Design and Evaluation of Cost-Effective Ultrasonic Sensors for Aggregate Temperature Measurement

Ali Amer Elyounsi

This thesis is submitted in partial fulfilment of the requirements of
Sheffield Hallam University
for the degree of Doctor of Philosophy

June 2024

DECLARATION

I hereby certify that the work described in this document is done without collaboration of anyone, except as indicated, the work described is entirely original.

1. I have not been enrolled for another award of the University, or other academic or professional organisation, whilst undertaking my research degree.

2. None of the material contained in the thesis has been used in any other submission for an academic award.

3. I am aware of and understand the University's policy on plagiarism and certify that this thesis is my own work. The use of all published or other sources of material consulted have been properly and fully acknowledged.

4. The work undertaken towards the thesis has been conducted in accordance with the SHU Principles of Integrity in Research and the SHU Research Ethics Policy.

5. The word count of the thesis is 26407 words

Name	Ali Amer Elyounsi
Award	PhD
Date of Submission	June 2024
Research Institute	Industry and Innovation Research Institute
Director of Studies	Alexander Kalashnikov

ABSTRACT

The development and verification of Ultrasonic Oscillating Temperature Sensors (UOTS) for measuring aggregate air temperature in residential settings is the primary focus of this thesis. Conventional temperature sensors, while commonly used, have limitations, including time lag and localised measurement. In contrast, UOTS provides a more comprehensive solution by offering rapid, responsive temperature measurements across the entire ultrasonic pathway using cost-effective piezo transducers. The research involved designing and experimenting with an air based UOTS system, specifically built using standard 20x20 aluminum profiles and ultrasonic transducers. This system was driven by an integrated circuit, equipped with dual operational amplifiers, and connected to conventional sensors (AHT20 and BMP280) via an I2C interface to serve as a reference temperature logger. Experimental setups included using A cardboard thermal testing enclosure and a domestic hairdryer to isolate the assembly from room air movements and rapidly heat the air, allowing for detailed monitoring of temperature changes. Key findings revealed that the UOTS responded much faster to abrupt temperature changes than conventional sensors. The UOTS demonstrated reliability over prolonged periods and varying distances (0.15 to 0.95 meters), showing sensitivity in the order of ~50 Hz/K. However, the research also concluded that while UOTS is effective for detecting rapid temperature changes, conventional sensors remain necessary for continuous monitoring, especially in environments with varying air movements. Overall, this research highlights the potential of UOTS in residential temperature control applications, offering a low-cost, efficient alternative to traditional sensor networks. The study opens the door for further advancements in temperature measurement technology, particularly in the context of smart homes and energy-efficient climate control systems.

ACKNOWLEDGEMENT

During my academic pursuits, I express deep gratitude to Allah for His guidance throughout my study period. I sincerely thank Dr Alexander Kalashnikov for his unwavering support, patience, supervision, and guidance throughout the research endeavour. Under his mentorship, I have been afforded an exceptional opportunity to acquire novel knowledge and develop a comprehensive understanding of temperature-sensing systems utilizing ultrasound waves. Additionally, I extend my heartfelt thanks to my second supervisor, Alan Holloway.

I also extend special thanks to my dear mother for her continual support and prayers.

My heartfelt thanks and appreciation go to the Sheffield Hallam University, encompassing faculty members, staff, and technicians, for providing an environment conducive to academic growth.

Special gratitude to my beloved wife Layla, my children Sakena, Esra, Abdou Arahman, Doaa and my little one Alaa, and all my friends for their endless love and unwavering support.

Additionally, I would like to thank the Libyan Ministry of Higher Education and the Libyan Embassy in the United Kingdom for their invaluable financial and administrative support.

PUBLICATIONS

A. Elyounsi and A. N. Kalashnikov, "Using Ultrasonic Oscillating Temperature Sensors (UOTSes) to Measure Aggregate temperatures in Liquid and Gaseous Media," 2021 IEEE UFFC Latin America Ultrasonics Symposium (LAUS), Gainesville, FL, USA, 2021, pp. 1-4.

A. Elyounsi and A. N. Kalashnikov, "Ultrasonic oscillating temperature sensor for operation in air," *Engineering Proceedings,* vol. 10, *(1),* pp. 62, 2021.

A. Elyounsi and A. N. Kalashnikov, "Evaluating suitability of a DS18B20 temperature sensor for use in an accurate air temperature distribution measurement network," *Engineering Proceedings,* vol. 10, *(1),* pp. 56, 2021.

A. Elyounsi and A. N. Kalashnikov, "Continuous rapid, accurate measurement of the output frequency of ultrasonic oscillating temperature sensors," *Engineering Proceedings,* vol. 27, *(1),* pp. 56, 2022.

A. Elyounsi and A. N. Kalashnikov, "Predictive IoT Temperature Sensor," *Engineering Proceedings,* vol. 27, *(1),* pp. 55, 2022.

A. Elyounsi, T. J. Mulroy and A. N. Kalashnikov, "Experimental Measurement of Air Temperature in an Enclosure Using Ultrasonic Oscillating Temperature Sensors (UOTSes)," *Engineering Proceedings,* vol. 58, *(1),* pp. 114, 2023.

A. Elyounsi and A. N. Kalashnikov, "Quantitative Experimental Evaluation of Ultrasonic Oscillating Temperature Sensors," 2024 IEEE UFFC Latin America Ultrasonics Symposium (LAUS), Montevideo, Uruguay, 2024, pp. 1-4, doi: 10.1109/LAUS60931.2024.10553028.

PRESENTATIONS

“**Quantitative experimental evaluation of ultrasonic oscillating temperature sensors.”** The 10th International Electronic Conference on Sensors and Applications IEEE UFFC Latin America Ultrasonics Symposium (LAUS 2024) Online https://2024.ieee-laus.org/

Friday 10 May 2024 [Montevideo, Uruguay]

“**Experimental Measurement of Air Temperature in an Enclosure Using Ultrasonic Oscillating Temperature Sensors, “**The 10th International Electronic Conference on Sensors and Applications (ECSA-10) Online https://ecsa-10.sciforum.net/#program

Monday 27 November 2023 [Singapore]

“Predictive IoT temperature sensor,” The 9th International Electronic Conference on Sensors and Applications. (ECSA-9) Online https://sciforum.net/paper/view/13337

Tuesday 1 November 2022 [Basel, Switzerland]

“Continuous rapid accurate measurement of the output frequency of ultrasonic oscillating temperature sensors”, The 9th International Electronic Conference on Sensors and Applications. (ECSA-9) Online https://sciforum.net/paper/view/13340

Tuesday 1 November 2022 [Basel, Switzerland]

“Sensing aggregate temperatures using ultrasound sensors,” Creating Knowledge 22

(SHU annual conference, CK-22 conference brochure

Wednesday15 June 2022 [Sheffield Hallam University]

“Ultrasonic thermometer for measuring aggregate temperatures in dwellings,” I2RI winter poster event (SHU), Eventbrite online announcement

Friday 4 March 2022 [Sheffield Hallam University]

“Evaluating suitability of a DS18B20 temperature sensor for use in an accurate air temperature distribution measurement network,” The 8th International Electronic Conference on Sensors and Applications (ECSA-8), Online https://sciforum.net/paper/view/11277

Wednesday 3 November 2021 [Basel, Switzerland]

"Ultrasonic oscillating temperature sensor for operation in air," The 8th International Electronic Conference on Sensors and Applications (ECSA-8), Online https://sciforum.net/paper/view/11276

Wednesday 3 November 2021 [Basel, Switzerland]

"Using Ultrasonic Oscillating Temperature Sensors(UOTSes) to Measure Aggregate temperatures in Liquid and Gaseous Media," LAUS Latin America Ultrasonics Symposium, (LAUS 2021) Online https://ieee-uffc.org/event/symposium/2021-ieee-latin-america-ultrasonics-symposium

Tuesday 5 October 2021 [Uruguay]

"Facilitating university-level analog electronics hands-on learning with a home lab kits." Transforming learning conference SHU 2021

Monday 13 September 2021 [Sheffield Hallam University]

"Using Internet services for low-cost intelligent management of industrial process equipment ," ICST21 International Scientific and Practical Conference, Online http://icst-conf.com/main-eng.html

Saturday 25 September 2021 [Odessa, Ukraine]

"Internet-of-Things application to automated control of process equipment," Creating knowledge Conference SHU Online https://shu.zoom.us/j/99375672508

Saturday 25 September 2021 [Sheffield Hallam University]

"Hands on learning of university level electronics at home," Creating knowledge

SHU Creating knowledge Conference SHU Online
https://shu.zoom.us/j/99375672508

Saturday 25 September 2021 [Sheffield Hallam University]

"Ultrasonic thermometer for measuring aggregate temperatures in dwellings," MERI Research Symposium Proceedings SHU Online

https://www.msn.com/en-gb/feed?rc=1&ocid=winp1taskbar&cvid=b1f2466ba05f4b979c1da6d18f95bc4f&ei=16

Tuesday, 08 June 2021 [Sheffield Hallam University]

"Student sensor lab at home: safe repurposing of your gadgets, "The 7th International Electronic Conference on Sensors and Applications (ECSA-7) , Online https://www.mdpi.com/2673-4591/2/1/

Tuesday17 November 2020 [Switzerland]

LIST OF CONTENTS

➢ **Contents**

LIST OF FIGURES

ABBREVIATIONS

AC	Alternating current
BAW	Bulk Acoustic Wave sensor
BPF	Band-Pass Filter
CAGR	Compound annual growth rate
CPU	Central Processing Unit
CWU	Continuous Wave Ultrasonic
DC	Direct current
DMA	Direct memory access
EMF	Electromotive Force
GUI	Graphical User Interface
IC	Integrated Circuits
I2C	Inter-Integrated Circuit
IR	Infrared
LED	Light Emitting Diodes
LPF	Low-Pass Filter
LUS	Laser Ultrasonic Sensor
MCU	Microcontroller Unit
NDT	Non-Destructive Testing
NTC	Negative Temperature Coefficient
OCXO	Oven-Controlled Crystal Oscillator
Opamp	Operating Amplifier
PC	Personal computer
PCB	Printed Circuit Board
PS	Phase Shift
PTC	Positive Temperature Coefficient
QCM	Quartz Crystal Microbalance
RH	Relative Humidity
RTD	Resistance Temperature Detectors
SAW	Surface Acoustic Wave
SD	Secure Digital
TCXO	Temperature Compensated Crystal Oscillator
TOF	Time-of-Flight
UART	Universal Asynchronous Receiver/Transmitter
UOTS	Ultrasonic Oscillating Temperature Sensors
USB CDC	Universal Serial Bus Communications Device Class
VGA	Variable Gain Amplifier

LIST OF TABLES

Chapter 1 : Introduction and background

The introductory chapter outlines the goals and purposes of the research. Temperature sensors are utilised in numerous industrial, scientific, medical, and residential applications, and their design and/or operating principles vary to better cater to specific requirements The global sensor market size was evaluated at USD 204.8 billion in 2022 and is expected to hit around USD 508.64 billion by 2032, growing at a CAGR of 8.40% from 2023 to 2032 The market's growth is fuelled by innovations in sensor accuracy, miniaturization, and the integration of IoT capabilities, which are increasingly critical in sectors such as healthcare, automotive, and smart home systems.[1] *While a single temperature sensor is often adequate for many applications, there are instances where a cluster of sensors is necessary to optimise a design, such as in the case of a refrigerator.*

Temperature measurements play a critical role in maintaining the safe and optimal functioning of nuclear reactors and aircraft engines Ultrasonic temperature measurement offers the advantage of responsive measurements throughout the ultrasonic pathway, unlike conventional temperature sensors that measure the temperature only at the point of their installation [2]. A range of conventional temperature sensors, including infrared temperature sensors [3], resistance temperature detectors [4], thermistors [5], and thermocouples [6], are discussed here.

1.1 Introduction

Temperature sensors have gained widespread adoption in various fields, including science, medicine, industry, and daily life. However, conventional temperature sensors can have limitations due to their operating principles, such as a time lag and response to temperature changes at only one localised point. In contrast, ultrasonic temperature sensors offer responsive measurements across the entire ultrasonic pathway, utilising the dependence of ultrasound velocity on the temperature of the propagation medium through pulse-echo and through-transmission principles. These sensors have demonstrated high sensitivity and reliable detection of fast temperature changes. Unfortunately, the high cost of the necessary ultrasonic instrumentation has limited their use. The development of Ultrasonic Oscillating Temperature Sensors (UOTS) was undertaken to address this issue, utilizing inexpensive, mass-produced narrowband ultrasonic sensors to lower the cost of the required instrumentation.

Piezoelectric transducers with a frequency range above 20 kHz are utilised in UOTS, generating sustained oscillations whose frequency corresponds to the temperature of the medium between the transducers. These sensors have demonstrated the ability to measure temperature in liquids with high responsiveness and low cost across an ultrasonic path of approximately 100 mm. The present study aims to extend the application of UOTS to measure temperature in air at varying distances, enabling the assessment of aggregate temperature in residential buildings using a single sensor.

1.2 Background

In a technical system, a sensor is a receptor that detects environmental changes. Temperature sensors are among the most frequently employed in industrial and domestic settings. As per [7], the market share volume of temperature sensors is expected to be expected to reach $11 billion by 2030 rising at a market growth of CAGR of 8.40% during the forecast period[1]

1.2.1 Ultrasonic thermometry

Ultrasonic thermometry relies on the correlation between ultrasound velocity and the properties of the medium, particularly its temperature. Accurate measurements of ultrasonic time-of-flight between two fixed points located at a known distance enable the determination of ultrasound velocity. Piezoceramic ultrasonic transducers are typically used to generate ultrasound waves by applying an AC voltage. The waves are either transmitted to an ultrasonic receiver or reflected by an object with an acoustic impedance that differs substantially from the environment, known as a reflector. In pulse-echo mode, the transducer is switched to receive mode before the reflected waves reach it, allowing for the detection of the echo, thereby eliminating the need for a separate receiver transducer.

Ultrasonic temperature sensors differ from conventional sensors in two significant ways: (a) they provide rapid and responsive temperature measurements, and (b) they detect temperature along the entire ultrasonic pathway. This makes them capable of replacing multiple conventional sensors that may be difficult to position within the object being monitored, such as for temperature monitoring within a dwelling's living area. It is possible to use more advanced and suitable devices.

The speed of sound in air is influenced not only by temperature but also by the moisture content, or humidity, present in the atmosphere. As humidity increases, the density of air decreases, resulting in an increased speed of sound. If humidity is not accounted for, this faster sound speed may lead the sensor to inaccurately interpret the data as indicating a higher temperature. Therefore, to ensure the accuracy of temperature measurements obtained from an ultrasonic sensor, it is essential also to measure the humidity level. By accurately determining both temperature and humidity, appropriate corrections can be applied to the sensor's readings, thereby enhancing the precision of the temperature measurement. In environments where humidity levels vary significantly, the integration of a humidity sensor alongside the ultrasonic temperature sensor facilitates real-time adjustments, ensuring that temperature readings remain accurate regardless of fluctuations in humidity.

Ultrasonic oscillating temperature sensors (UOTS) have been developed to solve the high cost of existing ultrasonic instrumentation. [2]. A UOTS operates by generating sustained oscillations at a frequency related to the temperature of the medium between the transducers. To implement a UOTS, a pair of ultrasonic transducers and driving electronics with supervisory control and output reporting are needed, The total cost of these components is below £20.[2]

Ultrasonic sensors are highly versatile instruments employed in both temperature measurement and object detection, playing essential roles in optimizing the efficiency and effectiveness of various applications. Their applications encompass maintaining precise temperature control in refrigeration systems, ensuring accurate heating in ovens, as well as enhancing robotic sensing capabilities and detecting irregular components in industrial processes.

1.2.2 Temperature measurements in residential buildings

Temperature is a crucial parameter in thermodynamics and kinetic theory, representing a system's thermal state. In physics, it is defined as the average kinetic energy generated by the particles in a system. It is commonly measured using Celsius, Kelvin, and Fahrenheit scales. Although there is no maximum temperature limit, the lowest possible temperature, called absolute zero, has been established, at which all molecular motion stops. To measure temperature, various physical parameters such as expansion coefficient, resistivity, voltage, and capacity are considered [8]. In the context of dwellings, the temperature is typically maintained between 15-30 degrees Celsius, which is considered comfortable and tolerable for humans. Some of the most used conventional temperature measurement methods or sensors are discussed below.

1.2.3 Types of conventional temperature sensors

Temperature sensors can be categorised into two primary types: contact and noncontact ones. Contact sensors necessitate the sensor and object to be in thermal equilibrium. The most used contact sensors include thermocouples, resistance temperature detectors (RTDs), thermistors, and integrated semiconductor temperature sensors. In contrast, noncontact temperature sensors estimate the temperature of a distant object by analysing its thermal radiation properties. These sensors calculate the thermal radiant power of infrared or optical radiation acquired from a predetermined area or volume [4] using techniques such as infrared (IR) sensors and remote thermal diode temperature sensors.

1.2.1.1 Thermistors

Thermistors are sensors that respond to changes in temperature by measurably altering their resistance. This relationship is nonlinear and requires some calculation to determine the temperature from the measured resistance. Thermistors consist of a material, such as ceramic or polymer, embedded in a system or encapsulated in epoxy resin or glass.

There are two types of thermistors: negative temperature coefficient (NTC) and positive temperature coefficient (PTC) thermistors. NTC thermistors are the most used, as their resistance decreases as the temperature increases [9]. Thermistors are frequently used in industry and home appliances due to their low cost. Another advantage of thermistors is their relatively high resistance. They have a variety of applications, such as in cars, to measure oil and coolant temperatures. Although they are generally less expensive than (RTDs), they are also less accurate. They allow for the monitoring of ambient temperature changes. Figure 1.1 shows the thermistor temperature characteristic curve.

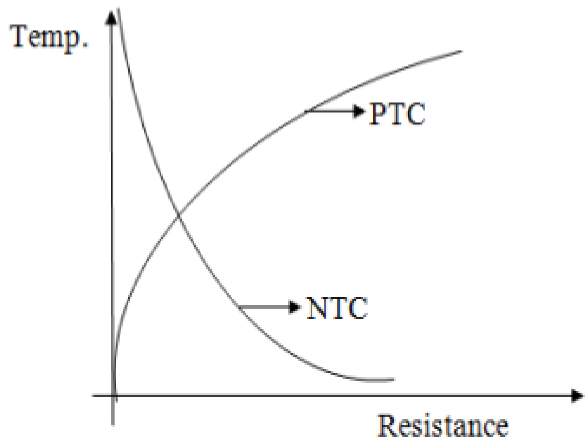

Figure 1.1: The thermistor temperature characteristic curve [9].

In contrast to other temperature sensors, thermistors typically operate within a limited temperature range but offer high accuracy and precision within that range. A common way of using a thermistor, shown in Figure1.2, is where a thermistor and a fixed value resistor form a voltage divider with its output connected to an ADC.

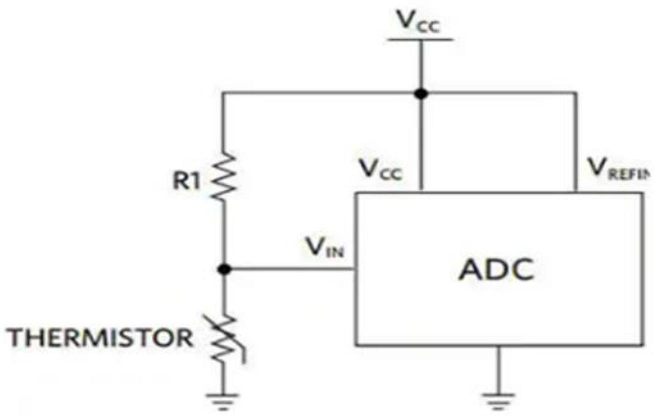

Figure 1.2: Typical Thermistor Interface [9]

1.2.1.2 Thermocouples

A temperature sensor known as a thermocouple measures temperature at a specific point by producing an electromotive force (EMF). This sensor contains two wires of different

conductive metals or alloys joined in a protective container called a thermowell. The voltage generated at the junction of these two wires is proportional to the temperature of the thermowell. Thermocouples have the benefits of being cost-effective, measuring a wide range of temperatures, and having a small size. However, they have drawbacks such as low voltage sensitivity, and their (EMF) may drift in a matter of hours or days, requiring frequent calibration [10]. As shown in figure 1.3

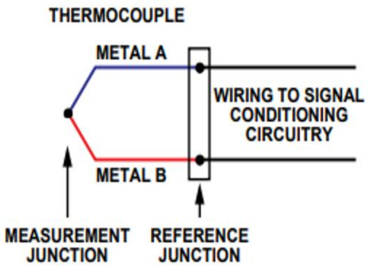

Figure 1.3: Construction of Thermocouple [10].

1.2.1.3 Resistance temperature detectors (RTDs)

Resistance temperature detectors use the correlation between the electrical resistance of conductive materials and their corresponding temperature, with platinum, nickel, and copper being common materials for constructing them. These materials are usually wrapped around a ceramic or glass core. The platinum option is especially favoured due to its highly linear resistance-temperature relationship [11].

One of the advantages of using (RTDs) for temperature measurement is that they do not require external temperature references, as the relationship between resistance and temperature is highly predictable.(RTDs) are effective in a temperature range of -200 to 600°C, which is adequate for many household and industrial applications. (RTD) sensors are increasingly employed in industrial settings and are even replacing thermocouples for temperature monitoring [12].

Compared to thermocouples, (RTDs) have a more accurate and linear behaviour over a more comprehensive temperature range. The benefits of using(RTDs) include a stable output over an extended time, precise readings over a narrow temperature range, and ease of recalibration. However,(RTDs) have some drawbacks, including a higher initial cost, less durability in high-vibration environments, and a smaller temperature range overall. To use(RTDs), an electrical current is required to produce a voltage drop across the sensor, which can then be measured using a calibrated read-out device A typical (RTD) is shown in Figure 1.4: Resistance temperature detectors (RTDs) [13].

.

Figure 1.4: Resistance temperature detectors (RTDs) [13].

1.2.1.4 Infrared temperature (IR) sensors

Noncontact temperature sensors make it possible to measure temperature without direct contact with the measured medium. Infrared radiation sensors are most widely used, as they can detect thermal changes in an object by measuring its infrared radiation. These sensors offer several advantages, including measuring the temperature of moving objects at a notable distance, a wide range of measurement capabilities, and fast reading times.

However, there are some disadvantages to using IR measurements. One major drawback is that differences in emissivity and reflectivity between objects can hinder the accuracy of temperature readings [14]. Additionally, these sensors are unsuitable for measuring gas temperatures and, therefore, for measuring the overall air temperature in dwellings.

The popularity of(IR)temperature sensors has risen significantly, mainly because they are compact and easy to operate. During the COVID-19 pandemic, they were used to reorganise social spaces and prevent the spread of the virus. Since fever is a common symptom of COVID-19, temperature measurement is one of the most frequently used screening protocols. Many countries have regulations that mandate temperature checks before entering public buildings, workplaces, and shops, as shown in Figure 1.5.

Figure 1.5: Infrared radiation (IR) temperature sensors.[14]

1.2.1.5 Semiconductor Temperature Sensors

Over the past few decades, semiconductor temperature sensors have become increasingly popular and widely used in various applications. These sensors are integrated circuits (ICs) and are thus commonly called(IC) temperature sensors They are typically manufactured on thin silicon wafers and divided into individual chips[15]

Semiconductor temperature sensors can be classified into five main categories: voltage output, current output, digital output, resistance output, and silicon diode temperature sensors. These sensors provide highly linear outputs within a temperature range of -40 to +120°C [14]. They have the advantages of being relatively small in size, low in cost, highly accurate (within ±2°C or less), and low in power consumption. However, it is important to note that these sensors may not consistently maintain adequate thermal contact with the measured surface. Table 1.1 summarises the main features of the different temperature sensors mentioned above.

Table 1.1: shown Summarises the main features of the different temperature sensors.

Main characteristics	Thermistors	RTDs	Thermocouples	IC sensors
Temperature range	0ºC to +100ºC	–200ºC to +850ºC	–184ºC to +2300ºC	–55ºC to +150ºC
Typical accuracy	Low	Best	Fair	Good
Linearity	Worst	Best	Fair	Good
Sensitivity	Good	Fair	Worst	Best
Ease of use	Fair	Difficult	Difficult	Easy
Cost	Cheapest	Highest	Moderate	Moderate

1.3 Use of ultrasound for temperature measurements

The term "ultrasonic" originates from the Latin words "ultra," meaning "beyond," and "sonic," meaning "sound." Ultrasound refers to sound waves with frequencies higher than the human hearing range, typically between 20 Hertz and 20 kilo Hertz for healthy individuals, hence, above 20 kHz. In 1912, the sinking of the Royal Merchant Ship Titanic after a collision with an iceberg prompted efforts to develop submerged detection methods. Researchers quickly discovered that higher-frequency waves were more effective for iceberg detection, leading to the development of ultrasonic technology to replace audible waves. This technology was pioneered by the father of ultrasonic Langevin, and the first underwater transducers were developed during World War I [16].

Ultrasonic waves possess unique characteristics that enable their use across a broad range of fields, including engineering, biology, medicine, oceanography, and others. Ultrasonic waves are characterised by their longitudinal nature in gases and liquids and transverse nature in solids. Despite travelling at a slow speed of approximately 100,000 times slower than electromagnetic waves, they can travel long distances, providing enough time for the transmission and reception of information. Unlike other forms of radiation, ultrasonic waves can penetrate opaque and conductive materials, generate heat within them, and produce images of their interior, making them suitable for non-destructive, non-invasive, and non-ionising applications such as non-destructive testing (NDT). Notably, ultrasonic waves are useful in creating images of tumours in the human body without the need for surgery, making it a safe alternative for patients [16].

There are two main categories of ultrasound applications: low-intensity, primarily for non-destructive testing (which is the focus of this research), and high-intensity applications, such as ultrasonic machining in industry and focused human tissue heating in medicine. Ultrasound is used for temperature measurement by taking advantage of the fact that the velocity of ultrasonic waves depends on the temperature of the medium. As temperature changes, the propagation delays of ultrasound between a fixed transmitter and receiver pair also vary. Variations in temperature can cause significant changes in the propagation delays of ultrasound between a fixed transmitter and receiver pair. Similarly, fluctuations in humidity can alter the speed of sound, further impacting the precision of ultrasound measurements. To ensure accurate readings, it is crucial to regularly calibrate the system, accounting for both temperature and humidity variations. Such calibration is essential for mitigating the effects of environmental factors, thereby preserving the reliability and accuracy of ultrasound measurements.

The first report on using ultrasound for temperature measurement was published in 1873 [17], and by 1975, around 500 industrial ultrasonic thermometers capable of measuring temperatures up to 20,000 °C in gases had been developed, In contrast to conventional temperature sensors, which respond to the temperature at their location only after a noticeable response time, ultrasonic temperature measurement provides responsive measurements throughout the entire ultrasonic pathway.

1.3.1 Types of acoustic thermometers

Temperature measurement using ultrasound has a rich history Temperature measurement using ultrasound has a rich history dating back to 1873 [17]. Various techniques for measuring temperature in solids, liquids, and gases have been developed. The use of ultrasound has enabled measurement with sub-millisecond response times, allowing for temperature monitoring in extreme conditions and high temperatures. For instance, in shock tubes, temperatures as high as 9000°C have been measured 18].

Similarly, in plasmas, ultrasound-based methods have been able to measure temperatures exceeding 20,000 °C. In situations, where conventional temperature measurement tools like thermocouples, resistance instruments, or optical pyrometers are not feasible, thin-wire sensors have been used in industrial and nuclear applications. These sensors can continuously monitor nuclear reactors at temperatures above 2000°C. However, ultrasonic equipment has been unaffordable in the past due to its size and cost. To improve sensor protection, some sensors require airtight enclosures, which can delay sensor response due to the need to achieve temperature equilibrium [19].

1.3.1.1 Acoustic Temperature Sensor (ATS)

The propagation of an acoustic wave through a medium is a function of temperature, which is the basis for the operation of an acoustic temperature sensor, Due to their poor accuracy, they are, however, not the best option [20].

1.3.1.2 Surface Acoustic Wave sensor (SAW)

SAW (Surface Acoustic Wave) technology utilises thermal expansion and propagation delay to create devices that have found numerous successful applications. These devices offer the necessary complex frequency responses at a reasonable cost [21]. SAW sensors function by initiating a surface acoustic wave on a piezoelectric material and detecting any alterations in the wave's frequency, amplitude, or velocity as it passes through a sensitive region. Although these sensors can be manufactured inexpensively, they have drawbacks, such as interference with chemical sensors and reduced selectivity due to fabrication tolerances [22]. One way to improve the performance of these sensors and lower their cost is to use less expensive materials.

1.3.1.3 Laser ultrasonic sensor (LUS)

By employing laser ultrasound inversion to determine the temperature distribution within a material, a new(SAW)-based propagation delay method was introduced. Laser ultrasound has an advantage over(SAW) in that the inversion process does not require surface boundary restrictions [23]. Laser ultrasonic sensors are used in a variety of applications, including non-destructive testing (NDT) of materials, thickness measurement of coatings and films, and measurements of the elastic properties of materials.

1.3.1.4 Bulk Acoustic Wave sensor (BAW)

For decades, the simplest and most ancient form of acoustic temperature sensor has been utilised as a thin film monitor in thermal evaporators. These sensors are based on the Quartz Crystal Microbalance (QCM) and consist of a small-sized thin film resonator, similar to a quartz crystal. The resonator contains a piezoelectric film sandwiched between metal films.

BAW (Bulk Acoustic Wave) sensors, characterised by their linear operation under extremely high temperatures and pressure [24], have sensitivities in the nanogram range, making them suitable for testing gas and liquid samples, BAW sensors present several distinct advantages over alternative sensor types, notably in terms of their high sensitivity, rapid response times, low power consumption, and potential for miniaturization. Specifically, BAW sensors can achieve sensitivity levels up to 1.5 ng/cm² in mass detection applications, enabling the detection of extremely subtle mass changes. Their response times are also notably rapid, typically less than 1 millisecond, which is essential for applications requiring real-time monitoring. Furthermore, BAW sensors operate at ultra-low power levels, typically consuming less than 10 μW, a figure significantly lower than that of many other sensor types. This low power requirement makes them particularly well-suited for use in battery-powered, portable devices. Additionally, the capacity of BAW sensors to be miniaturized to sub-millimetre dimensions further underscores their suitability for integration into compact, portable electronic device [25]

1.3.2 Notable developments in ultrasonic thermometry

Ultrasonic temperature measurement relies on the observed relationship between the velocity of ultrasonic waves and the object's temperature through which they travel [26]. As the sound velocity of a material is dependent on its temperature, The temperature can be determined by measuring the propagation velocity of ultrasonic waves. Thus, Temperature measurement is based on the practical observation that ultrasonic velocity correlates with temperature. This principle posits that the speed at which ultrasonic waves propagate through a material depends on its temperature, providing a foundation for temperature measurement across various materials. To numerically establish this correlation [27], the following steps are typically undertaken:

1-Ultrasonic velocity is measured at different known temperatures through controlled experiments. Ultrasonic transducers, employing either the pulse-echo or through-transmission technique, are used to measure the velocity at each temperature with precision. This process is repeated across a range of temperatures to compile a dataset of temperature values paired with corresponding ultrasonic velocities.

2-The collected data is plotted, with temperature on the x-axis and ultrasonic velocity on the y-axis. A trend is observed, typically linear or nonlinear depending on the material, illustrating a clear relationship between temperature and velocity measurement can thus be calculated as shown in equation 1.1

$V(T)=V_o+ \alpha \cdot T$ (1.1)

V(T) is the ultrasonic velocity at temperature T.

V0 is the ultrasonic velocity at a reference temperature

α is the temperature coefficient of ultrasonic velocity.

To Calibration and Validation, the derived equation is validated by comparing predicted ultrasonic velocities at various temperatures with experimentally measured values. Calibration involves adjusting the model's coefficients to minimize the error between the predicted and observed values.

Once this correlation is established, ultrasonic velocity can be measured in real time within an unknown environment, allowing the corresponding temperature to be inferred using the established mathematical model. This method is widely utilized in industries for non-invasive temperature measurement in various processes. Ultrasonic temperature measurement is founded on this practical observation of the correlation between ultrasonic velocity and temperature.

In 1972, Lynnworth et al. applied for a patent to measure temperature profiles in high-temperature gaseous and liquid media. Ultrasound propagated in a metal rod with equally spaced discontinuities, which reflected it to the transducer. By measuring the delay between the neighbouring echoes, it was possible to assess the aggregate temperature in the rod's section between the specially placed discontinuities [28].

In 2004 Liao et al. used inexpensive 40kHz air ultrasonic transducers for air conditioning thermometry in an automobile. The change in air temperature between the transducers resulted in an associated change in the velocity of the ultrasonic waves, which was measured using the time-of-flight (TOF) and phase shift (PS) techniques. The estimated air temperature was within 0.4 centigrade of the temperature measured by the reference thermocouple. This outcome, which was achieved using relatively expensive electronic instrumentation, was considered adequate for automobile air conditioning systems [27].

In 2008, Malyarenko et al. used ultrasonic system thermometry to determine small temperature changes caused by the therapeutic cancer treatment radiation in order not to exceed safe levels of the latter. They developed analog variable-frequency and digital phase monitor laboratory prototypes. In particular, the analog prototype tracked the signal phase by continuously adjusting the output frequency to compensate for phase shifts due to changing temperature. The phase detector consisted of a mixer followed by a lowpass filter. The prototypes detected changes in the order of tens of microkelvin averaged over the acoustic path of about 60 cm at room temperature in water with root-mean-squared noise of about 5µK [29].

In 2016, Lévesque et al. implemented integrated ultrasonic transducers (IUTs) on a small firearm at 3 locations. They were used to measure the inner bore temperature during actual firing. The firing test included both single shots and several shot firings sequences. Ultrasonic delay measurements were conducted with a resolution of less than one ns. Processed data provided indications for the average temperature rise through thickness after each shot and were fed into a simple 1D model of heat conduction. This model was found to be useful in predicting the inner bore temperature [30].

Afaneh et al., 2011 applied an acoustic sensor of pulse-echo type to various liquids (aqueous solutions of different salinity and acidity). In this study, a 20 MHz ultrasonic transducer and a reflector that was mounted inside a dipstick probe were placed inside a controlled temperature tank filled with the solution of interest. The reflector featured a cavity filled with deionised water used as the reference. The temperature was estimated by measuring two delays in the propagation of the acoustic wave through the medium of interest and deionised water. The results showed success in detecting and quantifying the changes in the Temperature of the solution when compared with a conventional thermometer with a resolution of 0.1 K [31].

The instrumentation employed encompasses high-speed electronics capable of capturing and processing signals with exceptional temporal precision. Key components, such as digital sampling oscilloscopes (DSOs), arbitrary waveform generators (AWGs), and low-jitter clock sources, are integral to these systems. Additionally, laser-based systems may be utilized in certain configurations to generate or detect ultrasonic waves with high temporal accuracy.

The high precision of these instruments often results in significant cost implications, owing to the requirements for ultra-fast electronics, low-noise environments, and advanced signal processing capabilities. For example, high-speed oscilloscopes with bandwidths exceeding 20 GHz and sampling rates in the hundreds of giga samples per second are commonly employed in cutting-edge ultrasonic thermometry.[32].

The developments mentioned above utilised high-resolution delay measurements requiring expensive electronic instrumentation. In addition, most of these used high-frequency, rather expensive, ultrasonic transducers, which prevented the use of ultrasonic temperature sensors in a wider context.

1.4 Ultrasonic oscillating temperature sensors

In order to decrease the high cost of ultrasonic instrumentation associated with ultrasonic temperature measurements, ultrasonic oscillating temperature sensors (UOTS) were developed, which can be made practical using mass-produced transducers and electronic parts at a fraction of the cost of conventional high-resolution ultrasonic measurement equipment. The lower-cost UOTS system consists of inexpensive narrowband piezo transducers with driving electronics. The operating principle of the ultrasonic oscillating temperature sensor is to produce continuous oscillations at a frequency that corresponds to the temperature of the medium of interest between the transducers. To achieve this, the narrowband ultrasound transducers should operate in the through transmission mode and use a positive feedback loop to sustain oscillations, which is similar to the mechanism used in surface acoustic wave (SAW) oscillators [2].

The previous developments mentioned relied on high-resolution delay measurements, requiring costly electronic instrumentation. Specifically, these systems used time-of-flight (ToF) measurements with resolutions in the nanosecond range (typically around 10–100 ns), which demanded expensive electronics such as high-speed counters and digital oscilloscopes. This high resolution was necessary to detect small changes in the propagation time of the ultrasonic waves due to temperature variations, but it significantly increased the cost of the system.[33].

An amplifier is utilised between the input and output transducers in order to maintain sustained oscillations, as depicted in Figure 1.6.

The UOTS operating principle involves the gradual development of oscillations at various frequencies, depending on the initial conditions, due to input noise. The amplifier is required to compensate for all the conversion and transmission losses in the electrical and ultrasonic pathways and ensure that the overall gain in the signal loop is greater than or equal to unity. The phase shifter, which is optional, may be used to adjust the output frequency at a particular temperature. The UOTS oscillates at the frequency where the overall phase shift in the open loop equals n × 360°, where n is an integer. Furthermore, a bandpass filter can be added to restrict oscillations to a specific frequency range only [2]

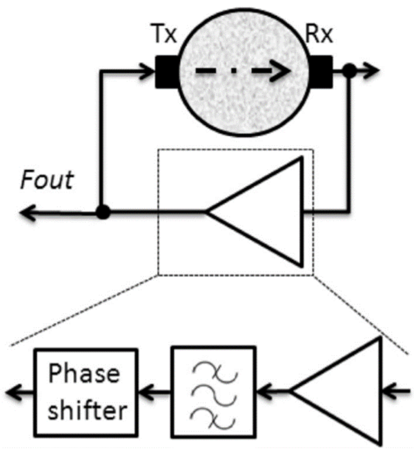

Figure 1.6: Operating principle of an UOTS [2].

A basic oscillating ultrasonic sensor can be created by positioning a pair of ultrasonic transducers coaxially and utilising a variable gain amplifier (VGA) to compensate for losses in conversion and propagation. However, this setup is insufficient for obtaining consistent output readings within a single frequency range. The addition of a phase shifter (PS) and a band pass filter (BPF) allows for the limitation of the output frequency to a specific defined range and sets it to the required value at a reference point.

These circuits necessitate control by a microcontroller, which also measures the output frequency and sends the data to a PC [34]. (See Figure 1.7)..

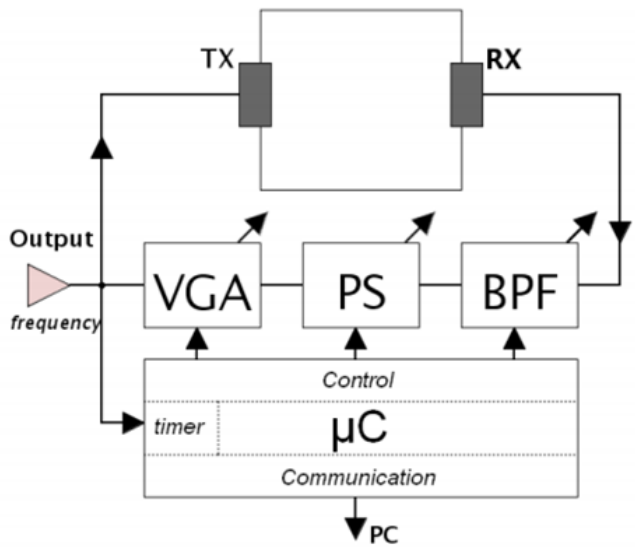

Figure 1.7: Complete diagram of a UOTS [34]

1.5 Previous developments in ultrasonic oscillating sensors

The UOTS technique relies on the dependence of ultrasonic sound velocity transmitted through a substance on temperature changes. The speed of ultrasonic waves through different substances ranges from hundreds of meters per second to several kilometres per second, allowing interrogation at almost zero settling time. The objective of most of these studies is to produce and develop UOTS devices that can be obtained at a cost comparable to that of conventional sensors while providing higher accuracy and reliability. Acoustic temperature measurement studies have been conducted in gases, liquids, and solids, with many of them accompanied by conventional temperature sensors for calibration, integration, and data fusion [35]. Some of the previous work is discussed and summarised below.

1.5.1 Temperature measurement in deionized water.

In 2010, Alzebda et al. developed a method for using air ultrasonic transducers to transmit ultrasound through a liquid to estimate its temperature. The two transducers were placed at a fixed distance in a deionised water tank, facing each other. An amplifier was used to compensate for the loop losses and maintain sustained oscillations. A phase shifter was also incorporated for calibration, and a bandpass filter was used to select the desired resonance. The output frequency depended on the propagation delay of ultrasonic waves between the transducers, which, in turn, depended on the temperature of the liquid medium. The temperature estimation was based on the several frequency resonances in the liquid instead of a single resonance in the air. A sensitivity of around 280 Hz/K at 26 to 32°C was achieved with reasonable consistency [36]. The sensitivity of a system or sensor is defined as the degree to which its output varies in response to a change in an input variable. In the context of this study, the sensitivity is quantified as 280 Hz/K, where Hz (hertz) denotes a unit of frequency and K (kelvin) represents a unit of temperature. This implies that for each 1 K increase in temperature, the system's frequency output changes by 280 Hz. To further illustrate the sensitivity, consider the temperature range from 26°C to 32°C, which encompasses a span of 6°C. Given that the temperature difference in °C is numerically equivalent to the difference in K, the sensitivity of 280 Hz/K allows us to calculate the corresponding frequency change over this range by applying the Equation (1.2).

$$\text{Frequency Change} = \text{Sensitivity} \times \text{Temperature Range} \qquad \text{Equation (1.2)}$$

$$\text{Frequency Change} = 280\,\text{Hz/K} \times 6\,\text{K} = 1680\,\text{Hz}$$

So, the frequency would change by 1680 Hz over the temperature range of 26°C to 32°C.

This sensitivity means that within this specific temperature range, a relatively small temperature change can cause a significant change in frequency, which could be crucial for applications requiring high precision. Was achieved with reasonable consistency.

The study used low-cost encapsulated ultrasonic transducers. The fast response time was obtained when the temperature was averaged across a path between sensors rather than at a single isolated point. Figure 1.8 shows the block diagram for the sensor developed by the authors.

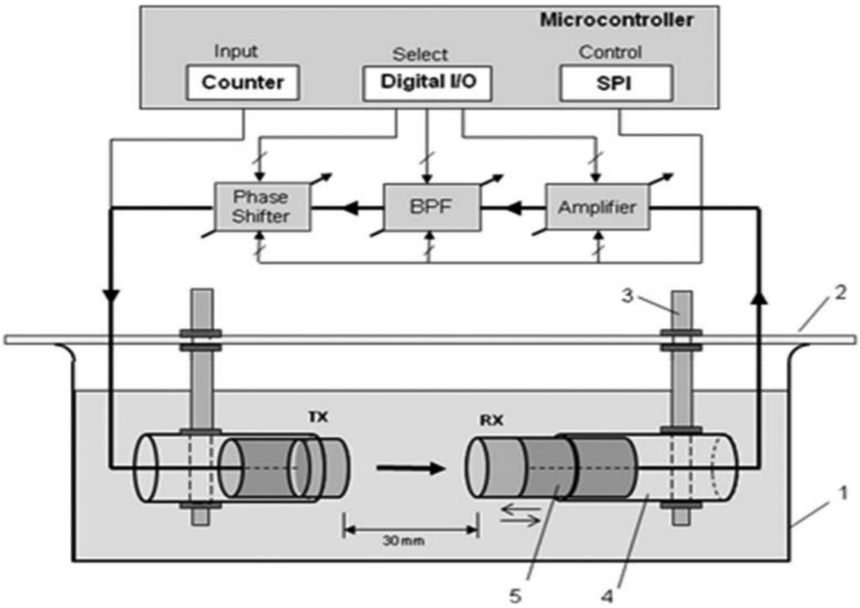

Figure 1.8 Block diagram of the developed sensor (1 – plastic vessel, 2 – aluminium plate, 3 – threaded steel rods, 4 – plastic tube to direct a transducer ,5- nylon tube to isolate the side and back of the transducer from the test medium.) [36].

1.5.2 Ultrasonic temperature measurements in aqueous solutions

In 2011, Afaneh et al. achieved a sensitivity of approximately 40 Hz/K at an operating frequency of roughly 25 kHz and a distance of 190 mm. The sensor circuit generated oscillations at the frequency where the overall gain exceeded one, and the total phase shift equalled 360◦. Measuring the frequency was relatively straightforward compared to measuring the phase shift, as the output pulses could be counted over a defined time. Using a set time of 1 second, the frequency measurement resolution was 1 Hz, which was well below 0.01% for ultrasonic frequencies. The sensor is advantageous due to the low cost of the transducer and supporting electronics (around $20). However, improvements to the transducer were required to provide accurate readings across a wider temperature range [37].

The measurement results indicate that the velocity of ultrasound in the aqueous solutions used differed from the velocity in seawater with the same salinity and temperature. This suggests that ultrasonic measurements have the potential to distinguish between similar chemical substances if they are maintained at the same temperature. Figure 1.9 shows schematic of the experimental setup

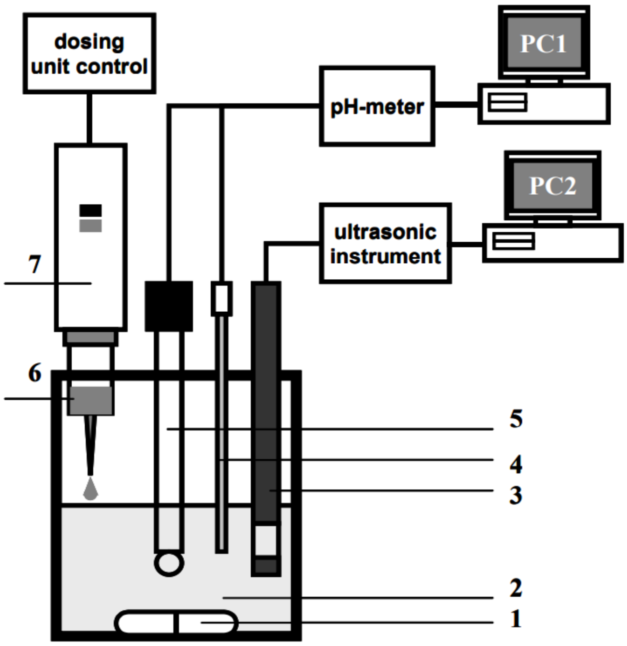

Figure 1.9: Schematic of the experimental setup (1 – magnetic stirrer, 2 – test solution, 3 – ultrasonic probe, 4 – temperature probe, 5 – pH probe, 6 – a tip of the dosing unit, 7 – dosing unit) [37].

1.5.3 Ultrasonic Temperature Measurements in Water

In 2019, Hashmi et al. utilised narrowband piezo transducers in the form of ultrasonic UOTS to measure water temperature in an ultrasonic calorimeter. The cylindrical experimental vessel was equipped with three sets of sensors: two conventional sets at the cylinder's ends and one set of UOTSes in the centre. The vessel could hold over 3.0 kg of water, which acted as a thermal buffer to prevent sudden temperature changes around the sensors. The experimental setup was placed inside a thermal chamber and heated, leading to an increase in the vessel's temperature. After being heated for some time, the heater was turned off, and the vessel cooled down gradually, returning to thermal equilibrium with the environment. The temperature and UOTS readings reported as text strings were continuously recorded into separate files by the host PC.

The UOTS was implemented by pairing one transducer with a modular ultrasonic driver consisting of two modules. The first module was responsible for amplifying and bandpass filtering the loop signal. In contrast, the second module measured the (UOTS) output frequency and communicated it to the host via a suitable USB interface. To measure the output frequency, an additional 10 MHz oven-controlled crystal oscillator (OCXO) was utilised as a reference frequency due to its temperature tolerance and stability. Data fusion was performed by combining readings from a conventional sensor with those from the(UOTS)to obtain temperature estimates without the hysteresis inherent to piezoelectric materials. This approach improved resolution and reduced response time compared to the conventional temperature sensor alone. It overcame the dependence of (UOTS) readings on the sign of the temperature gradient[38] .Figure 1.10 shows full view and close-up photographs of the vessel with transducers [38].

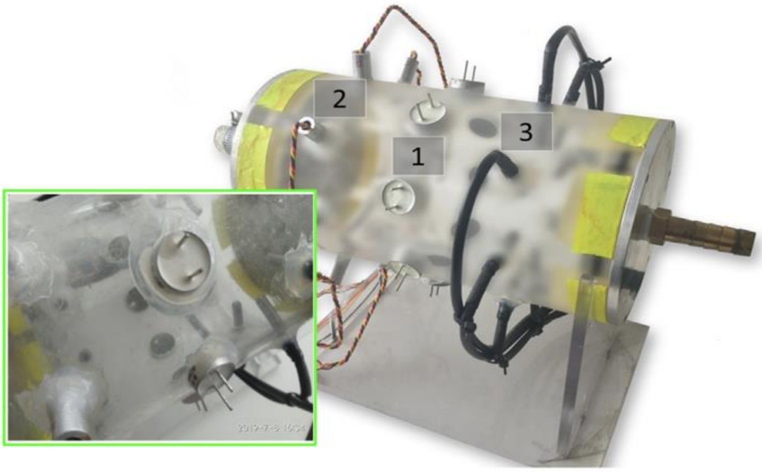

Figure 1.10: Full view and close-up photographs of the vessel with transducers (1) Ultrasonic transducers, (2) Case less DS18B20, (3) Encased DS18B20) [38]

1.5.4 Summary of previous developments in ultrasonic oscillating sensors

Previous experiments have been carried out to measure temperature of a liquid using UOTSes. In one such experiment, a transparent plastic tube was filled with water and placed inside a thermostatic chamber. The experiment also revealed that the output frequencies of transducer pairs placed at the same distance could be similar or different at different stages of the temperature-changing process. This inconsistency was attributed to thermal hysteresis, which is common in piezoelectric devices.

Attempts have been made to overcome hysteresis by adjusting the parameters based on the current output frequency to maintain the use of ultrasound data. Hysteresis refers to a phenomenon in which the output of a system is contingent not only on its current input but also on its historical states. In other words, the system exhibits lag or path-dependent behaviour, wherein its present state is influenced by its previous conditions. Hysteresis is commonly observed in dynamic systems, including ultrasound, where it may manifest as a delay or lag in the response of a system parameter such as output frequency—to variations in an input parameter. This temporal lag can result in the system behaving differently depending on whether the input is increasing or decreasing, leading to loop-like behaviour in input-output plots.

The presence of hysteresis in ultrasound data systems poses significant challenges, particularly in applications demanding high precision. However, by identifying the sources of hysteresis and implementing strategies such as dynamic parameter adjustment, algorithmic compensation, feedback loop tuning, temperature compensation, and meticulous material selection, it is possible to mitigate its adverse effects. These interventions help ensure that the system maintains the desired output frequency and produces accurate and reliable ultrasound data, even under conditions that would typically induce hysteresis.

Hysteresis is thus a critical concept in the study of systems where history and path dependence play a pivotal role in determining both current and future states [39].

During the plastic tube use, eight conventional DS18B20 sensors were also installed in the thermostatic chamber. The temperature profile for the experiment consisted of two intervals with increasing temperature, each followed by an interval with decreasing temperature. In another experiment designed purely for temperature measurement, oscillating ultrasonic sensors were found to have less variation in tilt measurement compared to a commercially available industrial accelerometer The test involved placing two coaxial ultrasonic transducers in water, with half of their front faces covered, and driving them using electronics assembled on a custom PCB [36].

Additional experiments were performed at low tilts, which indicated that an industrial tilt sensor, previously used as a reference sensor, had a limited output change sensitivity near the level position, whereas the frequency of the oscillating ultrasonic sensor still varied. Another research study employed a continuous wave ultrasonic (CWU) device with frequency output to conduct submerged sensor tests for high-resolution liquid temperature measurements [36].

The researchers later decided to use the (CWU) electronic driver alone to measure the output frequency. They conducted a feasibility study on using a(CWU) oscillator to measure low-frequency tilt inputs with high resolution. Their test cell, electronic instrumentation, and test rig allowed for stand-alone and comparative measurements within the -5°…+5° tilt range. Results from an experimental comparison with an industrial tilt sensor showed a smaller output scatter for the (CWU) oscillator. However, this may have been influenced by the adopted time base inherent to the frequency measurement procedure.

Nevertheless, the (CWU) oscillator demonstrated the ability to measure angles with a resolution below one minute and a capture rate above 150 Hz. How the resonant frequency of the water mass affects the device's frequency response remains to be determined [36]. Table 1.2 provides a summary of previous developments in ultrasonic oscillating sensors.

Table 1.2: Summary of Previous Developments in ultrasonic oscillating sensors.

Paper	medium	Application	Arrangement	Apparatus	Temperature Estimation	The result
Afaneh,et al. 2011	Aqueous solutions	Pulse-echo	A controlled temperature tank filled with a solution of interest and dipstick probe of 20 MHz ultrasonic transducer with a designed reflector.	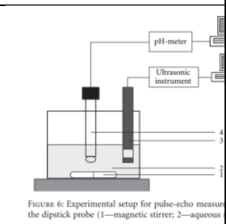	Via the delay of the propagation of the acoustic wave through the medium	Measured fast changes over conventional sensors
Alzebda., et al 2010	Deionised Water	Through transmission (pulse operation)	To modify inexpensive narrowband transducers designed for operation in air they were held in a tank. The test cell was complemented by an amplifier microcontroller, phase shifter and bandpass filter.	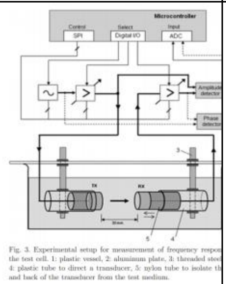	The generated output frequency depends on the delay of the ultrasonic waves between the transducers.	A sensitivity of 280 Hz/K at 26 - 32℃. Several frequency resonances in liquids instead of the single resonance in air achieved.
Afaneh,et al. 2011	Aqueous solution	Through transmission of continuous wave	Similar to exp.2 The circuit produces oscillations at the frequency where the overall gain exceeds 1, and the overall phase shift equals to 360◦. Sensitivity of about 40 Hz/K at the distance of 190 mm and the operating frequency of about 25 kHz.	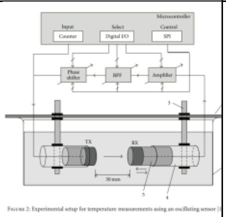	The phase shift of the wave propagated through the medium was measured instead of pulse delay. Resonances at 25 kHz frequency was chosen for good temperature resolution.	Worked between 20 -35◦C with a sensitivity 280 Hz/K at 328 kHz frequency. Ambiguous output of the sensors because two resonances instead of one for the transducers used.
Hashmi., et al 2019	water	Narrowband piezo transducers (UOTS)	The experimental water filled vessel with 2 conventional temperature sensors, and 1 USOTS set.	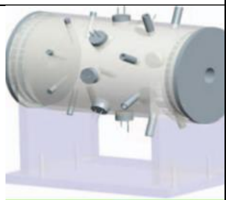	Due uneven temperature distribution inside the tube, the sensors reading were integrated. Averaging the temperatures across the sensor array was done. (STDs) were computed for each sensor.	The data fusion increases temperature resolution and decreases response time. Overcome dependence of UOTS readings on the ultrasonic path length

1.5.5 Utilisation of UOTSes for this study

This study aims to develop an ultrasonic sensor for measuring aggregate temperature in residential settings. While previous projects have focused on submerged ultrasonic sensors in liquid media, this sensor will be used in the air. An electronic driver with MCU control will be designed, and the entire operation process of the developed ultrasonic temperature sensor will be tested in various real-world scenarios against conventional temperature sensors.

1.6 Why using UOTSes in air

The cost of maintaining comfortable indoor temperatures in modern buildings is high and contributes to greenhouse gas emissions. In the US, for instance, 38% of residential greenhouse gas emissions are attributed to heating and cooling rooms, while the UK estimates that 19% of its greenhouse gas emissions result from warming up indoor spaces. Temperature Sensors Market size, share, and trends 2024 to 2034. The global temperature sensors market size was estimated at USD 9.1 billion in 2022 and is projected to be worth around USD 18.15 billion by 2032, registering a CAGR of 7.20% during the forecast period from 2023 to 203[40].

Moreover, the distribution of air temperature within a room can be uneven, necessitating the use of several conventional temperature sensors for optimal and eco-friendly temperature control that prioritises environmental comfort. Ultrasonic oscillating temperature sensors (UOTSs) have the capability to measure temperature almost instantly across the entire ultrasonic pathways [2], making them a promising candidate to replace conventional temperature sensors for indoor climate control purposes. This research introduces a newly developed air UOTS and provides experimental findings on its response to air temperature step changes while concurrently recording the responses of AHT20 and BMP280 conventional air temperature sensors.

1.7 Outcomes for the present research

To make ultrasonic thermometers more widely used, their cost must be reduced. This can be achieved using low-cost ultrasonic transducers that are mass-produced and have a narrow frequency range. The introduction of ultrasonic oscillating temperature sensors (UOTSs) in the 2010s demonstrated that ultrasonic temperature sensor components could be reduced to below £20 [41]. Additionally, (UOTSs) have an advantage over other electronic architectures that use narrowband ultrasonic wave transducers because of their simplicity due to their self-sustaining oscillator operating principle [42]. Initially, testing took place within the controlled confines of a laboratory, where baseline data was forged, and the technology itself was tested. This phase focused on crafting prototypes and gathering the vital data needed. Looking ahead, the technology may be tested in real residential homes.

1.7.1 Motivation

Highly accurate temperature measurement is essential for various applications, including estimating the power loss of electric motors, aircraft, and spaceship engines, as well as determining the energy released through waste burning. However, devices offering accuracy better than ±0.15 K are often prohibitively expensive. This disparity underscores the imperative need for the development of a low-cost yet precise temperature measurement device. Low-frequency and low-intensity oscillating ultrasonic sensors, coupled with additional data processing and calibration, hold the potential to attain high accuracy at a substantially reduced cost.

1.7.2 Aims and objectives.

This research aims to develop, fully prototype, and verify an ultrasonic sensor for measuring aggregate temperature in dwellings (residential buildings). The aim is to be achieved by completing the following objectives:

1. Develop a test rig for the oscillating temperature sensors that can be isolated from any air movement inside the room to fully develop the electronics and characterise the sensor, equipped with calibrated conventional temperature sensors placed along the ultrasonic pathway.

2. Designing an electronic driver with (MCU)control and frequency reporting and a suitable low-cost frequency reference oscillator.

3. Verify the operation of the developed sensor against conventional temperature sensors.

4. Testing operation of the developed sensor for various distances.

Regarding the development of a test rig that isolates the sensors from air movement, while this setup may seem ideal for refining the sensor's functionality, it might not fully represent typical residential conditions. However, it is realistic for the developmental stage of the project. Isolating the sensors in this manner ensures that environmental factors like drafts or ventilation systems do not interfere with the sensor’s performance. Once the sensors are calibrated and optimized in the lab, they can be tested in real-world settings, where additional factors such as air movement and varying humidity levels can be accounted for.

Therefore, while the test rig offers controlled conditions that may not entirely reflect the real-life environment, it serves a crucial role in the sensor development process. This setup ensures that the core technology is sound before field-testing the sensors in more dynamic and uncontrolled residential environments.

1.8 Novel Contributions to Future Research Developments in (UOTS)

During this research and through several experiments conducted, certain limitations require addressing in future work concerning the measurement of air temperature using an ultrasonic oscillating temperature sensor for operation in the air.

1-Verify performance of an UOTS in a temperature-controlled chamber that will also enable more comprehensive study of hysteresis in the output frequency.

2- Verify performance of an UOTS against an array of conventional temperature sensors, independently measuring air temperature along the complete ultrasonic pathway.

3-Extend the distance between the transducers in order to achieve operation at the distance of several meters that is typical for residential buildings.

4-Establish convenient and unobtrusive ways of commissioning an UOTS into a residential environment.

1.9 Structure of the thesis.

This chapter introduces conventional and ultrasonic technologies used for measuring temperature, providing an overview of their background and historical development. Various types of temperature sensors, encompassing both conventional and, notably, ultrasonic sensing devices, are briefly examined and contrasted. The Oscillating Ultrasonic Temperature Sensor (UOTS) is introduced. Additionally, ultrasonic oscillating sensors employed in prior research projects are discussed. The project's aims and objectives are further discussed in the concluding section of this chapter.

Chapter 2 focuses on and underscores the potential for achieving consistent relative measurements despite challenges in absolute accuracy. Placing sensors within a standardized enclosure with limited air volume can lead to closer-than-anticipated readings, with sensor biases addressed during subsequent processing. Two experiments are being conducted: one utilizes Pt100 RTD and DS18B20 sensors, chosen for their prevalence in the industry and networking capabilities, respectively, while the other employs BMP280 and AHT20 sensors on a board with solid thermal contact. These experiments comprehensively evaluate the suitability, reliability, networking convenience, and cost-effectiveness of conventional temperature sensors for the present study.

Chapter 3 introduces the design and testing of the supporting electronics necessary to operate the ultrasonic oscillating temperature sensor (UOTS) system. The chapter briefly overviews constructing an ultrasonic driver circuit and outlines the system requirements. The research focuses on frequency measurement, which is crucial for developing UOTS, as their output frequency changes with the sensed temperature. Different methods for frequency measurement using MCUs' built-in timers are explored. Various techniques leverage the timer peripherals of modern MCUs to continuously and accurately measure the output frequency of UOTS Lastly, a low-cost and reasonably accurate frequency meter is being devised, complemented by the appropriate selection of the clocking reference.

Chapter 4 delineates various approaches for recording experimental temperature data from a conventional temperature sensor and a UOTS across three distinct scenarios: rapid heating of air within an enclosure, long-term monitoring of air temperature inside an enclosure, and long-term monitoring of air temperature in an open-plan office. The UOTS output frequency is measured across two specific intervals: 0.1 seconds and 6.25 milliseconds. Finally, the comparison between the conventional sensor and UOTS output frequencies is conducted at 150 mm, revealing that the UOTS offers faster response to temperature changes whilst ensuring capture of the same temperature profiles over long time as the conventional reference sensors.

Chapter 5 details the methods used to record experimental temperature data from a conventional temperature sensor and a (UOTS) in two scenarios: long-term monitoring of air temperature inside an enclosure and long-term monitoring of air temperature in an open-plan office. The UOTS output frequency is measured at 6.25 milliseconds. The comparison of the conventional sensor and UOTS output frequencies is being conducted over 300 mm and 500 mm, with the outcomes being broadly in line with these observed at the smaller distance.

Chapter 6 implements various scenarios to measure temperature within controlled and open environments at a distance of 920 mm between the transducers. Conducting experiments outside the box in an open office aims to replicate an uncontrolled environment. These conditions are systematically applied across extended time intervals. The other scenarios implemented in this chapter include the rapid and slow heating tests. The rapid heating test utilizes a hair dryer for forced convection, creating dynamic airflow that rapidly increases the temperature within the enclosure. Heat conduction is the primary mechanism in the slow heating test, involving a soldering iron, and is complemented by forced and natural convection. The interplay of these mechanisms influences the overall heat transfer, providing insights for tailored thermal processes.

Chapter 7 offers a comprehensive summary of the findings from the preceding chapters and provides insights into the system's performance. An overarching project summary is included, focusing on the significance of cost in deploying a UOTS and the study's objective to assess temperatures ultrasonically at the lowest feasible expense. Additionally, recommendations for potential future advancements in this field are discussed.

Chapter 2 : Instrumentation and procedures for logging frequency reported by the UOTS

This chapter will describe components for operating an UOTS and measuring its output frequency. The general procedure of most of the experiments will be outlined. Any methodology specific to individual chapters will be discussed there.

2.1 Ultrasonic transducers

2.1.1 Introduction

Typically, ultrasonic transducers comprise both a transmitter and a receiver, with their performance varying based on temporal and spatial factors. Over time, ultrasonic transducers change in response due to ageing. Thus, different types of ultrasonic transducers are available to suit varying levels of accuracy and application needs [43].

One significant advantage of ultrasonic transducers is their ability to operate in harsh environments, surpassing the capabilities of other measurement methods. Moreover, ultrasonic sensors are relatively inexpensive compared to their competitors. Research has also found that ultrasound can provide more accurate data than conventional thermometers These sensors can monitor several parameters, such as viscosity, displacement, density, and temperature [44]. Figure 2.1 below illustrates an ultrasonic transducer.

Figure 2.1: Ultrasonic Transducer [44]

2.1.2 Working principle of an ultrasonic Transducer

An ultrasonic transducer operates within a specific frequency range and generates a sound wave by applying an electrical signal. As the sound waves propagate, they bounce off any obstacles encountered, and the echo information is reflected to the transducer. The transducer then converts this echo into an electrical signal at its output.

The time taken for the sound wave to travel and the echo signal to return is measured by the transducer, determining the distance of the obstacle from the sensor. Ultrasonic sensors emit pulses with a frequency of 40 kHz and are highly advantageous compared to infrared sensors as they are not affected by smoke, dark materials, and other environmental factors. Furthermore, they can reduce background noise, making them highly desirable [45]. Figure 2.1 below Working principle of ultrasonic transducer.

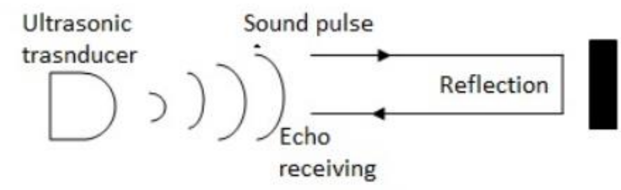

Figure 2.1: Working principle of ultrasonic transducer.

Ultrasonic transducers can be used to measure distance to remote objects using ultrasonic waves. The distance can be calculated using the equation 2.1

$$D = \frac{1}{2} * T * C \qquad (2.1)$$

where D indicates the distance, T shows the time difference between the sending and reception of ultrasonic waves, and C indicates the speed of sound.

1.2.3 Ultrasonic Transducer Types

The development and fabrication of ultrasonic transducers are tailored to meet specific application requirements. The selection of the appropriate transducer is crucial to ensure accurate ultrasonic measurement. Ultrasonic transducers are available in various types to suit different needs.

a. Piezoelectric transducers: These transducers use the piezoelectric effect to convert electrical energy into mechanical energy (ultrasonic waves) and vice versa. They are commonly used for both transmitting and receiving ultrasonic waves.

b. Magnetostrictive transducers: These transducers use the magneto-strictive effect to convert electrical energy into mechanical energy (ultrasonic waves) and vice versa. They are typically used for high-power ultrasonic applications.

c. Electrostatic transducers: These transducers use the electrostatic effect to convert electrical energy into mechanical energy (ultrasonic waves) and vice versa. They are less commonly used in ultrasonic applications due to their relatively low efficiency.

d. Electromagnetic transducers: These transducers use the electromagnetic effect to convert electrical energy into mechanical energy (ultrasonic waves) and vice versa. These are also less commonly used.

e. Laser-based transducers: These transducers use laser beams to generate ultrasonic waves. They are used in non-destructive testing, medical imaging, and industrial measurements. Depending on the needed range, various temperature sensors (or transducers) are utilised.

2.2 Operational Amplifier

"Op-amp" is a shortened form of "Operational Amplifier," which refers to a DC-coupled, high-gain electronic voltage amplifier with a differential input and a single-ended output. Typically, the voltage differential between an op-amp's input terminals and the output voltage is hundreds of thousands of times higher.

Op-amps serve as fundamental building blocks for circuit design as the characteristics of a circuit containing one are determined by external components. This makes op-amps less susceptible to temperature changes or manufacturing variances. Operational amplifiers are considered one of the most valuable and significant components of analog electronics, and they are commonly found in scientific, industrial, and consumer products.

2.2.1 Working principle of an Operational Amplifier

An operational amplifier, commonly called an OP, OPA, or OPAMP, is a voltage amplifier with a single-ended output and a differential-mode input that is DC-coupled. Its name originated from its primary use in arithmetic circuits such as adders and multiplyers. Several features are necessary to meet ideal op-amp characteristics, including infinite input impedance, zero output impedance, infinite open-loop gain, and infinite standard bandwidth.

2.2.2. 1MCP6022 - Rail-to-Rail Input/Output Op Amps

The MCP6022 is an operational amplifier (Op Amp) with rail-to-rail input/output and a gain-bandwidth product of 10MHz. It has a low operating current of 1.0mA and an offset voltage of less than 0.5mV. This Op-Amp utilizes Microchip's advanced (CMOS) technology, which provides high-speed operation, rail-to-rail output swing, high open-loop gain, and low bias current.

The MCP6022 is suitable for various applications requiring low or battery power. It is also ideal for low-end audio applications, portable equipment, data-gathering, and test equipment.

With the supply voltage as low as 2.5V, the MCP6022 can operate using less than 1.35mA of quiescent current per amplifier.

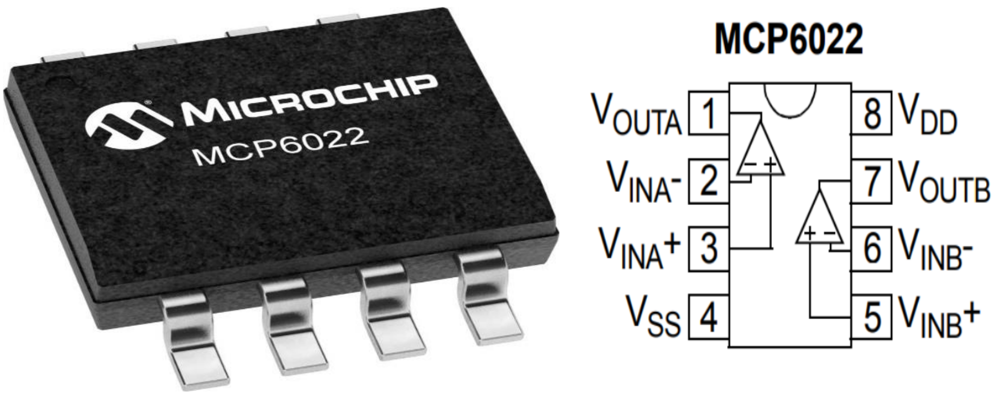

Figure 2.2:Microchip MCP6022 temperature sensor.

Features:

Rail-to-Rail Input/Output

Wide Bandwidth 10MHz (typical)

Low Noise 8.7nV/√Hz at 10kHz (typical)

Low Offset Voltage

Temperature Range

Industrial -40°C to +85°C

Extended -40°C to +125°C

2.3 Frequency counter PLJ-8LED-C

The main purpose of the 8-digit, cost-effective PLJ-8LED-C module is to display the operating frequency in a radio transceiver and other communication devices. Additionally, it can be applied to regular frequency measurements. The module provides low-cost, reliable, high-performance operation with a small, clear display.

Figure 2.3: 8-Digit LED Frequency Counter Module Model PLJ-8LED-C

The main features:

a. Microchip PIC16F648A forms the core of the 2.4GHz frequency meter.

b. Frequency reference using a temperature-compensated voltage-controlled crystal oscillator (2.5 ppm VC-TCXO).

c. Unique gate control with precise time algorithm (No timer interrupt).

d. Gate (display refresh) times include 0.01, 0.1 and 1.0 seconds to allow a real-time frequency display.

2.3.1 Measuring Frequencies

Frequency measures the number of occurrences of a repeating event per unit of time. It is commonly measured in Hertz (Hz), the number of occurrences per second. For example, a frequency of 20 Hz means an event occurs 20 times per second. Frequencies can be measured using a frequency meter, a standalone instrument or a function built into other equipment, such as an oscilloscope or a multimeter. The RF IN (signal input) port needs to be wired up with the signal that will be monitored. This signal input can be connected to several test points or the local oscillator output of a transceiver. The Light Emitting Diodes(LED) display will show the frequency in real time once connected.

The high-impedance input design lessens the counter's load on the transceiver's local oscillator circuit. The signal being monitored, though, needs to be higher than 60mVpp. For instance, the oscillator signal from the popular NE602/NE612 is weak, which may prevent the counter from obtaining a consistent frequency value. A signal amplitude of 59 mVpp is deemed insufficient as it is slightly below the critical threshold of 60 mVpp, which is necessary for reliable operation. Such a marginally deficient signal will likely cause inconsistent readings due to its proximity to the operational limit. Signals with significantly lower amplitudes, such as one mVpp, would be even more problematic, rendering the frequency counter unable to produce stable frequency measurements. In this context, any signal with an amplitude below 60 mVpp can be classified as "weak," with the probability of operational failure escalating as the signal amplitude diminishes further below this threshold. For the frequency counter to function correctly, the input signal must exceed the 60 mVpp requirement.

2.4 Cardboard Thermal Testing Enclosure.:

A cardboard thermal testing enclosure was used to house the temperature sensors in a confined space. It has a length of 1700mm, width of 280mm and height of 195mm. We utilised a domestic hair dryer rated at 2kW to quickly heat up the air inside the enclosure as shown in Fig (2.5).

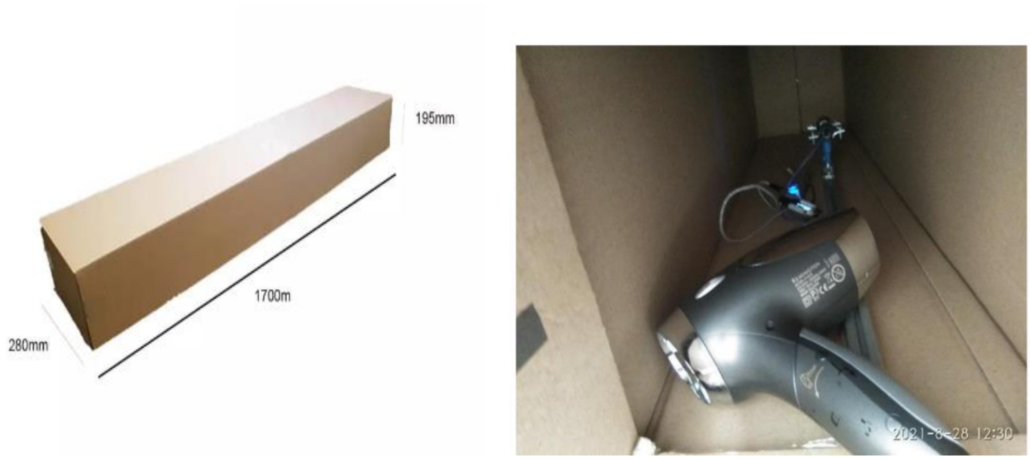

Figure 2.4: Cardboard enclosure.

Contact Name:

Contact Number:

Contact Email:

All Dimensions quoted are internal & are shown as - Length x Width x Height.

Qty Required	Product Code	Product Description	Unit Price £	Net £
1.00	7000	1100mm x 250 x 250 0201 DW INC DELIV	28.000000	28.00

Sales Order Tax Breakdown:	Tax Rate	Total Net	Total Tax
	20.00%	28.00	5.60

2.5 USB Oscilloscope Instrustar ISDS 205

The ISDS205 digital oscilloscope is a dual-channel device designed to achieve high performance at an affordable price. It boasts a well-designed bandwidth of 16 MHz and a sampling rate of 48 MHz, with two channels that support X-T and XY alternating patterns for the virtual oscilloscope. Additionally, it includes a spectrum analyser and data recorder. Oscilloscopes are vital to testing and measuring equipment in laboratory settings, as they allow for the display, recording, and analysis of voltage waveforms, typically in the time domain. The INSTRUSTAR ISD205 is a portable USB oscilloscope that can be used for various applications, including electronics testing, automotive diagnostics, and educational purposes. Other notable features of this device include automatic measurements and a built-in function generator. The device can be powered via a USB connection and comes with software for both Windows and Mac operating systems. The spectrum analyzer feature of the INSTRUSTAR ISDS205 was employed to analyze the frequency components of the signals under measurement. This tool proved particularly effective in identifying and isolating noise or interference within specific frequency ranges, which was essential for fine-tuning and optimizing the signal integrity of the system under investigation. Utilizing the spectrum analyzer allowed for the visualization of the distribution of signal power across various frequencies, thereby enabling the detection and mitigation of unwanted frequency components that could potentially impact overall performance.

Figure 2.5: USB Oscilloscope INSTRUSTAR ISDS205

2.6 Comparing UOTS responsiveness with that of the conventional temperature sensors

26.1 Materials & Methods

The UOTS utilizes a pair of ultrasonic transducers and an electronic driver, which includes a dual operational amplifier (OpAmp) MCP6022, as shown in Figure 2.6. The opAmp has two buffers: buffer U1 amplifies the signal, while buffer U2 is for the eight-digit frequency counter PLJ-8LED-C. Additionally, resistances and capacitors are used in the UOTS setup.

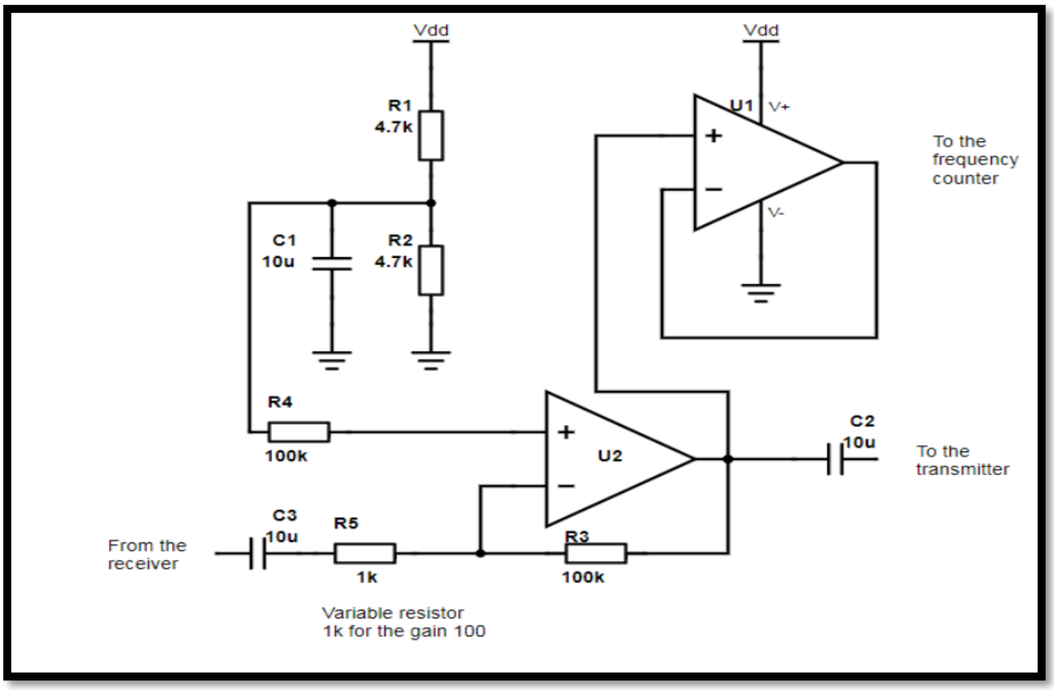

Figure 2.6: Schematic diagram of the electronic driver.

Conventional temperature sensors AHT20 and BMP280 were connected to an I2C interface on a Seeedstudio Xiao microcontroller board mounted on the same circuit board to measure air temperature. The setup also included a 40 kHz air ultrasound transducer that was attached to a standard 20 × 20 aluminium profile at 125 mm using Munsen rings, as shown in Figure 2.7.

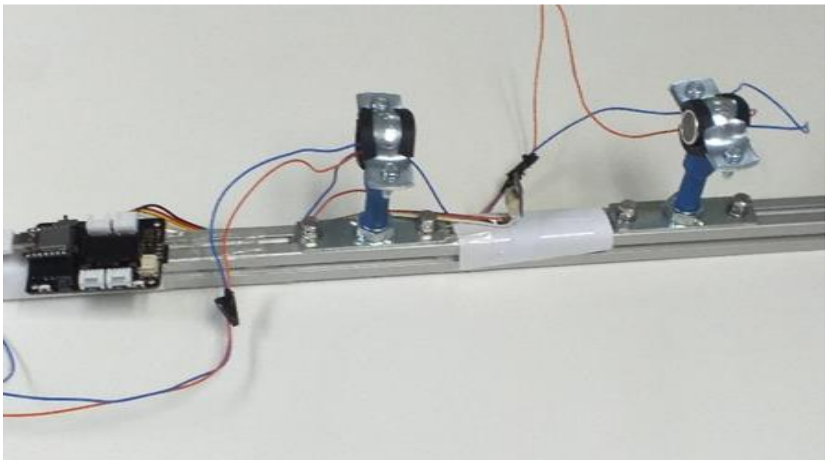

Figure 2.7: Fixture for ultrasonic transducers.

A USB power bank was used as a button to start/ stop the oscillating readings and record data to an SD card. A domestic hair dryer rated at 2 kW was used for temperature step changes, and a cardboard enclosure to house the temperature sensors in a confined space Figure 2.8

Figure 2.8: A domestic hair dryer used for preferred change temperature steps.

Finally, a power supply to provide DC voltage and an INSTRUSTAR ISD205 oscilloscope were used to show waveforms. The temperature measurement setup in operation is shown in (Figure 2.9).

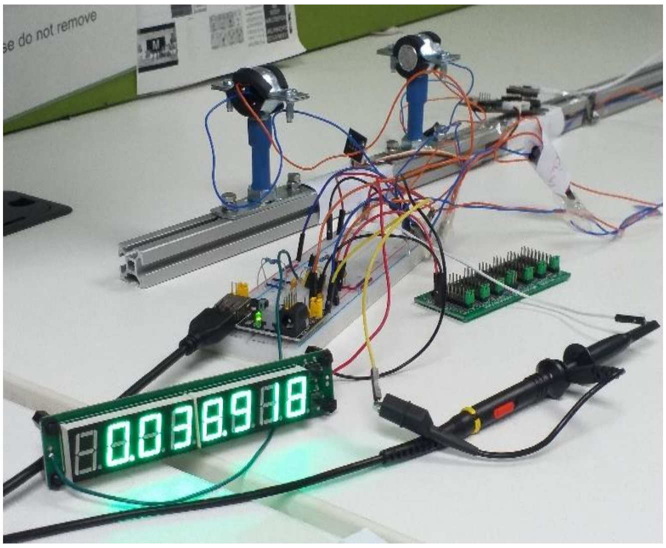

Figure 2.9: The UOTS in operation.

2.6.2. Experimental setup and procedure:

The experimental setup was placed inside a cardboard thermal testing enclosure. It contained the conventional temperature sensors, a UOTS to measure air temperature; an Seeeduino Xiao was used to measure the temperature of conventional sensors. The hairdryer provided step changes in temperature. The air temperature was measured using conventional temperature sensors AHT20 and BMP280 mounted on the same circuit board. The board was connected via an I2C interface to a Seeeduino Xiao [46] with an expansion board and a USB power bank, as illustrated in Figure 2.10.

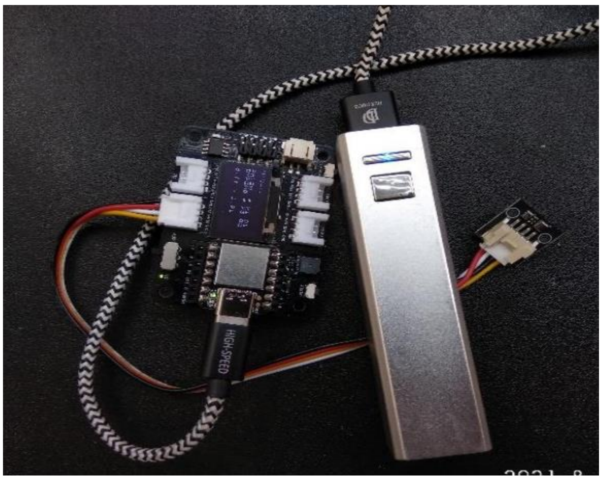

Figure 2.10: Temperature measurement setup with conventional air temperature sensors AHT20 and BMP280.

The steps of the experiment are as follows:

a. A stopwatch was set for 15 minutes.

b. The readings of the conventional temperature sensors started after the power bank was switched on and were recorded to a secure digital (SD) card every second.

c. After 3 minutes, the video recording starts, and a cell phone facing frequency meter to record the displayed UOTS frequency every 1 sec.

d. After 15 seconds passed, the hairdryer switched on for 4 seconds. The first jump was completed, followed by a one-minute wait.

e. The hair dryer was switched on remotely for 6 seconds for a second jump.

f. One minute of waiting after the hairdryer switched off. Then, the video recording turned off.

g. After 10 minutes, the hairdryer switched off. Up to this point, the hairdryer was switched on two times.

h. Data was transferred from the SD card to a personal computer. The transfer of data from the SD card to the personal computer was performed manually. This process involved physically removing the SD card from the device and inserting it into a card reader connected to the computer. The data was then copied from the SD card to the computer's storage through standard file transfer operations

i. Frequency meter recordings were transferred to a personal computer. Used pauses to record changes in the measured frequency.

j. The average bias was calculated, and 1.48 ℃ was subtracted from the sensor's higher readings BMP280.

k. All the data was imported into a spreadsheet, and relevant graphs were plotted.

2.6.3. Experimental results:

The experimental results, collected and processed following the procedures outlined in the previous section, are depicted in Figure 2.11.

Graphs in Figure 2.11 from (C - E) present changes in the readings of both the conventional air temperature sensors and the UOTS (less 38 kHz) for three distinct temperature step change regions.

In each instance, readings increased rapidly until the hairdryer was turned off, after which they returned to pre-step levels quickly for the UOTS but more slowly for the conventional air sensors. On one occasion, the UOTS output frequency included a distinct single-point outlier (Graph E, right). We verified this point multiple times and are confident the value shown on the graph was recorded by the frequency counter. This anomaly could be an error (the only error of the frequency counter) or a rollover of the output frequency of the UOTS as the would-be oscillation frequency crossed over the passband of the closed signal loop.

The experimental results demonstrate that even properly thermally coupled conventional air temperature sensors placed on the same circuit board can record varying values within a range of −0.55 ℃ to +0.85 ℃ when air temperature changes rapidly. When the cause of the temperature step change was removed, it took a considerable time for the readings to return to their pre-step levels. In contrast, the UOTS readings increased sharply with a step change and decreased rapidly when the step change ended (Figure 2.11).

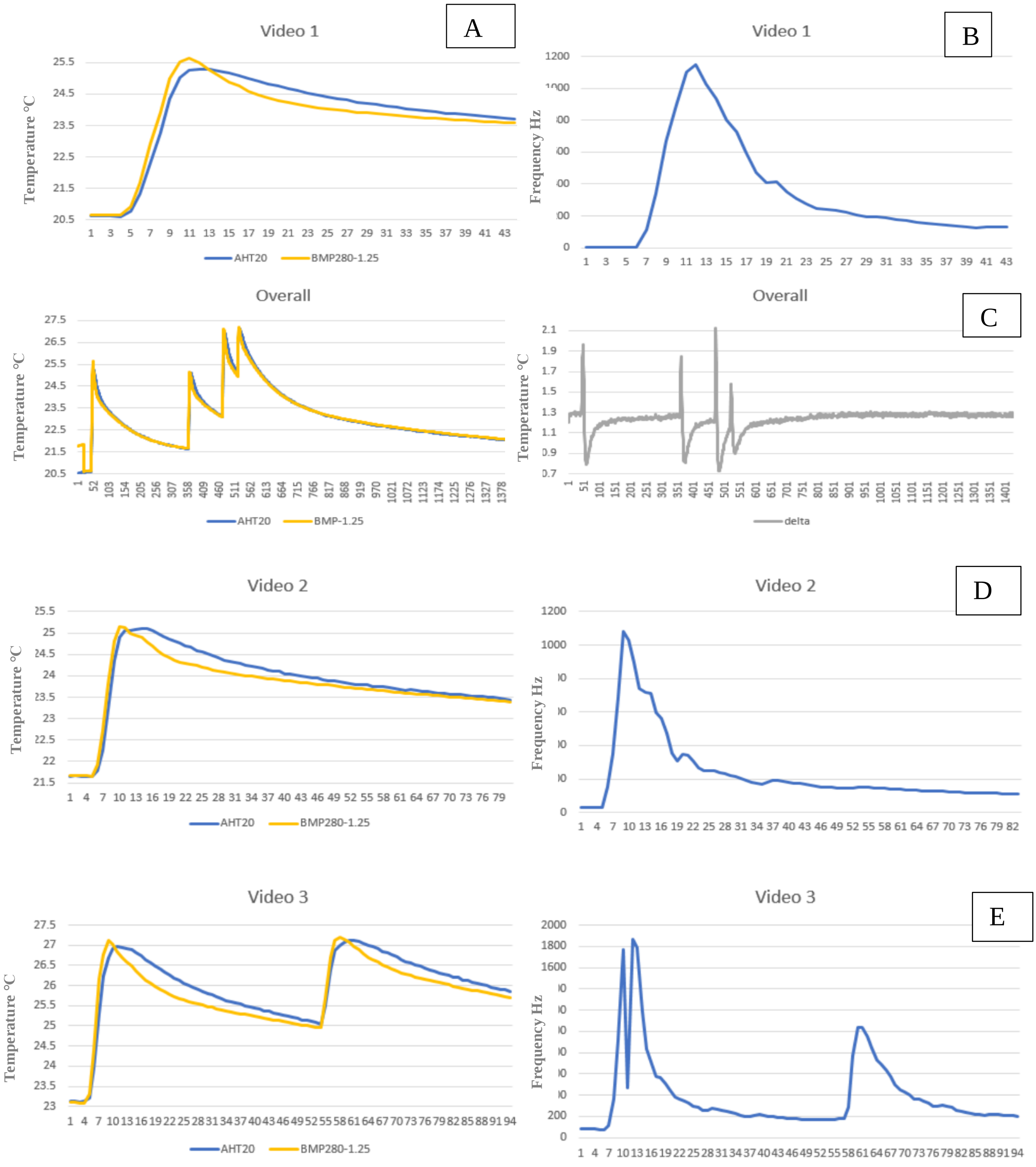

Figure 2.11: Four temperature step changes recorded via the conventional air temperature sensors (A). Difference between readings of the conventional air temperature sensors (B). Sensor readings for each second of the first step change (left: AHT20 and BMP280, in centigrade; right: the UOTS, in Hz) (C). Sensor readings for each second of the second step change (left: AHT20 and BMP280, in centigrade; right: the UOTS, in Hz) (D). Sensor readings for each second of the third and fourth step changes (left: AHT20 and BMP280, in centigrade; right: the UOTS, in Hz) (E)

To clarify how the Ultrasonic Oscillating Temperature Sensor (UOTS) was calibrated, the following detailed procedure was used:

Calibration Equipment: The calibration was conducted using a precision temperature bath or a controlled temperature chamber equipped with a high-accuracy reference thermometer. This ensures that the temperature at the sensor's location is well-defined and stable.

Sensor Placement: The UOTS was positioned within the temperature bath or chamber, ensuring it was exposed to uniform temperature conditions. The sensor's placement was checked to avoid any thermal gradients.

Data Collection: Temperature readings from both the UOTS and the reference thermometer were recorded at each calibration point. Multiple readings were taken at each temperature to account for any variability.

Data Analysis: The collected data were analysed to create a calibration curve or calibration table. This involves plotting the sensor readings against the known reference temperatures and fitting a curve to determine the sensor's response characteristics.

This calibration process ensures that the UOTS provides accurate and reliable temperature measurements by aligning its output with established temperature standards.

2.6.4. Conclusions

The experiment used appropriate equipment and experimental techniques to compare the response times of two conventional air temperature sensors, AHT20 and BMP280, and a prototyped air UOTS. The experiment's qualitative findings suggest that the UOTS can detect fluctuations in ultrasonic velocity across the air pathway, influenced by temperature and humidity, with a significantly faster response time. However, it is not possible to quantify this result accurately using this setup. To achieve this, a frequency meter that can measure the input frequency of the UOTS with high accuracy and at high resolution, recording values multiple times per second, needs to be developed. This can be achieved by utilising a temperature-controlled crystal oscillator to provide the reference frequency and a microcontroller with a capture timer(s). Moreover, creating a measurement network that records temperatures across the complete ultrasonic pathway is needed for calibrating the developed UOTS accurately.

The ultrasonic sensor is subjected to a controlled, stable temperature environment, during which a reference sensor accurately measures the actual temperature, and the ultrasonic sensor records a corresponding reading. The recorded time delay of the ultrasonic waves, which is affected by the temperature-dependent variation in the speed of sound, is captured by the ultrasonic sensor. The data collected through this process is utilized to generate a calibration curve that delineates the relationship between the ultrasonic sensor's output and the reference sensor's measured temperature. This calibration procedure ensures that the ultrasonic temperature sensor is precisely calibrated, thereby enabling reliable temperature measurements in its intended application.

2.7 Continuous rapid accurate measurement of the output frequency of ultrasonic oscillating temperature sensors

2.7.1. Introduction

Ultrasonic oscillating temperature sensors (UOTSes) can sense the aggregate temperatures of an entire room and respond to temperature changes within milliseconds [47]. However, measuring their output frequency requires high accuracy and resolution (down to 0.01%) to realise the potential advantages of UOTSes. Therefore, a robust, inexpensive, and convenient method for widely measuring the output frequency is necessary to adopt these sensors. Different microcontrollers and methods for measuring frequency using built-in timers were evaluated. Direct memory access (DMA) was eventually selected for this purpose.

Frequency control and measurement play a crucial role in various electrical and electronic engineering areas, i.e., electricity networks and telecommunications. The significant advances in the field are associated with the development of crystal oscillators and atomic clocks, which enabled inexpensive but accurate oscillators and ultimate frequency accuracy and stability, respectively. The availability of such oscillators allowed precise synchronisation of generating electrical grids and high throughput communications. Interest in frequency measurement is primarily related to the development of UOTSes as their output frequency changes with the sensed temperature. Frequency measurement involves benchmarking the frequency in question Fx against a reference one Fr. Well-established approaches involve using a gated counter connected to both the clock sources (Figure 2.12). If Fr >> Fx, the Fx source enables the counter. Otherwise, the Enable input is connected to the source of Fr.

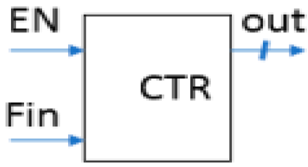

Figure 2.12: Gated counter for measuring frequency.

As these two clocks are generally not synchronised (i.e., derived from two different oscillators), the Fx/Fr (or Fr/Fx) ratio is fractional. The counter produces an integer value, effectively cutting off the fractional part of the ratio. The relative accuracy of frequency measurement can thus be calculated as in equation 2.2

$$\varepsilon \leq \frac{1}{\max\left(\frac{Fr}{Fx}, \frac{Fx}{Fr}\right) + 1} \tag{2.2}$$

Consequently, the higher the ratio between the frequencies, the higher the measurement accuracy

Although various sensors vary their output frequency as the response to the sensed value , interest towards measuring the output sensor's frequency is primarily related to the ultrasonic oscillating temperature sensors (UOTSes) that can operate in various media UOTSes can operate in liquids at the centre frequency of hundreds of kHz but require frequency measurement with an accuracy of a few Hz [48]. Because of such a relatively high frequency of operation, providing the Fr/Fx ratio in the order of 10,000 using an inexpensive reference oscillator is very complicated, if possible. A better solution would be to employ several (rather than one) gating pulses [49] Utilizing multiple gating pulses presents several significant advantages, including improved noise reduction, heightened precision, enhanced reliability, and optimized performance, particularly in complex or dynamic systems. These benefits render it a superior methodology in various technical applications, contributing to more effective system operation and increased accuracy as shown in Figure 2.13 .

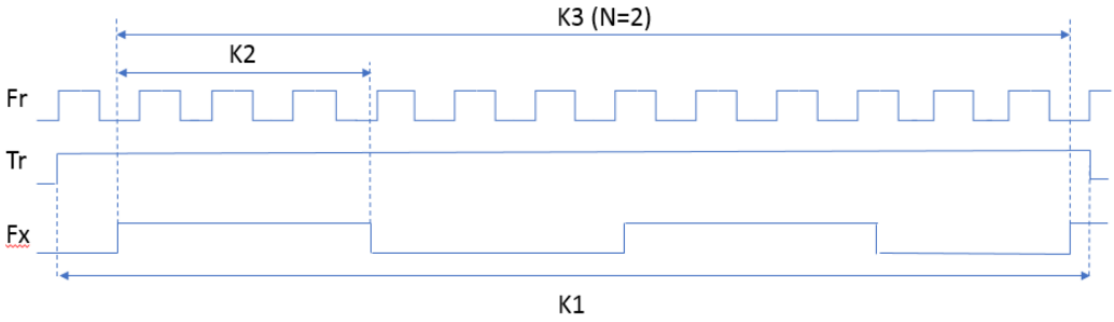

Figure 2.13: Waveforms illustrating various methods for frequency measurement waveforms.

If Fr > Fx (which holds for known UOTSes), the Fx pulses gate the counter that counts K2 Fr pulses. (If Fr pulses are used to define the reference time interval Tr, the interval is used at the Enable input of the counter, which counts K1 pulses of Fx. This mode was frequently employed in frequency meters in the past. By making Tr proportional to 10 s, 1 s, 0.1 s, etc., it became possible, by altering the position of the decimal point, to display the counter value as Fx directly.) If several UOTS pulses are used to gate the counter, the latter ends up with a considerably higher reading K3 (shown for the number of gating pulses N=2 in equation 3.2), which increases the frequency measurement accuracy accordingly:

$$\varepsilon \leq \frac{1}{N * \max\left(\frac{Fr}{Fx}, \frac{Fr}{Fx}\right) + 1} \tag{2.3}$$

This measurement scheme was successfully implemented by using discreet logic [5] and integrated circuits with proprietary architecture (namely, Programmable Systems on Chip PSOC-1 [48]. As tried using conventional microcontrollers (MCUs) in air UOTS design, various ways of using built-in MCU timers to measure the output frequency were compared. An STM32G474 MCU was used in our experiments because of our familiarity with this series, but the results apply to other (MCUs).

2.7.2. Different methods for frequency measurement using MCUs' built-in timers.

An MCU timer can be used for frequency measurement directly in its Capture mode, which operates similarly to the gated counter. Fr, usually generated internally, is supplied to the timer's clock input, and Fx, acting as the gating signal, is supplied to the Capture pin. The timer counts the clock pulses between the two consecutive edges of Fx. It then typically generates an interrupt that allows the central processing unit (CPU) to process the captured count. Unfortunately, typical MCU timers cannot keep counting for a few periods of Fx on their own.

Most MCUs feature multiple timers that can be combined a presents two timers that start counting Fx and Fr pulses simultaneously. When TMR1 has counted to the chosen value of Fx pulses N, it generates an interrupt, and MCU reads the accumulated value from TMR2. As responding to interrupt and reading TMR2 takes some CPU cycles, the read value might become inaccurate. Additionally, resetting the timers cannot be done synchronously, increasing measurement errors.

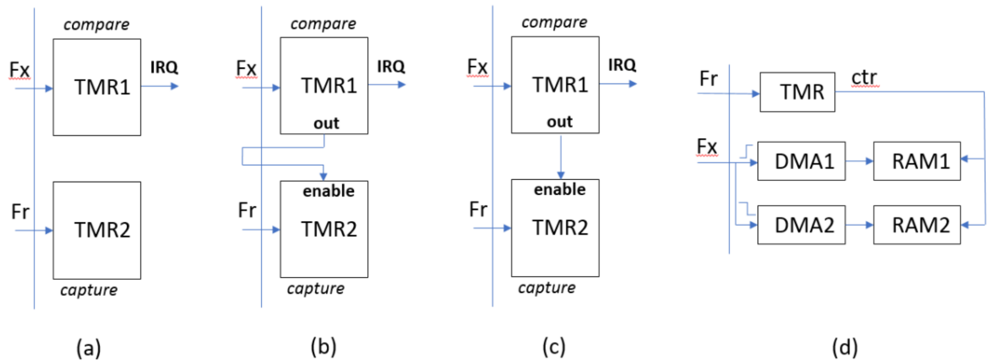

Figure 2.14: Measuring frequency using built-in timers (a – unlinked timers, b – externally linked timers, c – internally connected timers, timer in the DMA mode

Better accuracy can be achieved when the output of Fx-connected timer gates another timer for external connection, suitable for most MCU timers, and for timers with internal synchronisation, available for STM32 MCUs [61]. This way, the TMR2 stops counting after the set number of Fx pulses; thus, the MCU reads the accurate value. Unfortunately, the timers' tandem cannot operate for the following period of Fx because it takes MCU some time to read and store the count. For this reason, it is impossible to get a continuous stream of the counted values, which is desirable for UOTS measurements.

The CPU involvement can be avoided completely if the timer transfers counted values to the MCU memory using direct memory access (DMA) mode d). In our development, we followed a video walkthrough tutorial and relevant code to implement this mode of operation. Both rising and falling edges of Fx trigger the DMA transfers, and the CPU is notified by an interrupt when the Fr count for each half-period of Fx is captured and transferred to the MCU memory [50].

To verify the accuracy and convenience of this measurement arrangement, we used one STM32 timer (TMR2 in PWM mode) that generated 40 kHz Fx pulses from two primary oscillators –

high-speed internal (HSI, RC-oscillator with accuracy and stability in the order of ±1%) and high-speed external (HSE). The HSE oscillator was connected to the 24 MHz crystal available on the STM32 Nucleo-G474RE board, and its accuracy and stability were determined by the crystal, typically in the order of ±50 ppm. TMR3 was configured to operate in the DMA mode, counting the Fr pulses from the Vectron C4550A1 oven-controlled oscillator (OCXO) with the stability of ±50 ppb [51], as shown in Figure 2.15.

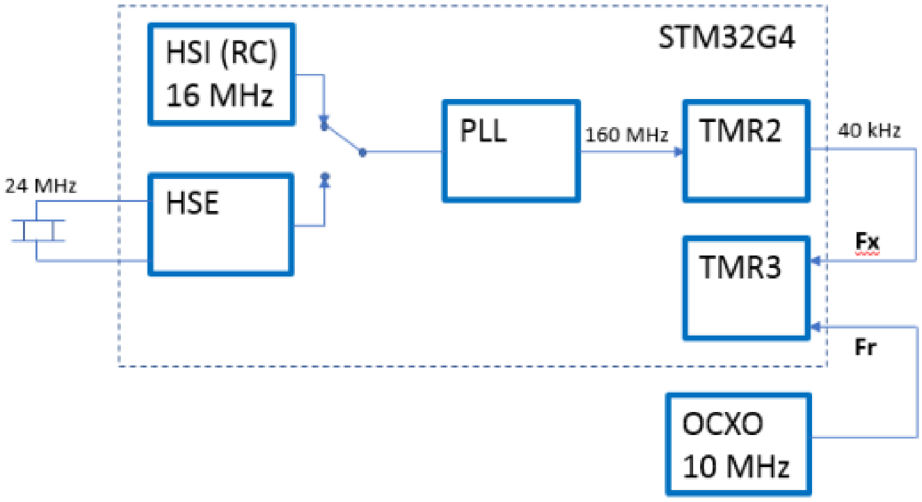

Figure 2.15: Frequency measurement verification setup.

The interrupt service routine counted the interrupts and flagged up when the data for a chosen number of Fx pulses N were fully collected in the memory buffer. The individual half-period counts were then averaged. A 100 ms delay was inserted before starting the following measurement.

2.7.3. Experimental results

Fig.3.14 presents measurement results for both primary oscillators.

Figure 2.16: Measured ratios Fr/Fx for 40 periods of Fx (100 ms delay between measurements)

As expected, Fx pulses derived from the HSI oscillator varied significantly compared to those derived from the HSE oscillator. The graph of the HSI estimates resembles some noisy process. In contrast, only three values were captured for the Fx pulses, derived from the HSE oscillator, confirming its much higher stability. The graphical representation shows that HSI-derived pulses appear noisy, while HSE-derived pulses are more consistent. Furthermore, the acquired time series and recorded data were processed to calculate statistical parameters like mean and variance, which are presented in Table 3.1. This table provides detailed statistical data confirming the observations about the stability and noise in the signals from the 24 MHz crystal oscillator and the 16 MHz RC oscillator.

Processing of the acquired time series resulted in the numerical estimates of their statistical Parameters. in Table 2.1 The data in the table clearly show that the 4000-period setting, presumably derived from the HSE oscillator, offers the highest stability with the least variability, as evidenced by the very low standard deviation and Std σ / Mean ratio. The HSI oscillator, with the 40-period setting, is the least stable, exhibiting a high standard deviation and a much higher ppm value, indicating significant noise in the signal. The Crystal 24MHz clock source at 40 Hz offers intermediate stability.

Table 2.1: Statistical parameters of the acquired time series

MCU clock source	Period acquired	Mean (average) Hz	Std σ Hz	Min (Hz)	Max(Hz)	Std σ /mean ppm
RC 16 MHz	40	249.8953	0.072212	249.5789	250.2105	1700
Crystal 24MHz	40	250.0058	0.009815	250	250.0263	236
	4000	250.0060	0.000080	250.0056	250.0063	2

It can be seen that the standard deviation for the HSE-derived pulses, despite being much smaller than that of the HSI-derived pulses, does not correspond well to the specified stability of the crystal oscillators. This was due to the insufficient averages, and the experiment was repeated with 4,000 averages instead of 40. The results confirmed that the moderate number of standards could be inadequate when evaluating the scatter of high-quality frequency sources. The HSI oscillator produces more variable and noisy signals compared to the HSE oscillator, which generates more stable and consistent outputs, as confirmed by both graphical analysis and statistical estimates

It can be seen that the standard deviation for the HSE-derived pulses, although much smaller than that of the HSI-derived pulses, does not align well with the specified stability of the crystal oscillators. This discrepancy was attributed to the initial use of insufficient averages. The experiment was therefore repeated with 4,000 averages instead of 40. The results confirmed that using a moderate number of standards might be inadequate when assessing the scatter of high-quality frequency sources. Specifically, the standards in question—likely calibration standards or reference oscillators—were insufficient in number or scope to capture the full range of variability in high-quality frequency sources. This inadequacy could be due to their limited precision, lack of coverage across the frequency range, or insufficient calibration accuracy. The time series data acquired from this revised experiment is presented in Figure 2.18.

The acquired time series is presented in Fig2.18 and features distinct values.

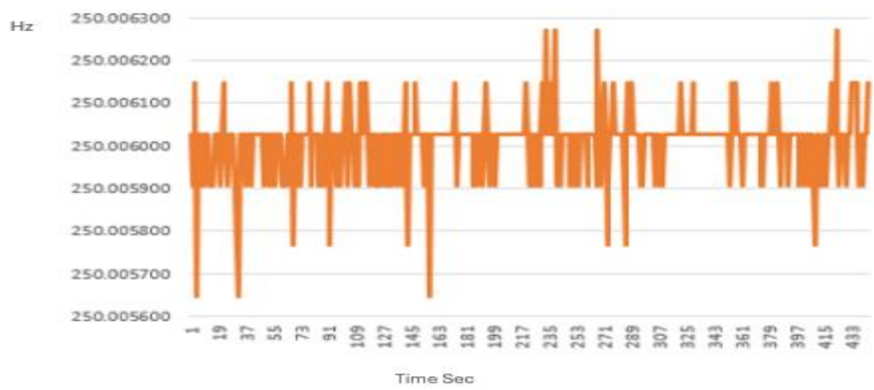

Figure 2.17: Measured ratios Fr/Fx for 4000 periods of Fx, derived from the 24 MHz crystal oscillator (100 ms delay between consecutive measurements).

2.7.3 Further enhancements to the procedure

In order to enhance the DMA frequency measurement process for measuring the UOTS output frequency, the following modification was used: the DMA started asynchronously with the UOTS output pulses at the notional frequency of 40 kHz, and the first reading needed to be discarded. This resulted in a negligible error for the more significant number of periods used (4,000 periods in the first experiment), but it was noticeable for the smaller number (250 periods in Experiment 2). For the 4,000-period measurement, the measurement time was around 0.1 s (4,000/40,000 Hz). The number of the counted 10 MHz clock pulses was approximately 1,000,000 (0.1 s * 10,000,000 Hz), resulting in a counting error of up to one pulse out of 1,000,000 or roughly 0.04 Hz frequency measurement error (40 kHz / 1,000,000). After each measurement, there was a 0.1-second delay before the next measurement began. For the 250-period measurement, each measurement was completed in 6.25 milliseconds (250/40 kHz). As the clock frequency was set to 160 MHz this time, the counting accuracy of frequency measurement was roughly the same as before, 0.04 Hz (40kHz/(6.25 ms*160 MHz)). The same 0.1-second delay was applied after each measurement.

2.7.4. Conclusions

Various frequency measurement methods using timer peripherals of modern MCUs to continuously and accurately measure the output frequency of UOTSes were compared. The required accuracy can be achieved by counting the reference pulses during several periods of the frequency source in question (40 periods were enough for a low-stability oscillator, but 4000 were required to assess a high-stability one). This operation is not achievable using a conventional

MCU timer’s Capture mode, though, even when using two timers, a continuous stream of frequency estimates is difficult to accomplish because the CPU needs to read the captured values that should be frozen during this time and the timers are challenging to restart at the very same time. Averaging was not the sole processing task undertaken. The CPU not only averaged the captured data for the required pulses but also communicated the results in a dependent manner. The communicated results indicate that the CPU likely performed additional processing steps either before or after the averaging process. These steps may have included data filtering, conditioning, error checking, or formatting the averaged data prior to communication. Moreover, given the use of two distinct oscillators—one low-stability RC and one high-stability crystal—for verification, it is plausible that calibration, compensation, or adjustment procedures were implemented to address differences in oscillator stability. Consequently, the processing extended beyond mere averaging

These inconveniences can be mitigated by employing a timer in the DMA mode when the captured values are stored in the MCU’s memory without any CPU intervention. The employed STM32G474 MCU could capture values at every edge of the incoming pulses, enabling measurement for every half period of these. The CPU averaged the captured data for the required pulses and communicated the result dependently. The design was verified using two separate oscillators: a low-stability RC one and a high-stability crystal oscillator. The obtained results were as expected. As the reference pulses are captured for every half-period of the input frequency, it becomes possible to provide a continuous stream of moving average estimates of the output frequency of UOTSes. Achieving the required accuracy with a conventional crystal oscillator connected to an MCU’s external high-speed oscillator seems feasible. As the derived timer’s clock frequency can be in the order of 100 MHz, the acceptable number of input signal periods should be in the order of ten. Therefore, a conventional MCU with external crystal seems sufficient to enable continuous accurate moving average measurement of the output frequency of UOTSes.

The complete experimental setup is presented in Figure 2.18.

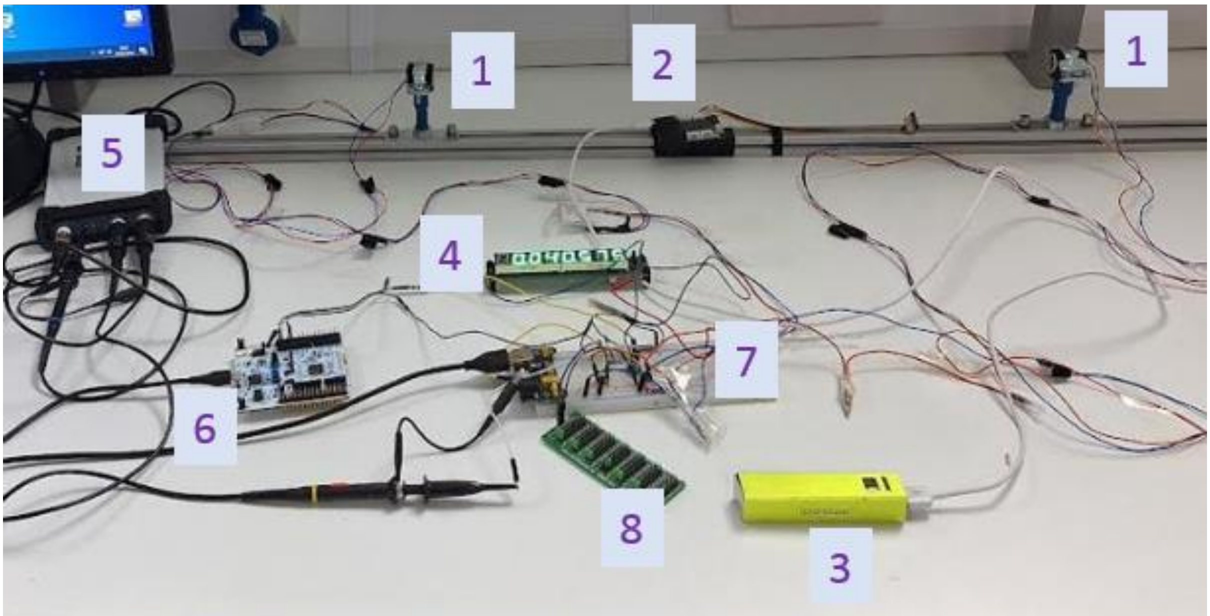

Figure 2.18: The complete experimental setup (1 – ultrasonic transducers, 2 – Seeedstudio Xiao board with the temperature sensor attached, 3 – power bank for the Xiao board, 4 – frequency meter, 5 – Instrustar oscilloscope, 6 – STM32G474 board, 7 – driver assembled on a breadboard, 8 – decade resistor for setting up the driver's gain)

Chapter 3 : Instrumentation and procedures for logging temperature reported by conventional sensors

This chapter will describe our experimental results to determine why the readings of different temperature sensors might vary notably in air despite being placed nearby.

3.1 Thermal measurement using conventional temperature sensors.

3.1.1 Introduction

Although achieving absolute accuracy can be challenging, obtaining consistent relative measurements by placing sensors inside a standard enclosure with limited air volume is possible. In such circumstances, the readings from different sensors can be much closer than anticipated based on the manufacturers' specifications. Any biases among sensors can be eliminated during subsequent processing. For example, in one experiment, the (Pt100 RTD) and the DS18B20 integrated circuit sensor were used. The former was chosen for its widespread use in the industry, and the latter for its networking capabilities and our positive past experiences [2]. In another experiment, two I2C combinational sensors (BMP280 and AHT20) were attached to an unbranded board with good thermal contact.

3.2 Simultaneous temperature measurement using Pt100 and DS18B20 air-gapped sensors.

3.2.1 Experimental setup and procedure:

The sensors were positioned inside a small A cardboard thermal testing and covered with air bubble packaging. The cardboard thermal testing was kept on the ground floor, away from windows and direct sunlight. Despite measures taken to ensure that the sensors responded to the same air temperature, including moving them closer to each other and adding layers of cover, there was a notable bias of up to 0.5°C and a scatter of up to ±0.2°C observed for more than three months. The recorded readings and computed changes collected approximately every 18 seconds over about three months sampling interval is selected to balance the need for detailed data collection, error minimization, and consistency with previous experiments despite the gradual environmental changes. Collecting data at this interval results in a more comprehensive dataset, which is beneficial for identifying trends or patterns. Furthermore, maintaining this interval ensures that any environmental changes can be directly compared to previous results, thereby preserving consistency and comparability, are shown in

Figure 3.1 The sensor values would be slightly skewed but generally follow each other, The observed bias of up to 0.5°C can be attributed to several factors, including thermal interactions between the sensors, insufficient ventilation within the test chamber, and the insulating properties of the cardboard thermal testing. Proximity between the sensors may lead to mutual radiative and conductive heat exchange, thereby influencing each sensor's readings. Furthermore, the addition of cover layers can trap heat, resulting in temperature gradients within the chamber, which further exacerbate the observed bias. The scatter, measured at up to ±0.2°C, is likely due to minor fluctuations in ambient conditions, slight variations in sensor placement, and inherent sensor noise. Over extended periods, these small variations can accumulate, contributing to the observed scatter. The persistence of bias and scatter over a period exceeding three months is likely related to the long-term stability testing of the sensors. Prolonged observation periods are essential for assessing the consistency and reliability of sensor data, ensuring the sensors maintain their accuracy under varying conditions, including potential environmental changes or sensor drift. Testing over a period of three months allows for the detection of any long-term trends or potential degradation in sensor performance.

as in previous trials using DS18B20 sensors in water [38]. However, the results were concerning, given the resulting scatter. It was within the DS18B20 standards, but it was not possible to isolate a single value of constant bias for the recorded dataset.

Regarding the recorded readings and computed changes collected every 18 seconds, I elaborated on the sampling interval choice. While the environment may vary slowly, the 18-second interval was selected to capture any subtle changes in the ultrasonic sensor's response. This frequent sampling allows for more precise detection of gradual shifts in temperature or environmental conditions, ensuring the data remains accurate over time. The relatively short sampling interval provides a buffer to account for any unanticipated fluctuations in the environment that might otherwise be missed with less frequent measurements.

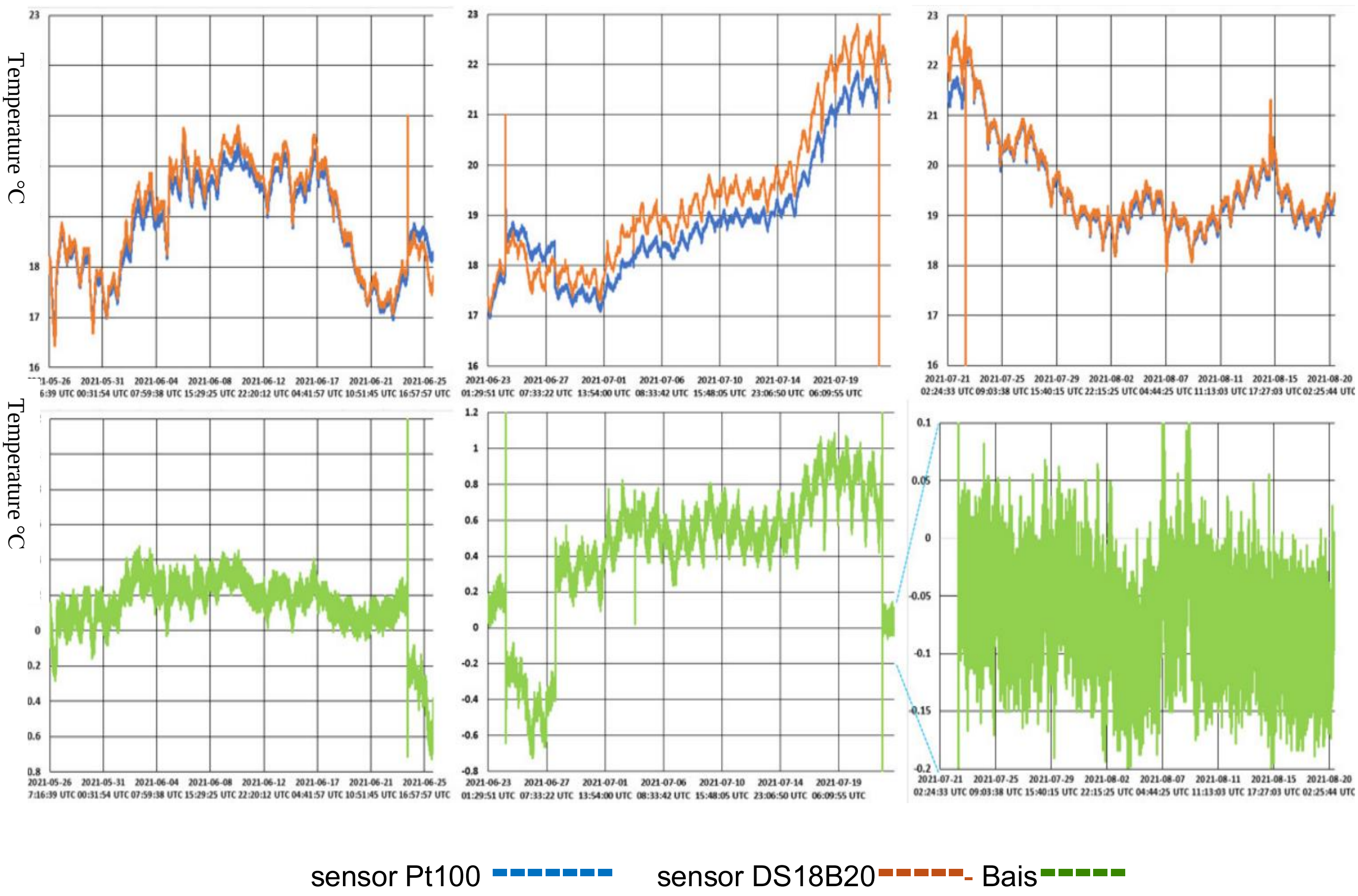

Figure 3.1: Temperature readings of Pt100 and DS18B20 sensors over three months.

On July 22, 2021, both sensors were placed in a plastic bag, and subsequent readings revealed excellent agreement, with an average bias of just 0.05°C and most of the dispersion falling within the range of ±0.08°C. The last part of the experiment was encouraging, as it indicated that the DS18B20 sensors could provide reasonably accurate readings of near-constant air temperatures.

3.3 Simultaneous air temperature measurement using AHT20 and BMP280 sensors mounted on the same board.

3.3.1 Introduction

This experiment was set to record the response to air temperature step changes and compare the results reported by the conventional AHT20 and BMP280 air temperature sensors. In this experiment, the air movement on the sensors and temperature readings from both sensors were monitored.

3.3.2 Experimental setup and procedure:

To conduct the experiment, the sensor board was paired with the Seeeduino Xiao, an Arduino-compatible microcontroller module [44], and connected to an expansion board with an OLED display, real-time clock, and SD card. The setup was placed on a computer table and monitored until approximately 22:00, after which the room was left unoccupied until the following morning. The setup's operation remained unchanged during this time. For the second setup, the sensor board was placed inside a plastic tube and covered with air bubble packaging material, and the room was also left unoccupied. Figure 3.2 displays the recorded readings, the calculated difference, and relevant photographs.

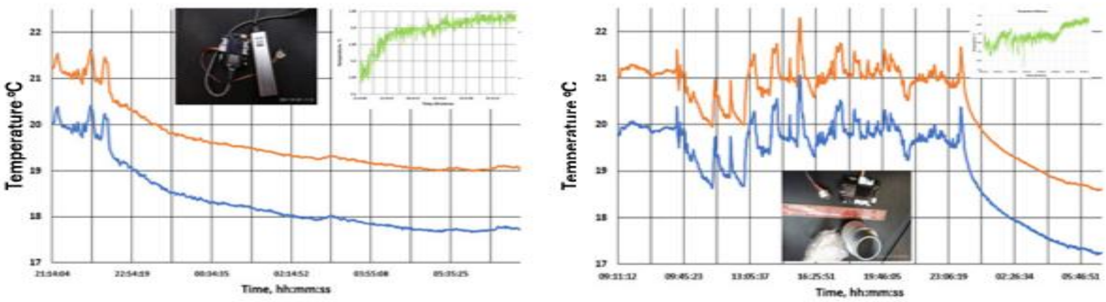

Sensor AHT20 ------- Sensor BMP280----- Bais-----

Figure 3.2: Recorded temperatures for the sensor board placed on a computer table on two occasions

The findings indicate that one of the sensors consistently produced higher readings, with a varying bias of around 1.25°C. When a person was nearby and working on a computer, spontaneous fluctuations of up to 1°C were detected, which were not observed at night when changes were within 0.1°C. Placing the sensor board in a plastic container further reduced these differences.

During the second experiment, the board was placed on a table where it would occasionally be exposed to sunlight filtering through the backyard shrubbery. When the sun's rays were present, they quickly heated the board, causing the bias to drop to 0.7°C, as illustrated in Figure 3.3. The other sensors' readings lagged due to this drop, as the sensor with lower values responded more rapidly.

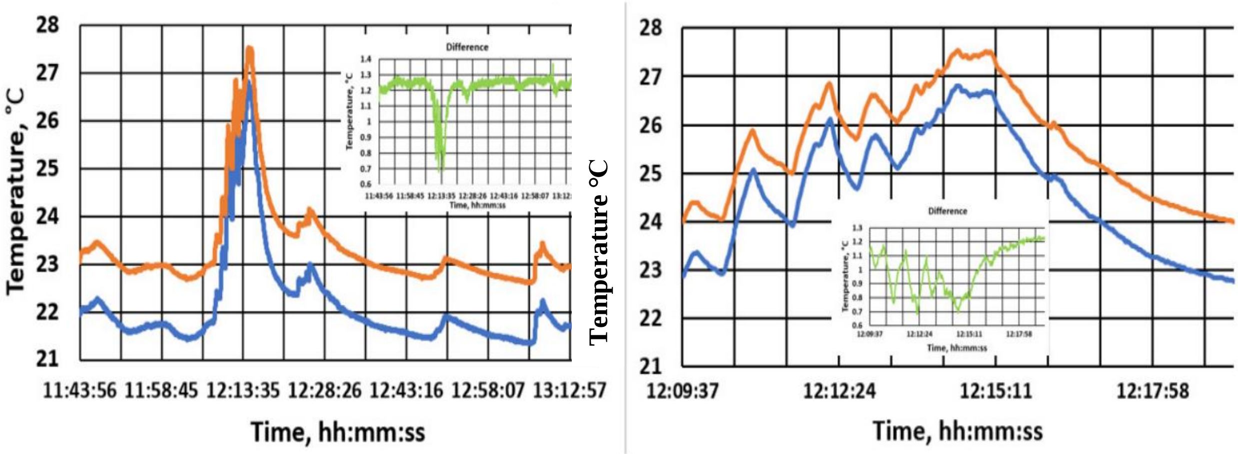

Sensor AHT20 ------- Sensor BMP280------ Bais-----

Figure 3.3: Temperatures recorded by the sensor board on a windowsill.

In the final experiment, the setup was situated inside a lengthy cardboard box with severely restricted airflow. In this environment, the readings of both sensors remained almost constant, fluctuating only within a range of ±0.1°Cover 80 minutes and consistently tracking each other. The calculated bias was highly stable, with a scatter of approximately ±0.02°C, as shown in

Sensor AHT20 ------- Sensor BMP280------ Bais-----

Figure 3.4.

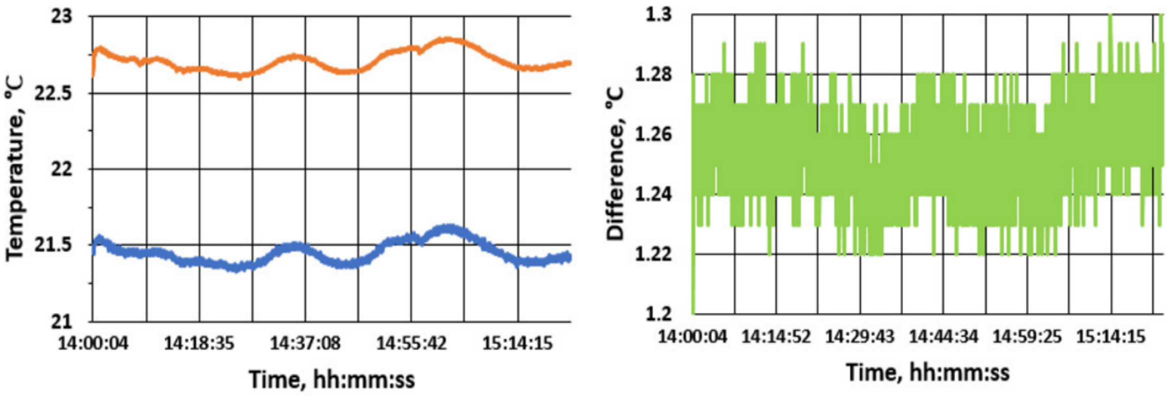

Sensor AHT20 ------- Sensor BMP280------ Bais-----

Figure 3.4: Temperatures recorded by the sensor board placed inside a long cardboard box.

When exposed to stable temperatures and no air movement, the sensors can produce readings very close to each other.

The experimental setup for collecting the temperature readings is presented in Figure 3.5.

Figure 3.5: Conventional temperature sensors AHT20, BMP280 and SD card adapter.

3.3.3 Conclusions

The findings of this experiment suggest that under stable temperature conditions with minimal air movement, temperature sensors can provide highly consistent and accurate readings. The close tracking between sensors and the minimal bias observed indicates that the sensors are well-calibrated and capable of providing reliable measurements in stable environments. The bias between the two sensors was calculated by comparing their readings directly, involving the subtraction of one sensor’s readings from the others to determine the bias at each time point. By processing the data in this manner, the experiment provided a comprehensive assessment of the sensors’ performance and reliability in a controlled environment. Overall, the experiment demonstrated that the sensors are capable of producing closely aligned readings when environmental conditions are controlled.

While achieving absolute accuracy may be challenging, relative measures can be relatively consistent if the sensors are enclosed in a limited air volume. The readings from different sensors may be closer than the manufacturers' specifications suggest, and any biases among sensors can be eliminated through processing. However, even closely placed sensors can produce significantly different readings if there are air movements. Quick temperature changes can result in substantial differences in sensor readings due to variations in response times.

Chapter 4 : Experimentation at a small distance between the transducers (150 mm)

This chapter presents an experimental record of conventional temperature sensors and UOTS when used inside an enclosure and an open-plan office over an extended period.

4.1 Experiments arrangement for 150 mm distance

In this chapter, two experiments were conducted at a 150 mm distance between the transducers. The distance was selected as a carefully considered compromise, effectively balancing signal integrity, practical feasibility, relevance to application scenarios, and the capabilities of the experimental setup. The first experiment was conducted at the frequency measurement interval of 0.1 s, and the second experiment was conducted at the interval of 6.25 ms. With every interval, three distinct sets of arrangement were applied. The arrangements for the total experiments performed in this Chapter are demonstrated in Figure 4.1.

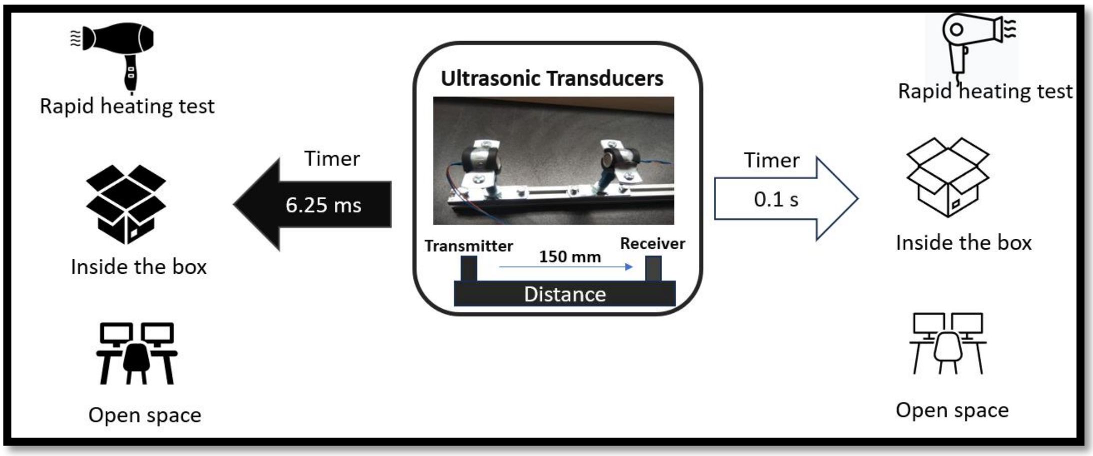

Figure 4.1: Schematic diagram for study arrangements conducted in this study.

The initial set involved a rapid heating test, where a hairdryer was employed to elevate the temperature inside the enclosure quickly. This allowed recording readings from the conventional temperature sensor and the UOTS, as previously explained in section 3.6.2. Once the hairdryer was switched on, some time was given for the heater and fan to reach maximum power before being directed into the enclosure.

The second and third sets present measurements taken over prolonged periods, typically overnight, in an open office environment. The heating was activated for roughly 5.5 hours in the afternoon, well after the start of the recording.

In the second set, the sensors were positioned inside the enclosure to minimize the impact of air circulation on the UOTS readings. It should be noted that enclosing the UOTS sensors also aided in reducing the scattering of their readings.

For the third set, the sensors were placed in an open space, as this arrangement is to be used for UOTS applications.

4.2 Experimental results for measuring the UOTS's output frequency for 0.1 s

4.2.1 Rapid heating test for 0.1 s

Upon initiating the recording of both temperature and UOTS output frequency, the hairdryer was removed from the enclosure, directed away from it, and switched on for some time to allow its heating element to reach the operating temperature. Subsequently, the hairdryer was directed inside the enclosure for a short while. The enclosure flap was closed to minimize air exchange with the environment. This sequence was repeated five times. Figure 4.2a shows these differences and how UOTS are showing a fast return to a lower temperature whilst it takes considerably longer for the conventional sensors to display the reduction in the temperature. Figure 4.2b demonstrated the second peak closely, and the UOTS took (74-73.25)*60=45 seconds to return to slightly above baseline, whilst the conventional sensor took around (77.5-73.25)*60=255 seconds to return to the same temperature.

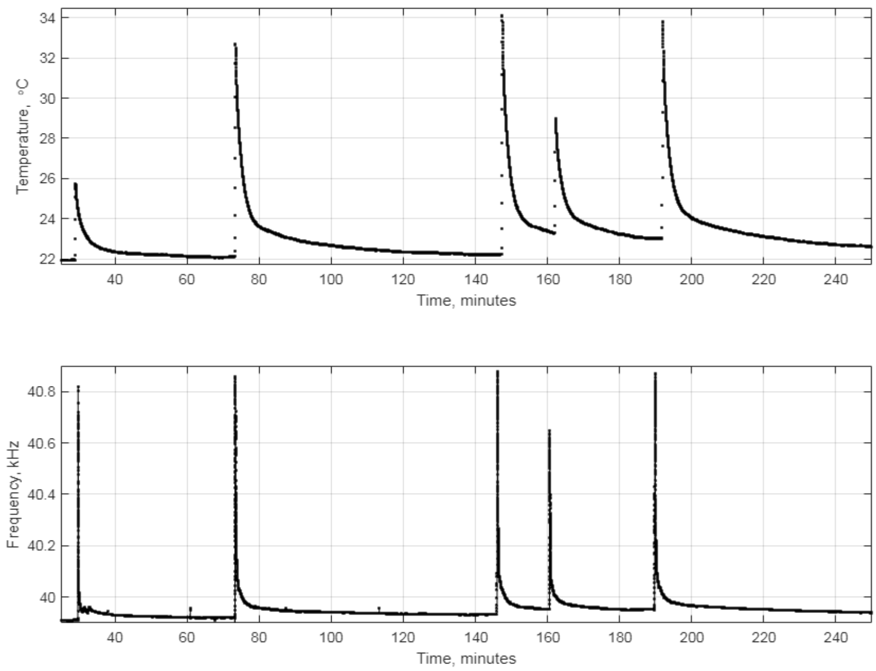

(a)

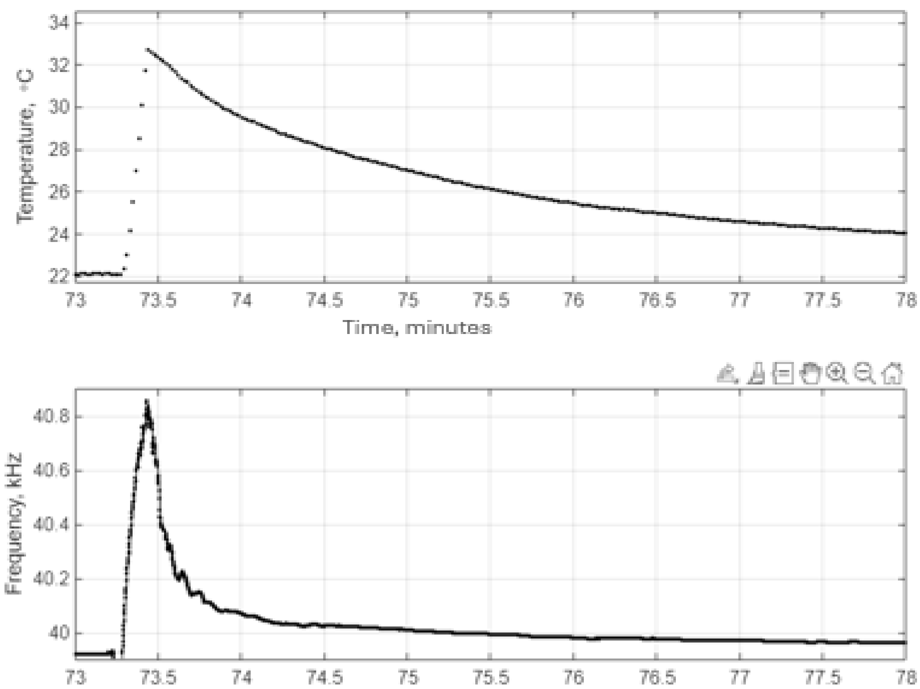

(b)

Figure 4.2: Experimental records for the rapid heating test (0.1 s measurement time) (a) Five subsequent heating cycles. (b) A section of the complete recording (second heating instance) is viewed at a closer scale.

4.2.2 Monitoring temperature inside the enclosure for 0.1 s frequency measurement interval.

Figure 4.3 Figure 4.3 shows a complete record of the temperature and UOTS frequency recorded inside the cardboard thermal testing enclosure. over a 22-hour period. The data collected from the conventional temperature sensor and the UOTS showed a strong agreement. During the period where the readings remained relatively constant over a certain period, it was noted that a variation of about 0.05°C corresponded to an approximately 2 Hz change in the UOTS's output frequency.

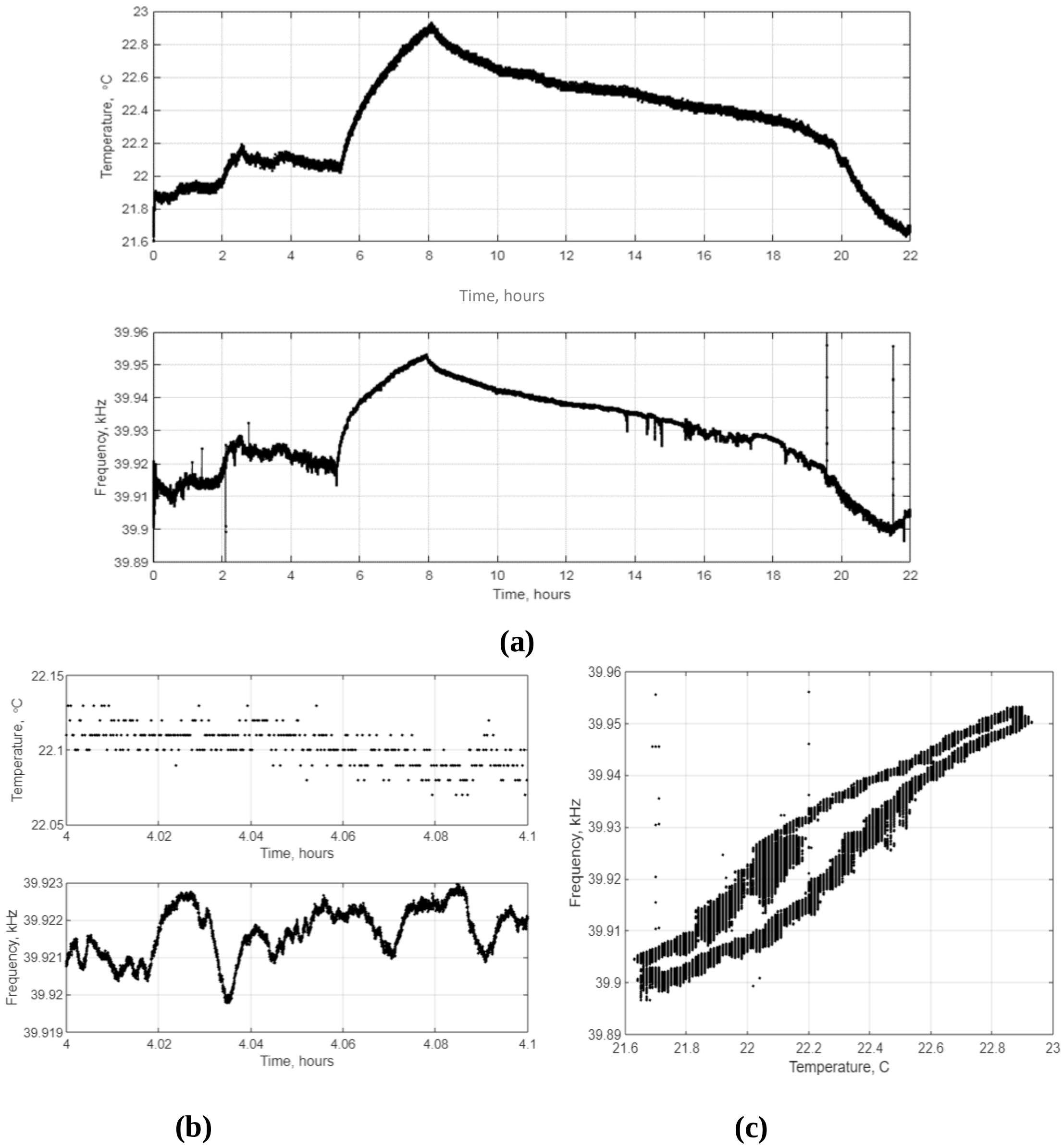

Figure 4.3: Records obtained from an experiment monitoring the air temperature overnight inside a container (0.1 s measurement time). (a) Overall recordings. (b) A section of the complete recording is viewed at a closer scale. (c) Temperature–frequency relationship showing hysteresis.

The relationship between frequency and temperature exhibited an estimated slope of 40 Hz per degree Celsius and calculated as follows:

$$Gradient\ (slope) = = \frac{\Delta\, dy}{\Delta\, dx} = \frac{change\ in\ frequncey(Hz)}{change\ in\ Temperature(°C)} \qquad (4.1)$$

Temperature difference $\Delta\mathcal{T} = 22.108(°C) - 22.053(°C) = 0.05°C$

Frequency difference $\Delta\mathcal{F} = 39.9228(Hz) - 39.9208(Hz) = .002 * 1000 = 2Hz$

Gradient=$\frac{\Delta\mathcal{F}}{\Delta\mathcal{T}} = 2(Hz)/0.05(°C) \ = 40Hz/°C$

The scatter plot reveals some hysteresis in the frequency of the UOTS, as evidenced by different frequency values at the same temperature.

4.2.3 Monitoring the temperature of the open space for 0.1 s frequency measurement interval

When taking readings outside the enclosure, it was observed that there was a significantly higher degree of variation in the readings of both sensors (Figure 4.4). The unconventional UOTS sensor was particularly sensitive to air movement, contributing to the increased variability. Nevertheless, the temperature graphs plotted for both sensors maintained a similar pattern.

The UOTS sensor demonstrated reduced fluctuations during distinct temperature trends. However, the correlation between frequency and temperature revealed a few irregular clusters without noticeable hysteresis. The gradient is calculated as follows:

Calculated using equation (4.1)

Temperature difference ΔT=22.04(°C)-21.88(°C) =0.15°C

Frequency difference ΔF =39.9915(Hz) -39.8923(Hz)= 0.023*1000=23(Hz)

Gradient=ΔF/ΔT=23(Hz)/0.15(°C) = 153 Hz/°C

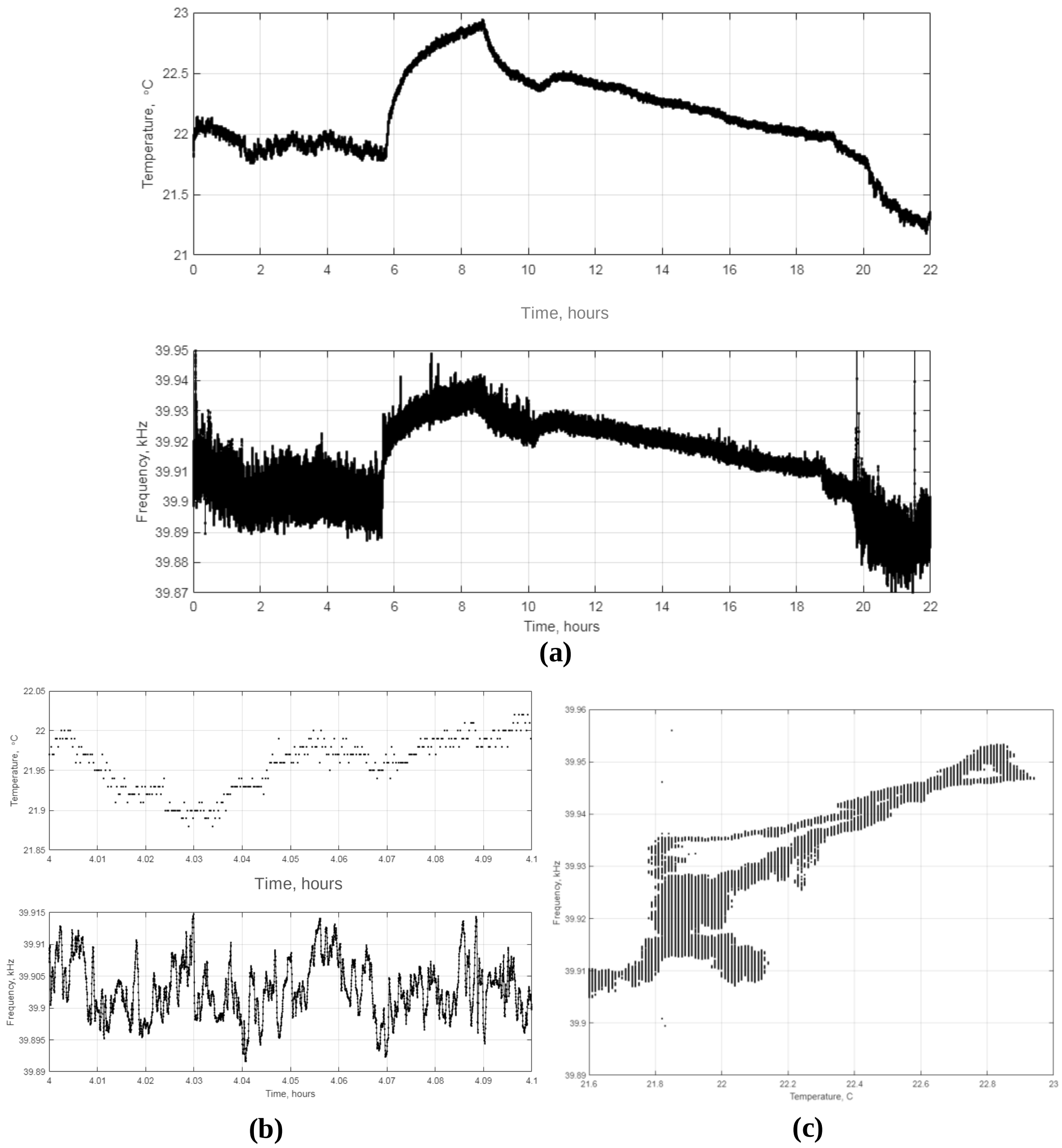

Figure 4.4: Records obtained from an experiment monitoring the air temperature overnight in an open-plan office setting (0.1 s measurement time). (a) Overall recordings. (b) A section of the complete recording is viewed at a closer scale. (c) Temperature – UOTS frequency relationship exhibiting a few irregular clusters.

Inside the Enclosure: The UOTS sensor exhibits a predictable relationship between temperature and frequency, though some hysteresis is evident. This hysteresis suggests potential limitations in the sensor's response, which may be attributable to its design or material properties.

Outside the Enclosure: The UOTS sensor's frequency readings display increased variability due to external factors. Nevertheless, the sensor maintains a general trend that correlates with temperature. The lack of noticeable hysteresis in this environment implies that the sensor's performance is less affected by the temperature history.

4.3 Measuring the UOTS's output frequency for 6.25 ms

4.3.1 Rapid heating test for 6.25 ms

In this experiment, the hot air was injected into the container regularly, by altering the direction of the hairdryer. In the graphs displayed in Figure 4.5, UOTS showed rapid responsiveness again, reaching its peak and returning to the baseline much faster. The peaks in both graphs are shown in Figure 4.5c, and their extent depends upon the hairdryer operation's duration in seconds. In Figure 4.5, conventional temperature sensors have a response time of 129 seconds, calculated as (8.35 - 6.20) * 60 = 129 seconds. In contrast, ultrasonic temperature sensors demonstrate a much faster response time of 18 seconds, calculated as (8.35 - 6.20) * 60 = 18 seconds.

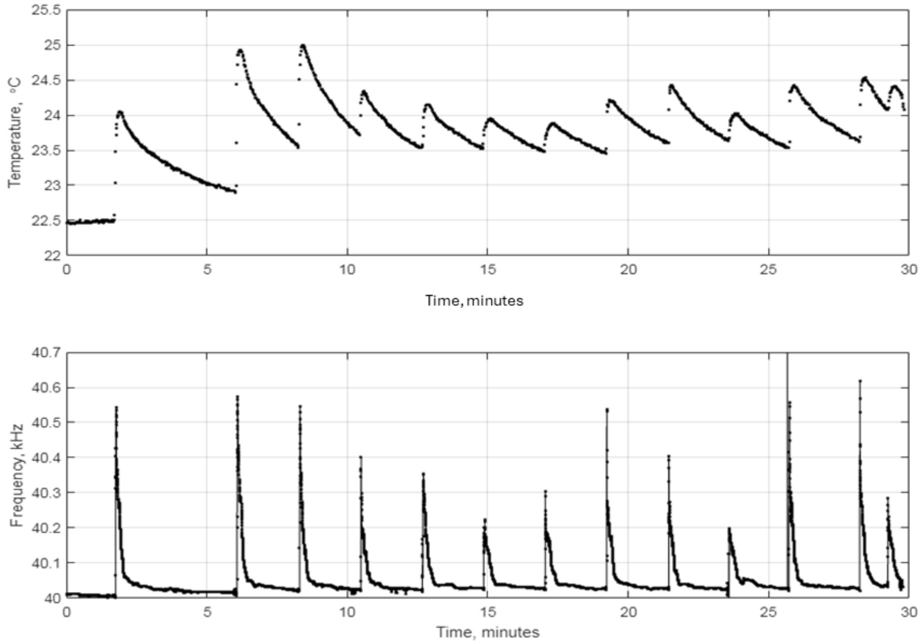

(a)

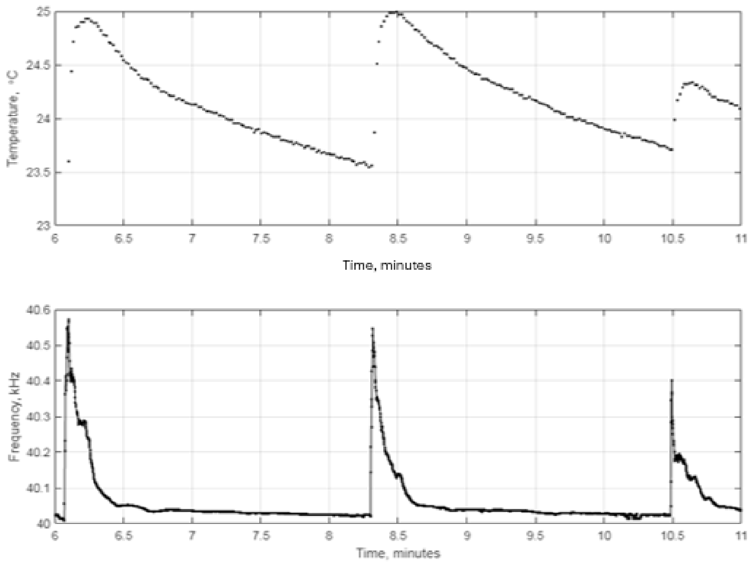

(b)

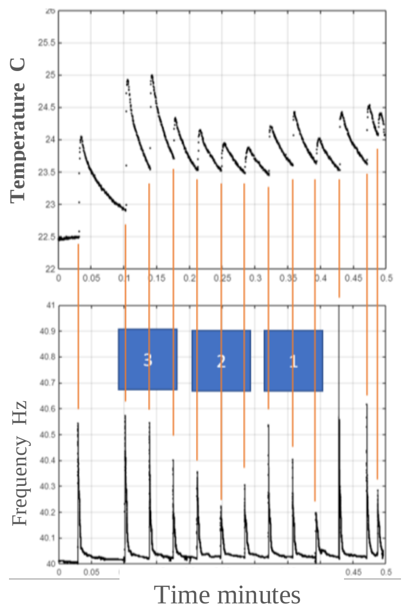

(c)

Figure 4.5: Experimental records for the rapid heating test (6.25 ms measurement time). (a) Overall recordings. (b) A section of the complete recording (from the second to the fourth heating instance) is viewed at a closer scale. (c) Concurrent peaks in both graphs show the simultaneous response of both sensors to the rapid heating test.

4.3.2 Monitoring temperature inside the enclosure for 6.25 ms

During a monitoring period that lasted for an entire weekend, the temperature curves recorded, displayed in Figure 4.6, showed a very close similarity. A correlation line was plotted to assess the similarity between the two graphs. A good linearity can be seen in Figure 4.6 c. displays a correlation line plotted to examine the linear relationship between frequency and temperature. This line, representing the best-fit line derived from linear regression analysis, quantifies the variation in frequency with changes in temperature.

Calculation of the Correlation Line:

The correlation line was established through linear regression, which fits a straight line to the data points. The slope of this line reflects the rate at which frequency changes with temperature. The slope of the correlation line was determined to be 0.045 Hz/°C. This value signifies the change in frequency per degree Celsius. This slope was calculated by analyzing the frequency variation over a specified temperature range and applying a linear model to the data.

Frequency Calculation: With a slope of 0.045 Hz/°C, the frequency change per degree Celsius is 0.045 Hz. Consequently, a temperature difference of 1°C results in a frequency change of 0.045 Hz. Calculated using Equation (4.1) Change in Frequency=0.045(Hz)/° 1(°C)=0.045Hz

For a temperature change of 1°C (from 22°C to 21°C), this results in a frequency change of 0.045 Hz. which equal 0.045×1000=45Hz/°C

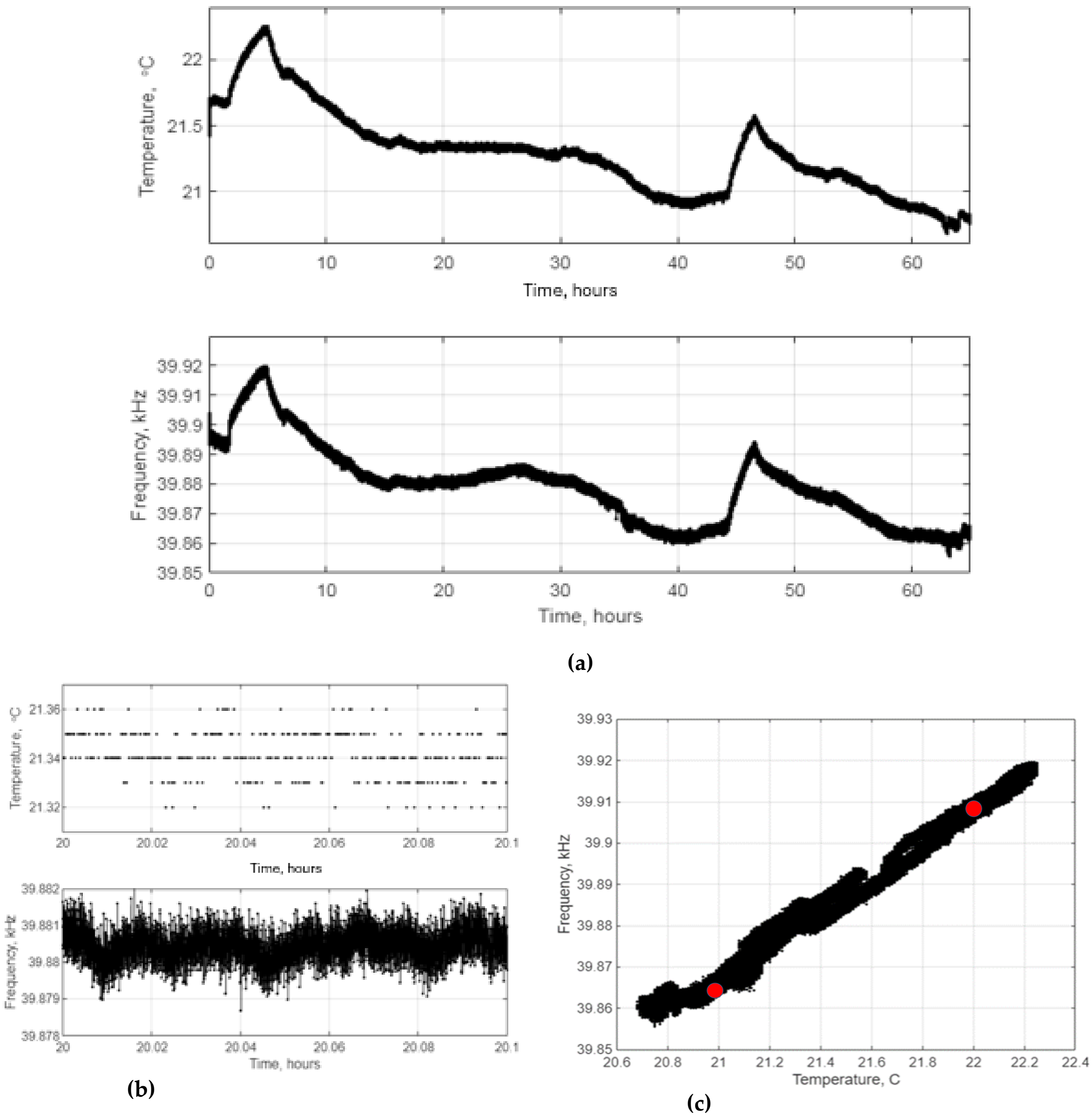

Figure 4.6: Records obtained from an experiment monitoring the air temperature inside a container over a weekend (6.25 ms measurement time). (a) Overall recordings. (b) A section of the complete recording is viewed at a closer scale. (c) The temperature–frequency relationship exhibits good linearity and slight hysteresis.

When the readings remained stable, it was noticed that a change of about 0.04°C was associated with a shift of roughly 10 Hz in the UOTS's output frequency. The relationship between frequency and temperature exhibited good linearity with a gradient of about 45 Hz/°C as calculated using the correlation line (Figure 4.6 c) and 44.4 Hz/°C as calculated in Figure 4.7, with a slight hysteresis. The gradient refers to the rate of frequency change with respect to temperature. It is the slope of the line when frequency (Hz) is plotted against temperature (°C). Figure 4.6 (c): A linear correlation line is drawn, and the slope gradient is reported as 45 Hz/°Figure 4.7: Another slope is reported as 44.4 Hz/°C, with a slight hysteresis.

The gradient or slope (m) of a line is calculated using the formula:

Calculated using equation (4.1)

Two data points for Figure 4.6(c):

Temperature difference ΔT=22(℃)-21(℃) =1℃

Gradient (slope) $= \frac{f_2 - f_1}{T_2 - T_1}$= (39.908(Hz) − 39.863(Hz)/(22℃-21℃)=0.045*1000=45Hz/°C

The same type of calculation was used for Figure 4.7

At the 10th hour:

Temperature difference ΔT=22.25(℃)-20.915(℃) =1.35℃

Frequency difference ΔF=39.92(Hz)-39.86(H)z= 0.060*1000=60Hz

Gradient=ΔF/ΔT=60(Hz)/1.35(℃) = 44.44Hz/℃

But the values differ slightly, which could explain the slope of 44.4 Hz/°C. Hysteresis, in this context, suggests that the relationship between frequency and temperature may not follow the same path during increasing and decreasing temperature cycles. This implies that the slope could vary depending on whether the temperature is rising or falling, hence the slight difference between 45 Hz/°C and 44.4 Hz/°C.

The gradient, or slope, represents the rate of change of frequency with respect to temperature. It was calculated as 45 Hz/°C and 44.4 Hz/°C using data points from Figures 4.6(c) and 4.7, respectively. The slight difference and the mention of hysteresis indicate a small discrepancy between the cycles of temperature change. However, both values are close, indicating a generally linear relationship.

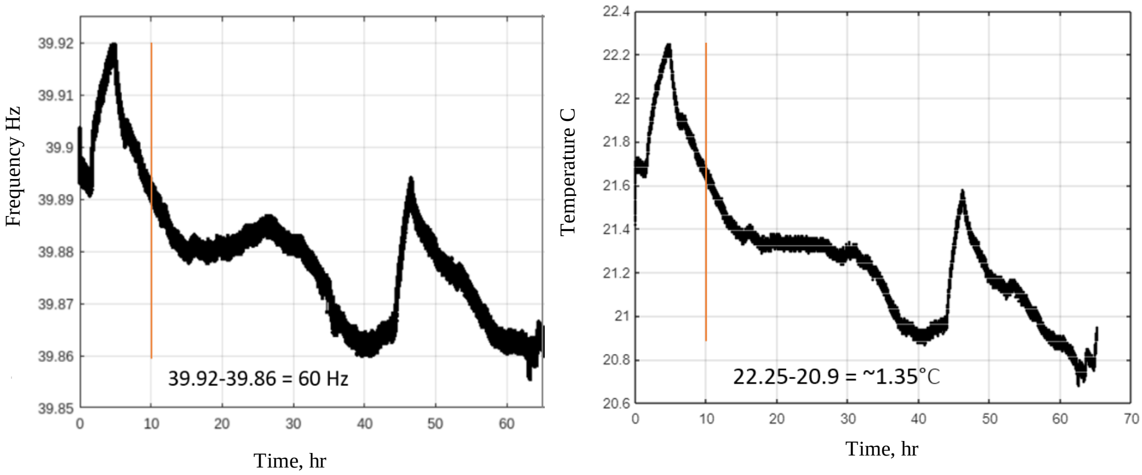

Figure 4.7: Calculation of the gradient frequency in regard to temperature.

To compare both sensors' output from a closer view, both graphs are zoomed at time 40 to 40.1 hours as shown in Figure 4.8 (A), and this was further ten times zoomed to show up to 40.01 Figure 4.8 (B), then to show up to 40.001 hr Figure 4.8 (C).

As can be seen from Figure 4.8, for the UOTS, a closer look shows a continuous and dynamic behaviour in the data revealed in continuous oscillation waves of frequency peaks that exhibit an up-and-down pattern. The scatter of the data becomes more apparent and can be easily calculated as in Figure 4.8 C, which is equivalent to 1.5 Hz. The frequency is calculated as 39.8630(H)z - 39.861(5Hz) = 0.0015 Hz, which equals 1.5 Hz.

On the other hand, the temperature data lines for the conventional sensor line are composed of intermittent measurement dots. This implies that the conventional sensors provide data in a more discrete or sporadic manner, as opposed to the continuous waves seen in the UOTS Figure 4.8 (C).

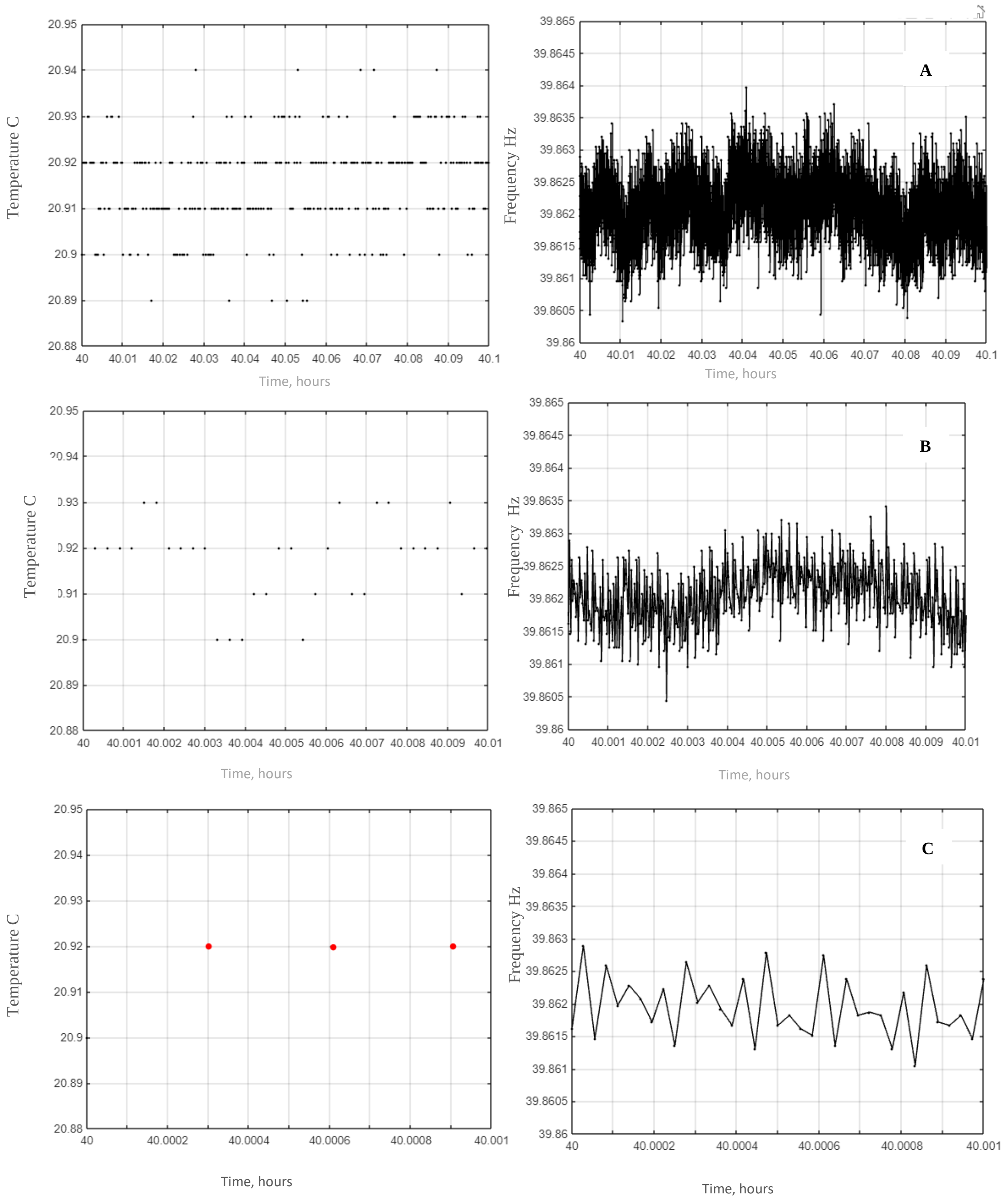

Figure 4.8: The UOTS frequency output and the conventional sensor temperature graph are zoomed at the same time and for three same scales: A, B and C.

The experiment was repeated to ensure the repeatability and stability of the outcome. Figure 4.9 shows a monitoring temperature period lasting 20 hours inside the enclosure.

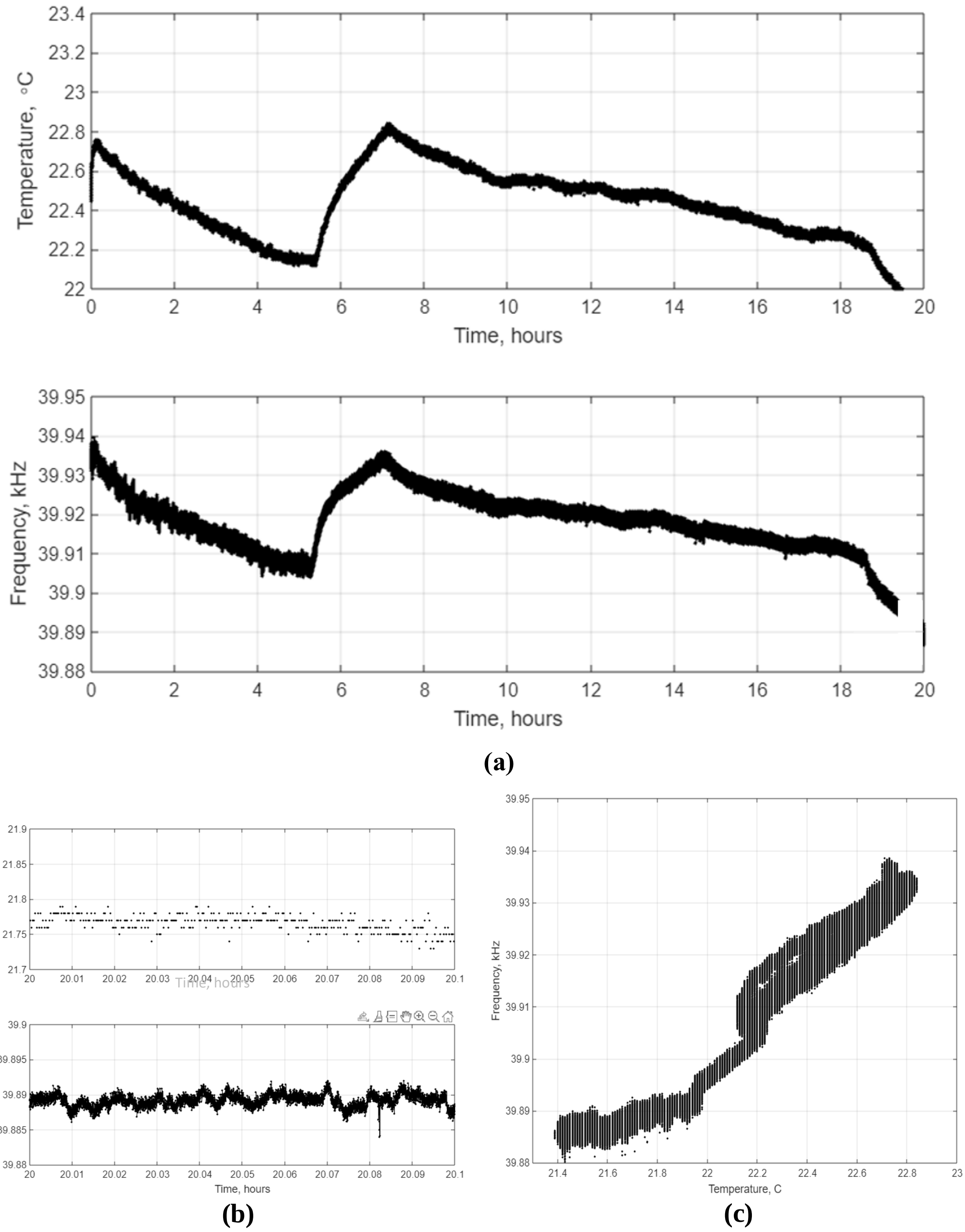

Figure 4.9: Repeat monitoring the air temperature for 20 hours inside the enclosure (6.25 ms measurement time). (a) Overall recordings. (b) A section of the complete recording is viewed at a closer scale. (c) Temperature –frequency relationship exhibiting hysteresis.

Figure 4.9 illustrates a similar outcome. The datasets from the two sensors produced comparable graphs without interruptions, exhibiting a gradient of approximately 45 Hz/°C. The gradient is calculated as follows:

Calculated using equation (4.1)

Temperature difference ΔT=22.6(°C)-21.6(°C) =1°C

Frequency difference ΔF=40.929(Hz)-39.883(Hz)= 0.045*1000=45Hz

Gradient=$\Delta F/\Delta T$=45(Hz)/1(°C) = 45Hz/°C

A correlation line was plotted to assess the similarity between the two graphs. A reasonable linearity can be seen in the temperature UOTS frequency relationship correlation line in Figure 4.9 C. However, the correlation is less linear comparing to the previous experiment.

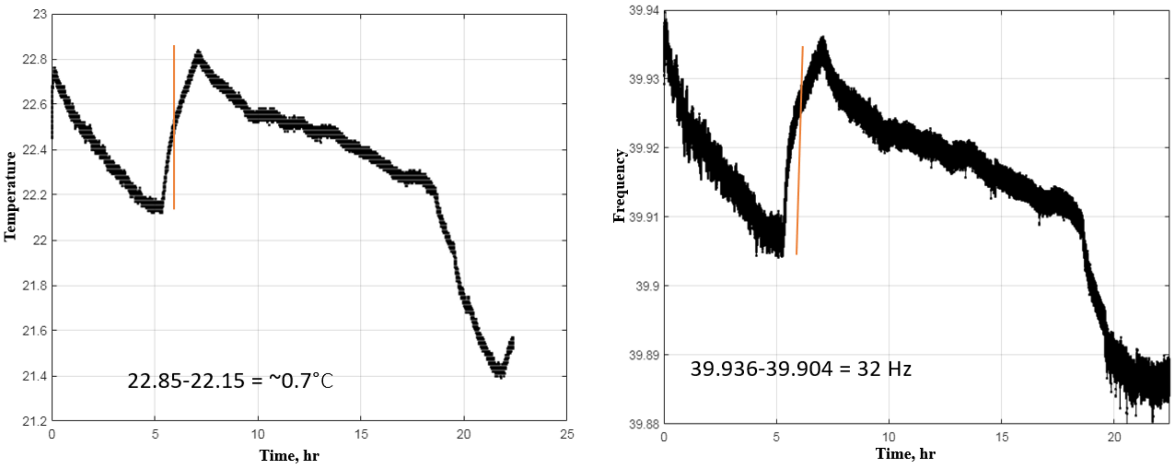

Figure 4.10: Calculation of the gradient frequency with temperature.

The relationship between frequency (F) and temperature (T) is linear, with a given gradient of 45 Hz/°C. This means that for every 1°C change in temperature, the frequency changes by 45 Hz

At the 5th hour:

Calculated using equation (4.1)

Temperature difference $\Delta \mathcal{T} = 22.85(℃) - 21.15(℃) = 0.7℃$

Frequency difference $\Delta \mathcal{F} = 39.936(Hz) - 39.904(Hz) = 0.032 * 1000 = 32Hz$

Gradient=$\frac{\Delta \mathcal{F}}{\Delta \mathcal{T}} = 32(Hz)/0.7(℃) = 45.71Hz/℃$

This calculated gradient (45.71 Hz/°C) is close to the provided 45 Hz/°C. The slight difference might be due to rounding or measurement errors, but it's close enough to consider the relationship valid. The calculations show that there zoomed at time 10 to 11 hours as shown in Figure 4.11 (A), then to show up to 10 to 10. 1 hr Figer 4.11(B). then to show up to 10 to 10.01 Figer 4.11(C).

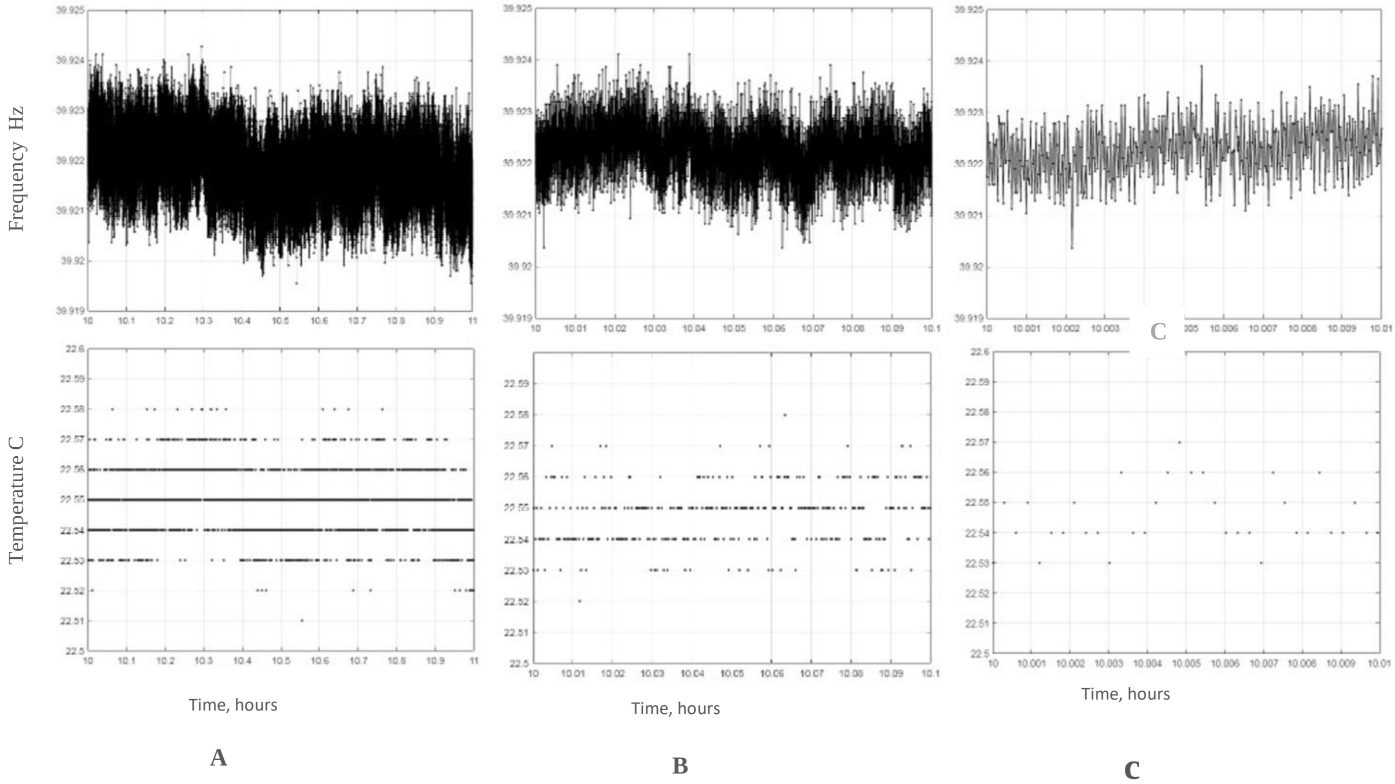

Figure 4.11: The UOTS frequency output and the conventional sensor temperature graph are zoomed concurrently for three scales: A, B and C.

The scatter of the data in Figure 4.9 is 2 Hz when the graph is further ten times zoomed. The frequency is calculated as 39.8925(Hz) - 39.8905(Hz) = 0.0020 Hz, which equals 2 Hz.

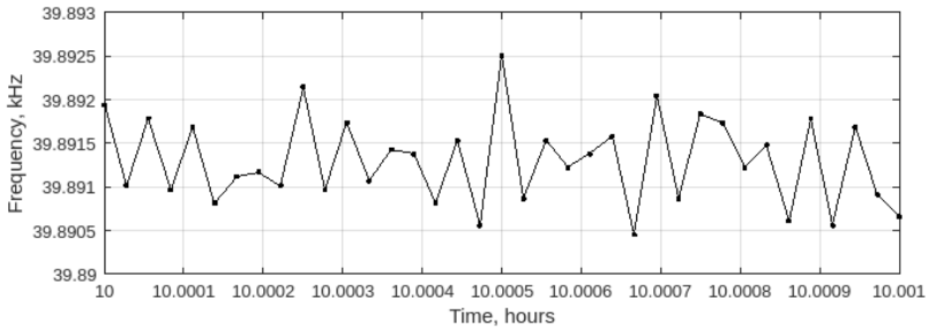

Figure 4.12: The zoomed segment of the UOTS output data shows the scatter of the data in this segment.

4.3.3 Monitoring the temperature of the open space for 6.25 ms frequency measurement interval

The following recordings, collected over the weekend, exhibited shapes comparable to each other but demonstrated greater variability compared to the recordings obtained in the enclosure. Although the relationship between frequency and temperature seemed to follow a linear pattern, it notably deviated at higher temperatures. Figure 4.13 shows the data collected over more than 60 hours. Figure 4.13 involves understanding how small changes in temperature and frequency were observed and how the gradient between these two quantities was calculated. Calculated using equation (4.1)

Temperature difference $\Delta\mathcal{T} = 21.74(°\mathrm{C}) - 21.67(°\mathrm{C}) = 0.07°\mathrm{C}$

Frequency difference $\Delta\mathcal{F} = 40.925(Hz) - 40.907(Hz) = 0.018 * 1000 = 18Hz$

Gradient=$\frac{\Delta\mathcal{F}}{\Delta\mathcal{T}} = 18(Hz)/0.07(°\mathrm{C}) = 257Hz/°\mathrm{C}$

The calculation in Figure 4.13 shows that over a period of more than 60 hours, the experiment recorded a small temperature difference of 0.07°C, which corresponds to a frequency difference of 18 Hz. The gradient, which is the change in frequency per unit change in temperature, was found to be 257 Hz/°C. This gradient is significant as it indicates the sensitivity of frequency to changes in temperature

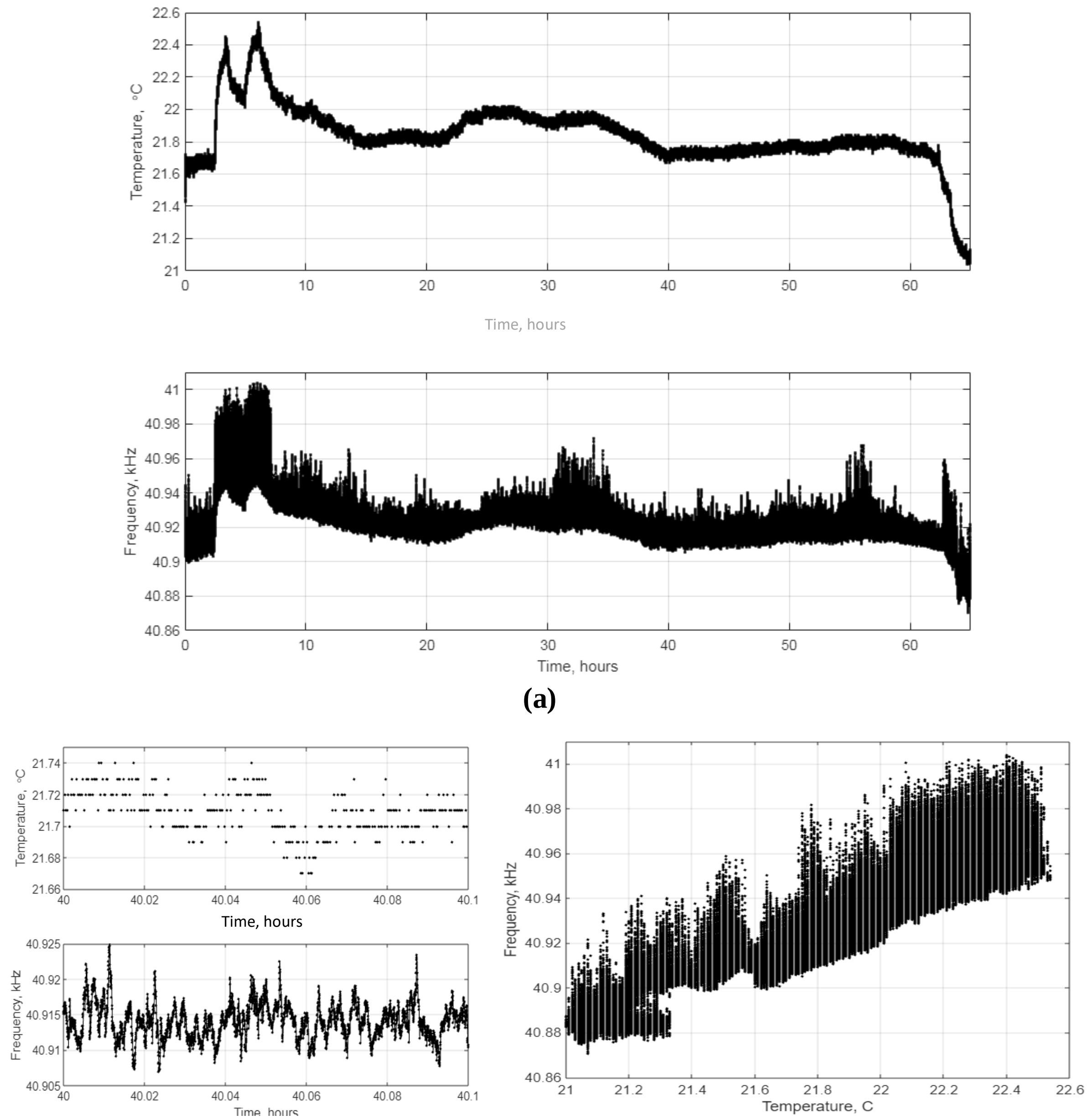

(b) **(c)**

Figure 4.13: Records were obtained from an experiment monitoring the air temperature over 65 hours in an open-plan office setting (6.25 ms measurement time). (a) Overall recordings. (b) A section of the complete recording is viewed at a closer scale. (c) Temperature – UOTS frequency relationship exhibiting some divergence at higher temperatures.

The gradient frequency regarding temperature in Figure 4.14 was estimated at 58 Hz/°C. It was higher than one inside the container, which was mostly 45 Hz/°C. The frequency gradient with respect to temperature. This value is higher than the gradient observed inside the container, which was approximately 45 Hz/°C

At the 10th hour Calculated using equation (4.1)

Temperature difference $\Delta\mathcal{T} = 22.55(℃) - 21(℃) = 1.55℃$

Frequency difference $\Delta\mathcal{F} = 40.98(Hz) - 40.894(Hz) = 0.90 * 1000 = 90Hz$

Gradient=$\frac{\Delta\mathcal{F}}{\Delta\mathcal{T}} = 90(Hz)/1.55(°C) \; = \; 58Hz/°C$

There seems to be a discrepancy in the values provided in the text. The calculated gradient based on the frequency difference of 0.086 Hz and temperature difference of 1.55°C is approximately 58 Hz/°C

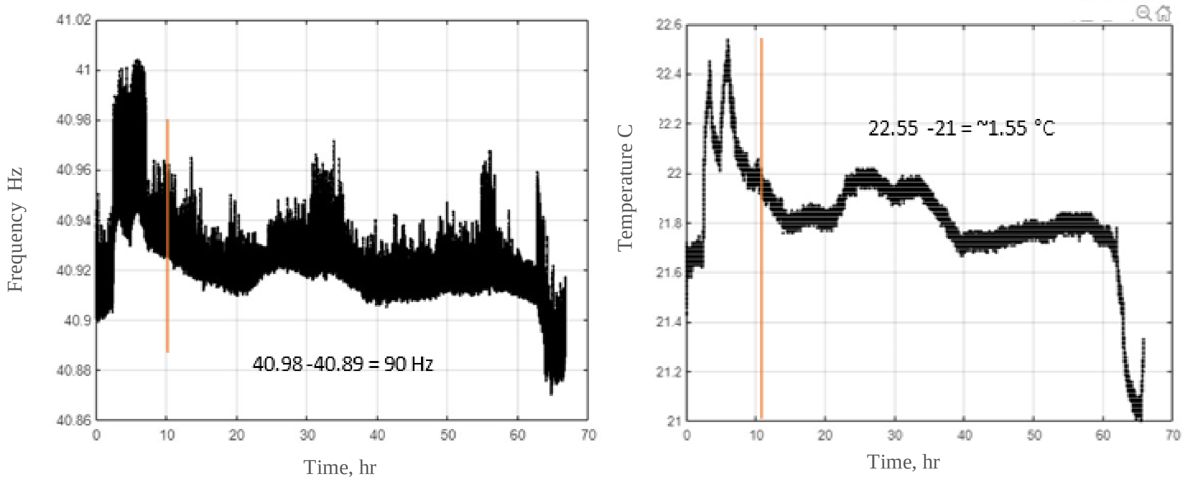

Figure 4.14: Calculation of the gradient frequency with respect to temperature.

By zooming the UTOS output record graph in Figure 4.13 (a) at the time of two hours (Figure 4.13 b), i.e. during a relatively stable curve segment, the first and last segment at time 2 and 2.09 hr were ten times further zoomed and shown in Figure 4.15 ; the temperature readings showed a scatter of 0.07°C. At the same time, the UOTS frequency exhibited a variation of 10 Hz in one segment and 25 Hz in the other. The temperature readings showed a variation of 21.64099(°C)- 21.57099(°C) = 0.07°C. This small variation suggests that the system remained relatively stable in terms of temperature during the observed period. UOTS Frequency Variation:

Variation Frequency Range in First Segment: The UOTS (Universal Oscillator Timing System) frequency varied from 40.9105(Hz) - 40.9005(H)z= 0.010*10= giving a variation of 10Hz

Frequency Range in Second Segment: The UOTS frequency varied from 40.92565Hz-40.90065(Hz0=0.025 *1000=25(H)z giving a variation of 25 Hz.

Despite the stable temperature, the UOTS (Ultrasonic Oscillating Temperature Sensors) frequency exhibited notable variations, indicating the influence of factors beyond temperature. Although the temperature appeared constant, other environmental conditions such as humidity, pressure, or electromagnetic interference may have contributed to these variations. The frequency fluctuations differed between the two segments—10 Hz in one and 25 Hz in the other. Over time, factors like component heating, aging, or drift may have caused these segments to respond differently. Even a slight temporal difference between segments could allow these factors to begin affecting the system.

Thus, a stable temperature does not necessarily equate to a stable UOTS frequency, as other variables likely contributed to the observed variations. The differences in frequency variation between segments suggest that external or internal conditions fluctuated in ways that uniquely impacted each segment. Understanding these influences is essential for enhancing the system's stability and accuracy.

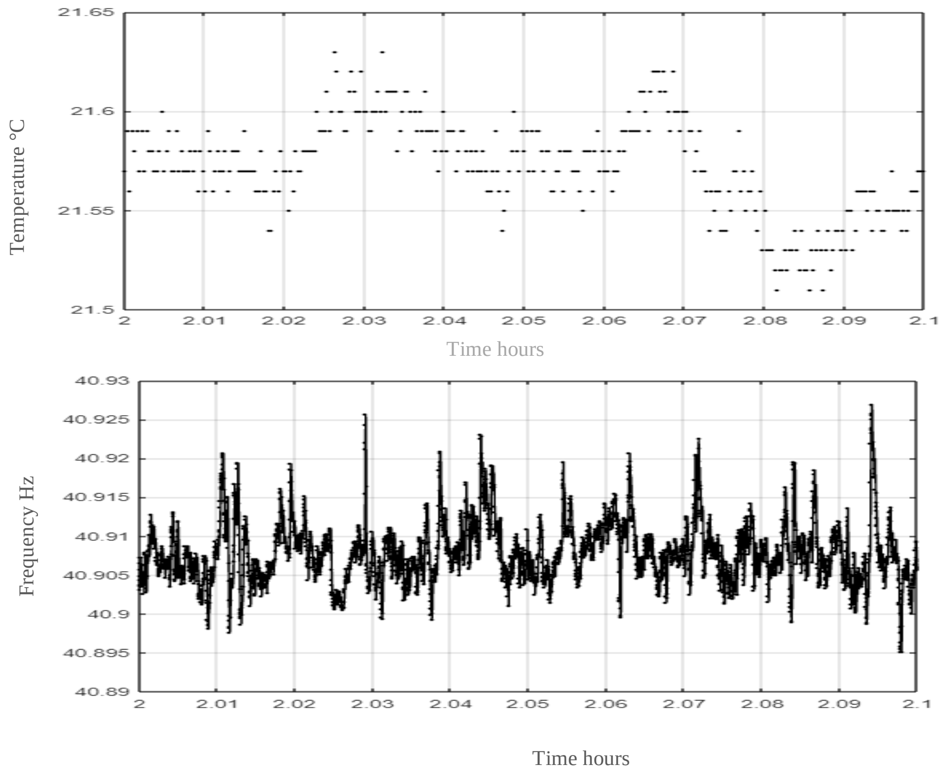

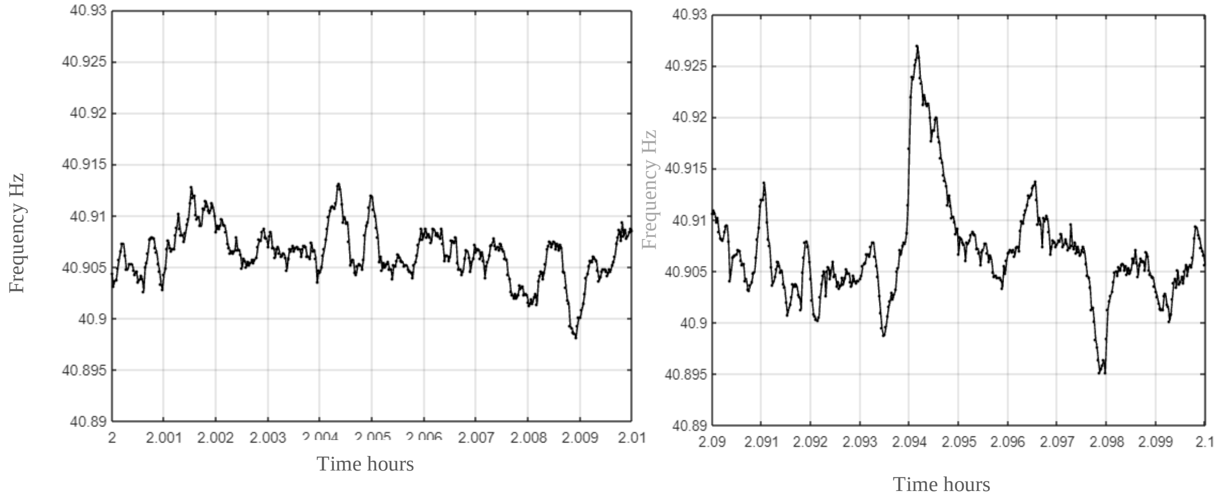

Figure 4.15: The zoomed segment of the UOTS output data shows the scatter of the data in two segments.

4.3.4 Repeated monitoring of the temperature of the open space (6.25msec)

These recordings, which were collected during the day, exhibited similar shapes to one another but demonstrated greater variability in comparison to the recordings obtained in the enclosure. During a relatively stable segment of the curve, the temperature readings displayed a scatter of 0.07°C. In contrast, the UOTS frequency exhibited a variation of 10 Hz as previously stated.

Despite the generally linear relationship observed between frequency and temperature, significant deviations were noted at higher temperatures. Figure 4.16 illustrates the data collected over more than 20 hours.

Temperature Variation: 21.25(°C) - 21.18(°C) = 0.07°C

UOTS Frequency Variation: 40.923 (Hz) - 40.913 (Hz)= .010*1000=10 Hz

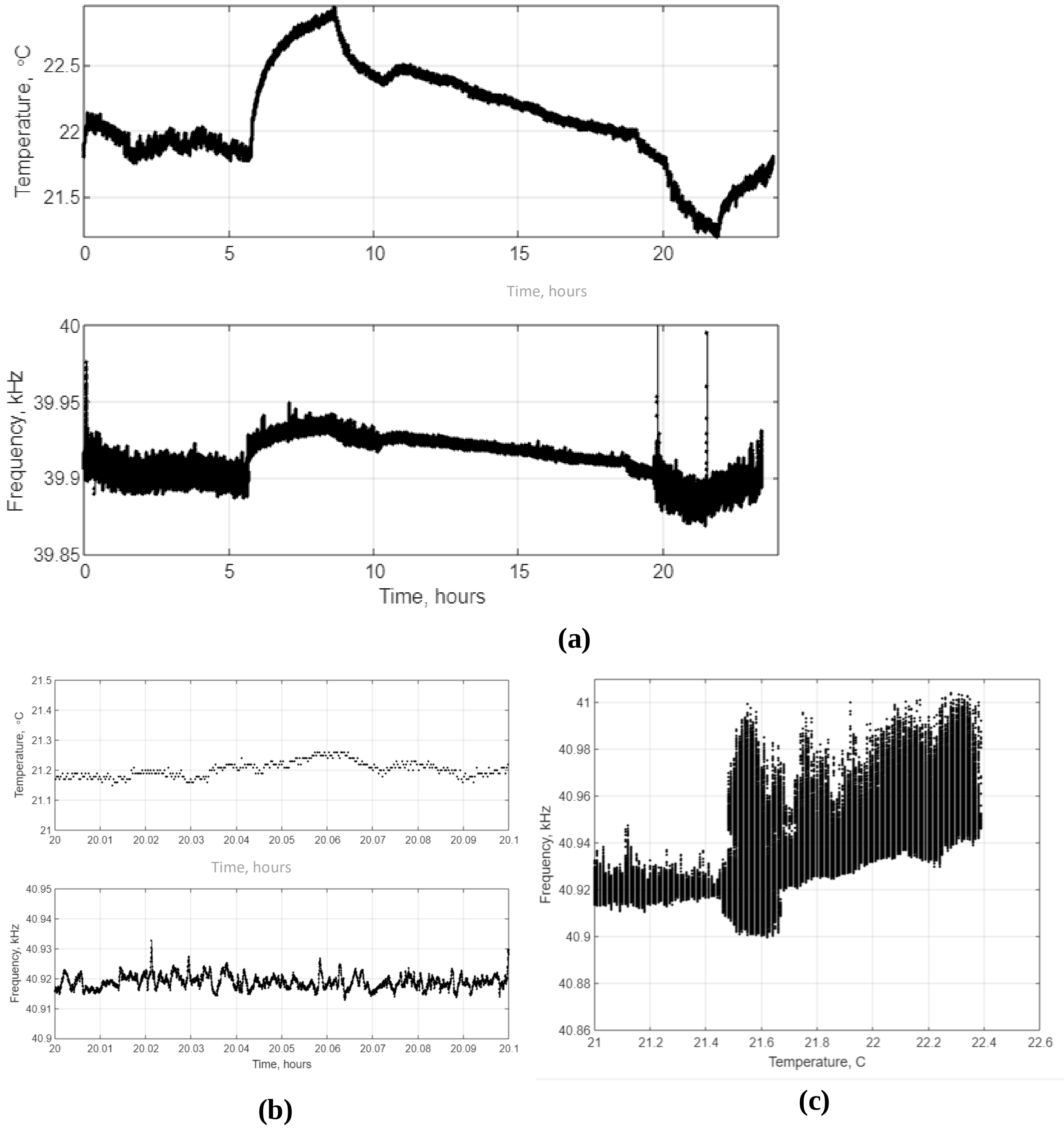

Figure 4.16: Second experiment monitoring the air temperature over a day in an open-plan office setting (6.25 ms measurement time). (a) Overall recordings. (b) A section of the complete recording is viewed at a closer scale. (c) Temperature – UOTS frequency relationship exhibiting some divergence at higher temperatures.

The gradient of frequency with respect to temperature, as depicted in Figure 4.17. This gradient is Calculated using Equation (4.1)

Gradient=$\frac{\Delta\mathcal{F}}{\Delta\mathcal{T}}$=88Hz/1.55°C =51.6Hz/°C This value indicates that for each degree Celsius increase in temperature, the frequency changes by approximately 51.6 Hz.

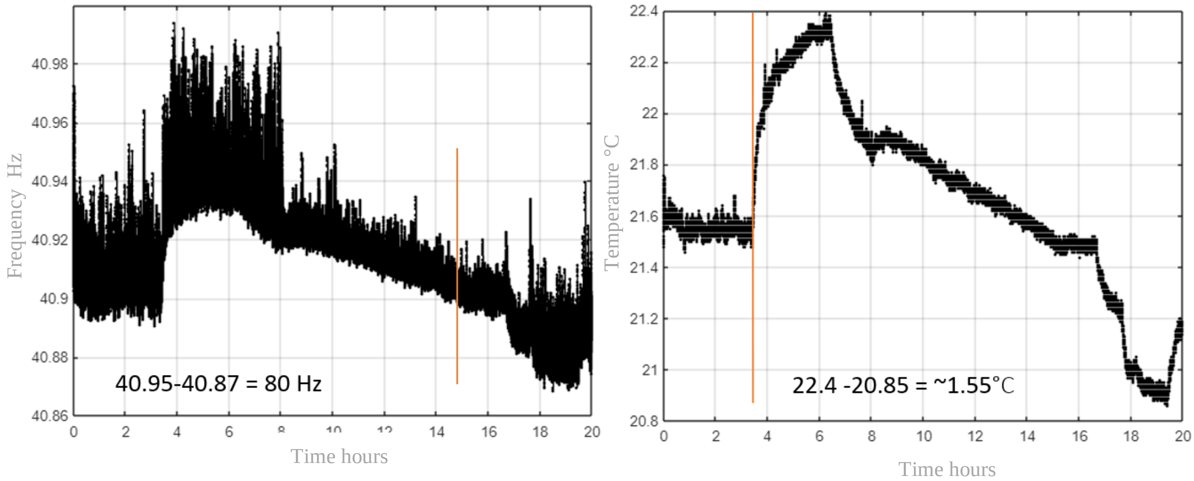

Figure 4.17: Calculation of the gradient frequency with respect to temperature.

4.4 Hysteresis analysis

Hysteresis should be considered when using inexpensive narrowband ultrasonic transducers in oscillating systems. The primary cause of this phenomenon is the deformation of the piezoelectric material due to temperature fluctuations. Although these variations are minimal, they cannot be disregarded because even a slight change in the thickness of the piezoelectric material leads to significant differences in the frequency response. It is important to note that the amount of hysteresis varies at the beginning and midway through the temperature cycle, making average hysteresis values inadequate for assessing performance at a specific distance. Instead, the results recorded different hysteresis values at various lengths.

The resulting hysteresis obtained under the various applied conditions and shown by the temperature–frequency relationship graphs (C) in Figures 4.3- 4.6 exhibit differences in their values and relationships. Even though all states exhibited a good relationship between frequency and temperature, the data recorded for the temperature inside the box over 60 hours Figure 4.5 (C) displayed the best linearity with the minimum hysteresis, where the relationship had a gradient of around 40 Hz/°C. However, the temperature recorded outside the cardboard box Figure 4.3 (C) and Figure 4.6 (C) with 0.1 s and 6.25 ms measurement time showed larger hysteresis. The analysis of temperature measurements inside a cardboard thermal testing reveals that hysteresis increases significantly as the measurement time is reduced from 0.1 seconds to 6.25

milliseconds. Hysteresis, defined as the lag between input (temperature change) and output (frequency response) in a system, in this context, reflects the system's ability to track temperature changes and the corresponding variation in frequency response. An increase in hysteresis suggests that the system's output frequency changes are increasingly delayed or dispersed relative to temperature changes, particularly as the temporal resolution of the measurements is heightened.

Explanation and Analysis:

Measurement Time of 0.1 Seconds (100 milliseconds) - Figure 4.3 (C):

Frequency Change: 39.951 (kHz) - 39.909 (kHz) = 0.0418*1000 = 41 Hz

Temperature Change: 22.88 (°C) - 21.88(°C) = 1 °C

At a longer measurement time of 0.1 seconds, the frequency change is observed to be 41 Hz, corresponding to a 1°C temperature change. This suggests that the system has sufficient time to respond to temperature changes, resulting in a smaller hysteresis effect. At this temporal resolution, the system can more accurately follow temperature variations with minimal delay or dispersion.

Measurement Time of 6.25 Milliseconds - Figure 4.6 (C)

Frequency Change: 39.908(kHz) - 39.863(kHz) = 0.045 *1000 = 45 Hz

Temperature Change: 22(°C) - 21 (°C) = 1 °C

When the measurement time is reduced to 6.25 milliseconds, the frequency change increases to 45 Hz for the same 1°C temperature change. This larger frequency change indicates a greater hysteresis effect, likely due to the reduced time available for the system to stabilize. As the time resolution increases, the system exhibits more pronounced fluctuations in frequency in response to the same temperature variation. This heightened hysteresis at shorter measurement times suggests that the system's frequency response to temperature changes becomes less stable, possibly due to the inherent thermal properties of the system and the influence of noise or transient effects that become more evident at higher sampling rates. This analysis underscores the critical role of measurement time in assessing temperature-related frequency changes in systems where hysteresis is present. Accurate interpretation of hysteresis effects requires careful consideration of the temporal resolution of the measurements, as shorter measurement intervals can lead to greater instability and more pronounced hysteresis in the system's response.

4.5 Results and discussion

The results showed some observations were common to all the experimental temperature records obtained from both a conventional temperature sensor and a UOTS in three different scenarios**.**

This comparison suggests that the UOTS captures a more continuous and dynamic representation of temperature changes, while the conventional sensors provide data in a more discrete and intermittent fashion.

4.5.1 Evaluating the responsiveness of conventional temperature sensors in the air using a UOTS

Experimental temperature recordings during rapid heating of the air inside the enclosure are presented in (Fig4.2) and (Fig. 4.5) In the first instance (Fig4.2), the hairdryer affected the air for a noticeable period, resulting in the output frequency reaching saturation at around 40.8 kHz. The records in (Fig. 4.2b) show various frequency peaks that can be used to estimate the maximum air temperature in the enclosure before the hairdryer was redirected elsewhere. The UOTS exhibited sensitivity to temperature changes ranging from 40 to 50 Hz/°C, as observed during the monitoring experiments. Based on the 400 to 500 Hz increase in the UOTS frequency (Fig. 4.5), one can estimate that the maximum air temperature in the enclosure was approximately 10°C higher than the environmental temperature. In contrast, the conventional temperature sensor recorded an increase of no more than 2°C. This difference can be explained by the high thermal inertia of the conventional sensor, as the air at an elevated temperature could not fully heat it up. When the hairdryer was removed from the enclosure, the sensor gradually cooled down due to its thermal inertia. Therefore, it seems potentially possible to use a UOTS for benchmarking and assessing the thermal responsiveness of air temperature sensors.

4.5.2 Need for additional conventional sensor when using a UOTS.

For view, while UOTSs have advantages, they are incapable of truly independent temperature measurement. The most beneficial use of UOTSs would be in open spaces without enclosures, reducing material and installation costs. However, the variability of the output frequency, as illustrated in (Fig 4.4) and (Fig.4.13), makes it difficult to determine the corresponding temperature accurately. For example, if the measured frequency in (Fig 4.13) was 40.92 kHz, the temperature could fall between 21°C and 22°C, undermining the high-resolution capability of UOTSes. Additionally, we noticed irregular behaviour in the output frequency during a few of our monitoring experiments, as shown in Figure 4.18.

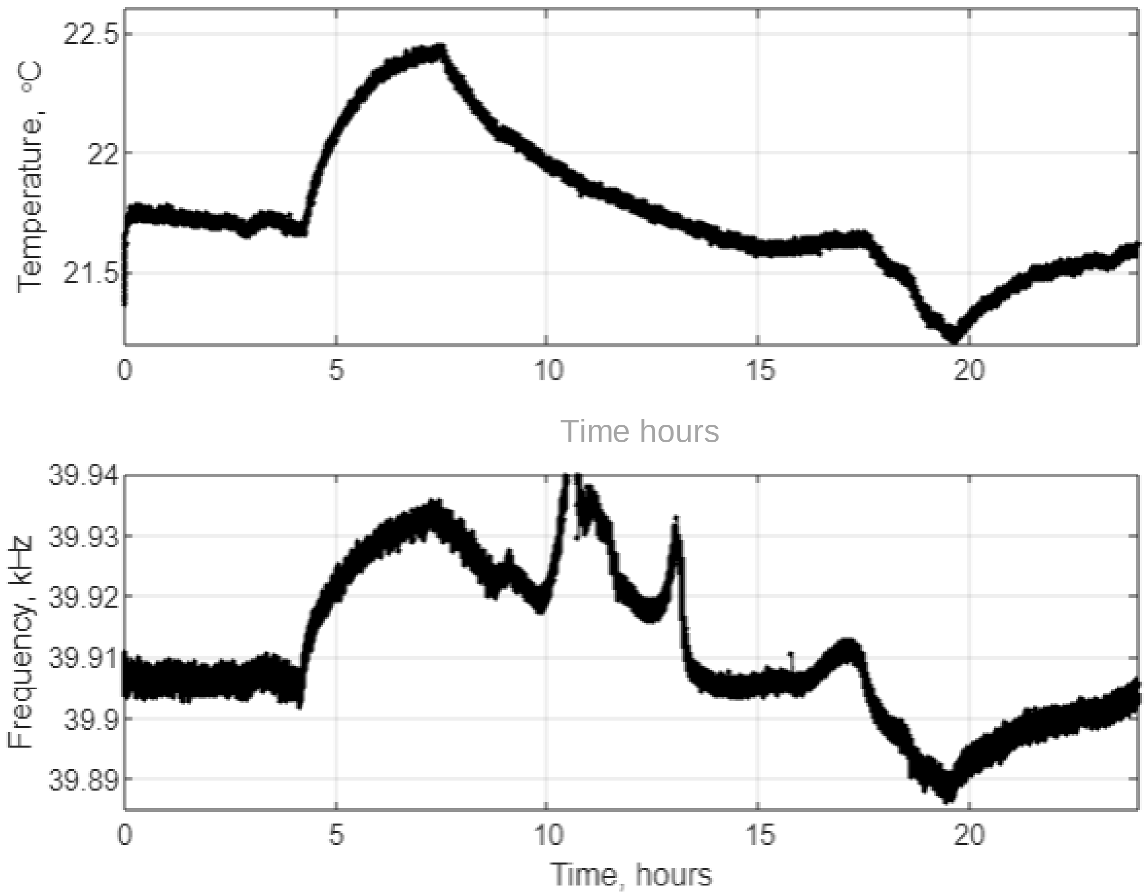

Figure 4.18: Records obtained from an experiment monitoring the air temperature overnight in the enclosure (6.25 ms measurement time) exhibiting deviation of the UOTS frequency curve from that of the conventional temperature sensor.

We cannot provide an explanation for either the deviation or the subsequent return of the readings to the conventional sensor's curve. Therefore, we recommend that a UOTS be supplemented with a conventional sensor, either to validate the UOTS reading or to conduct a sensor data fusion procedure [7].

4.6 Summary and conclusions

To summarise the key findings of the set of 150 mm distance experiments that have been done, Table 4.1 illustrates a comparison between 0.1 seconds and 6.25 milliseconds of UOTS output.

Table 4.1 Conventional temperature sensor vs UOTS output frequency measured over two-time intervals.

Sensor position & Temperature scenario		**Conventional sensor Vs UOTS output frequency measured over two-time intervals:**	
		0.1 seconds	6.25 milliseconds
1	Rapid heating of air inside an enclosure	-UOTS showed a faster response time than the CTS, which took time to return to baseline values.	-UOTS showed quicker time in reaching its highest point and returning to the baseline
2	Long term Monitoring temperature inside the enclosure	UOTS showed reasonable agreement with CTS data. -Within a constant readings period, UOTS showed a variation of 0.05°c corresponding to 2 HZ frequency. -The frequency-temperature relationship displayed hysteresis with a slope of 40 Hz/°C.	-Within 60 -hour period, UOTS showed a very close resemblance to CTS. -Within a stable readings period, UOTS showed a variation of 0.04°c corresponding to 10 Hz output frequency. -A linear relationship between temperature and frequency was achieved with a gradient of around 40 Hz/°C and slight hysteresis.
3	Long term Monitoring of temperature in open space	-Data collected by both sensors showed a comparable temperature pattern of significant variations compared to the data measured inside the enclosure. -The UOTS sensor was more sensitive to air movement, which contributed to increased variability. -UOTS sensor showed few irregular clusters with no notable hysteresis.	Both sensors showed similar temperature graphs with variations due to the open area. -The UOTS sensor was more sensitive to air movement.

This chapter presents experimental temperature records obtained from both a conventional temperature sensor and a UOTS in three different scenarios:

-Rapid heating of air inside an enclosure.

-Long-term monitoring of air temperature inside an enclosure.

-Long-term monitoring of air temperature in an open-plan office.

The UOTS output frequency was measured over two distinct time intervals: 0.1 seconds and 6.25 milliseconds. The results were similar, but the latter interval was preferred for more responsive measurements.

The UOTS demonstrated high responsiveness to rapid temperature changes, whereas the conventional temperature sensor underestimated the maximal temperature in the enclosure by approximately eight °C and took a substantial amount of time to return to baseline values.

The temperature curves recorded by both sensors were in very good agreement, particularly when monitoring the temperature in the enclosure. However, when monitoring the temperature in an open space, both sensors exhibited notable variability, with the UOTS frequency variability being higher due to its sensitivity to both local temperature and air movements between the ultrasonic transducers.

We believe that UOTSes are suitable for applications requiring the detection of rapid temperature changes, such as detecting leaks or thermal runaways or opening doors of storage compartments. However, for continuous temperature monitoring, a UOTS should be complemented by a conventional temperature sensor, especially in an open space environment. Combining sensors allows for sensing the aggregate temperature along the complete ultrasonic pathway and detecting instances where the UOTS reading might be unreliable.

Chapter 5 : Experimentation at medium distances between the transducers (300 and 500 mm)

This chapter explores the performance of the UOTS in air temperature measurements over different distances and in different scenarios and compares its functioning to conventional temperature sensors. The same settings were employed for the two systems, and the temperature was recorded by both systems over the same conditions.

5.1 Instrumentation and experimental procedures:

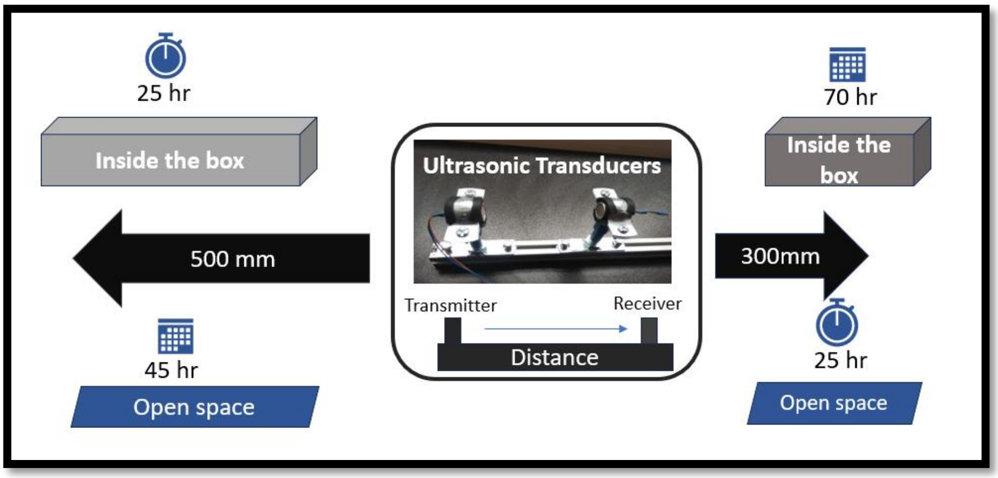

Figure 5.1: Schematic diagram for the study.

Different scenarios were implemented in this study to measure the temperature inside a controlled environment and in an open space environment. A cardboard thermal testing enclosure. Was used to represent the controlled environment to prevent air movement inside the enclosure. Conducting the experiment outside the box is to represent the uncontrolled environment. These conditions were applied over extended intervals and different distances. Figure 5.1 shows a schematic diagram for the experiment conditions conducted in this chapter.

5.2 Monitoring temperature inside the enclosure at a 300 mm distance

The setup was placed inside the cardboard thermal testing enclosure., and the temperature was monitored over prolonged periods of time (e.g., weekends). Figure 5.2 shows the records of the monitored air temperature from both sensors inside the enclosure over roughly 70 hours in November. In Figure 5.2, the conventional sensor data showed a change in the temperature ranging from approximately 19.7 °C to 21.9 °C, whereas the UOTSs showed a window of roughly from 40.285 to 40.384 kHz.

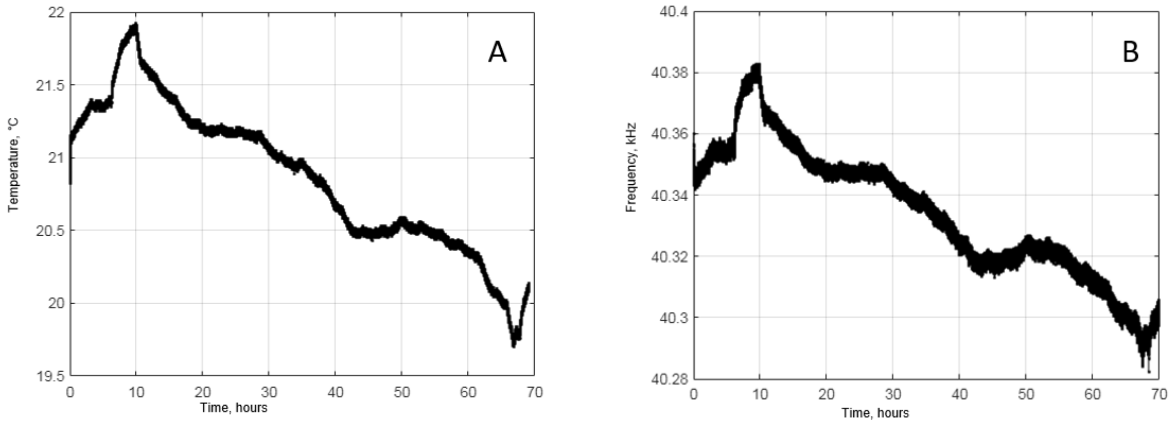

Figure 5.2: The monitored air temperature inside the enclosure was recorded by (A) conventional sensor, (B) UOTSs at 300 mm over 70 hrs interval (Run 1).

Figure 5.3 shows the relationship between the frequency UOTSs recorded and the temperature the conventional sensor. The recorded data, shown by the A and B curves in Figure 5.2, exhibit a close similarity when superimposed (Figure 5.3 A). A scatter plot can be seen in Figure 5.3

B with the gradient of around 45 Hz/°C. In Figure 5.3B, a scatter plot illustrates a frequency-temperature gradient of approximately 45 Hz/°C. This gradient is calculated based on the observed variations in temperature and frequency:

Calculated using equation (4.1)

Temperature Variation: 21.2(°C) - 20.2(°C) = 1°C

UOTS Frequency Variation: 40.348(Hz) - 40.303(Hz) = 0.045*1000=45 Hz

Gradient=$\Delta F/\Delta T$=45(Hz)/1(°C) = 45Hz/°C

This indicates that for each 1°C increase in temperature, the frequency changes by 45 Hz.

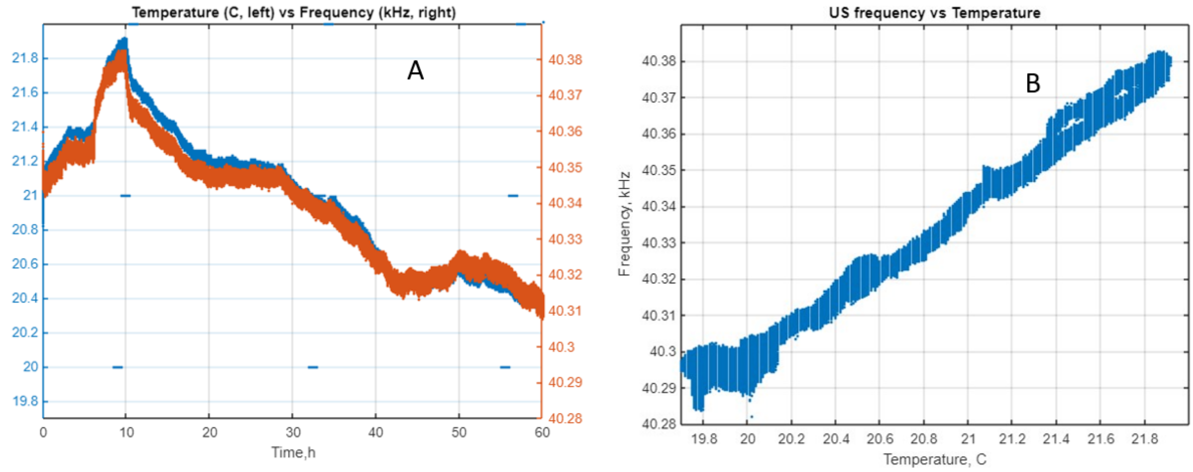

Figure 5.3: (A) The relationship between the monitored air temperature recorded by the conventional sensor and UOTSs inside the enclosure over 70-hour intervals. (B) Temperature – UOTS frequency relationship (Run 1).

This experiment was repeated to check consistency of the outcome; Figure 5.4 shows the results of temperature monitoring inside the enclosure over 70 hours at a distance of 300 mm.

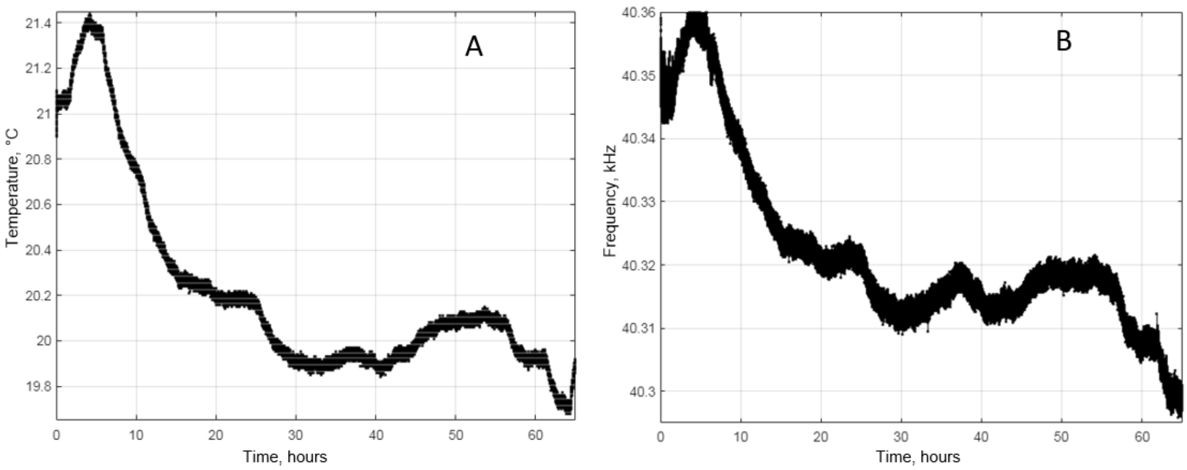

Figure 5.4: A repeat of the monitored air temperature inside the enclosure was recorded by (A) a conventional sensor and (B) at 300 mm over 70 hrs interval (Run 2).

Figure 5.5 displays collected records superimposed (A) and the relevant scatter plot (B). Comparing to the run1, the collected data superimposed less tightly, and the scatter plot exhibited a few small clusters away of the linear relationship. Figure 5.5 shows the relationship between the frequency UOTSs recorded and the temperature the conventional sensor. gradient is calculated as follows.

Calculated using equation (4.1)

Temperature difference ΔT=21(°C)-20(°C) =1°C

Frequency difference ΔF=40.349(Hz)-40.316(H)z=0.033*1000=33Hz, Gradient=ΔF/ΔT=33(Hz)/1(°C) = 33Hz/°C

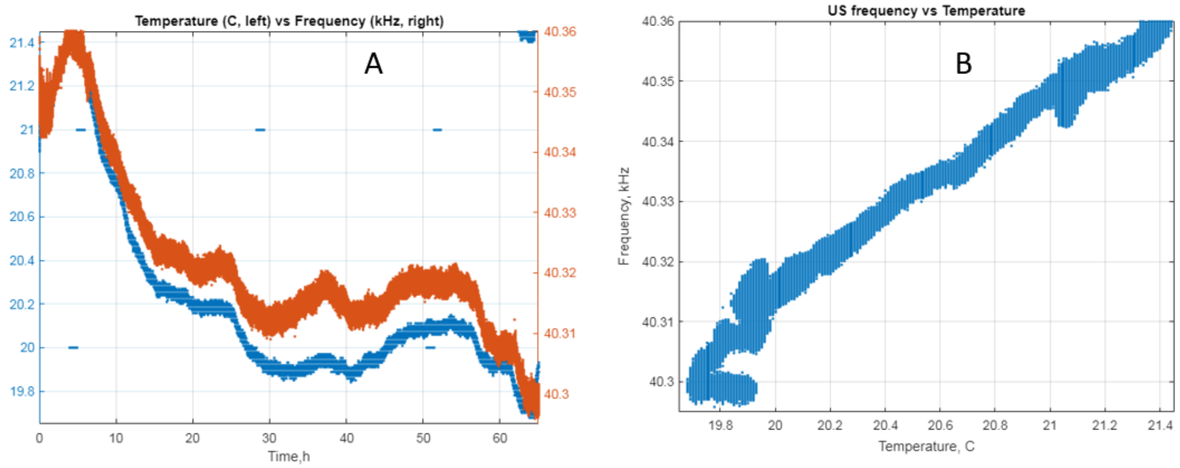

Figure 5.5 (A) The relationship between the monitored air temperature recorded by the conventional sensor and UOTSs inside the enclosure over 70-hour intervals. (B)Temperature – UOTS frequency relationship (Run 2).

5.3 Monitoring the temperature of the open space at a 300 mm distance

The setup was placed on a table inside an open office environment in November and left to record data for over 21 hours. The surrounding environment included operating computers and students moving around during the day. The recorded data for conventional sensors and UOTSs are shown in Figure 5.6. There is more variability in the open space UOTS frequency output recordings compared to those recorded in the enclosure, especially at higher temperatures.

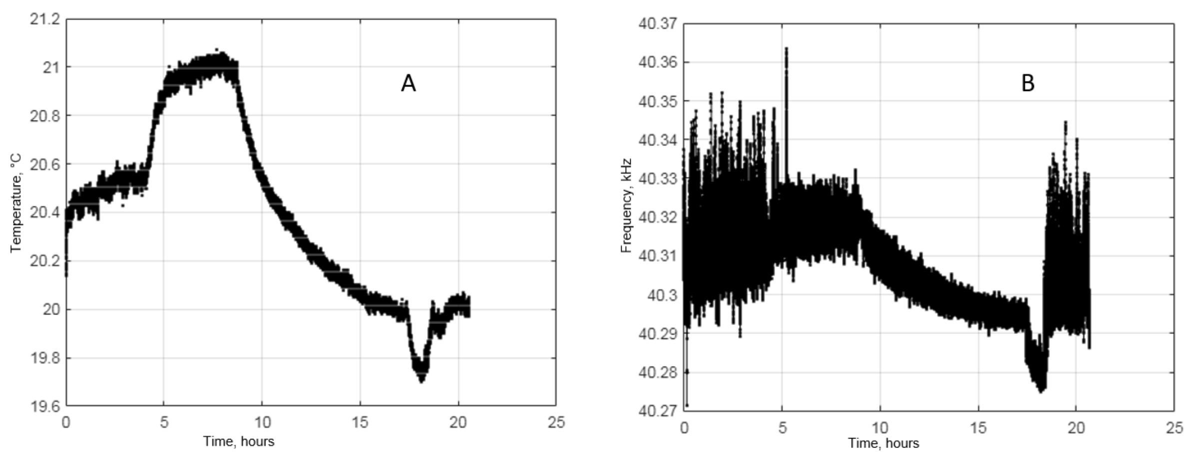

Figure 5.6: The monitored air temperature in an open space recorded by (A) conventional sensor (B) UOTSs at 300 mm over 21 hours (Run 1).

The scatter plot presented in Figure 5.7 illustrates a nearly linear relationship between temperature and frequency, with three distinct clusters deviating from this trend. The gradient of this relationship is approximately 27 Hz/°C.

This gradient is calculated as follows:

Calculated using equation (4.1)

This gradient is calculated as follows: Temperature Variation: 21. (°C) - 20. (°C) = 1°C

UOTS Frequency Variation: 40.318(Hz) - 40.291 (Hz)= 0.027*1000=27 Hz

Gradient=ΔF/ΔT=27(Hz)/1(°C) = 27Hz/°C

This indicates that the frequency changes by approximately 27 Hz for each 1°C increase in temperature

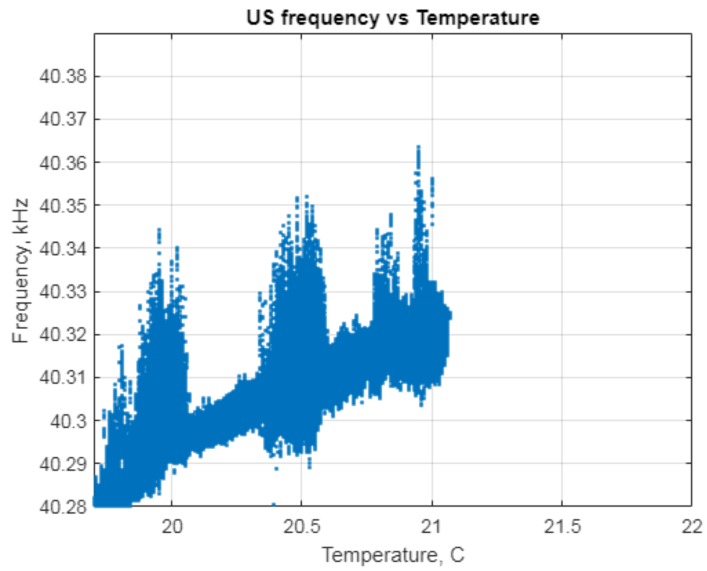

Figure 5.7: The correlation coefficient between the two data sets recorded at 300 mm by the conventional sensor and UOTSs in the open space over 21 hrs (Run 1).

The same experiment was repeated and collected data are presented in Figure 5.8 and Figure 5.9.

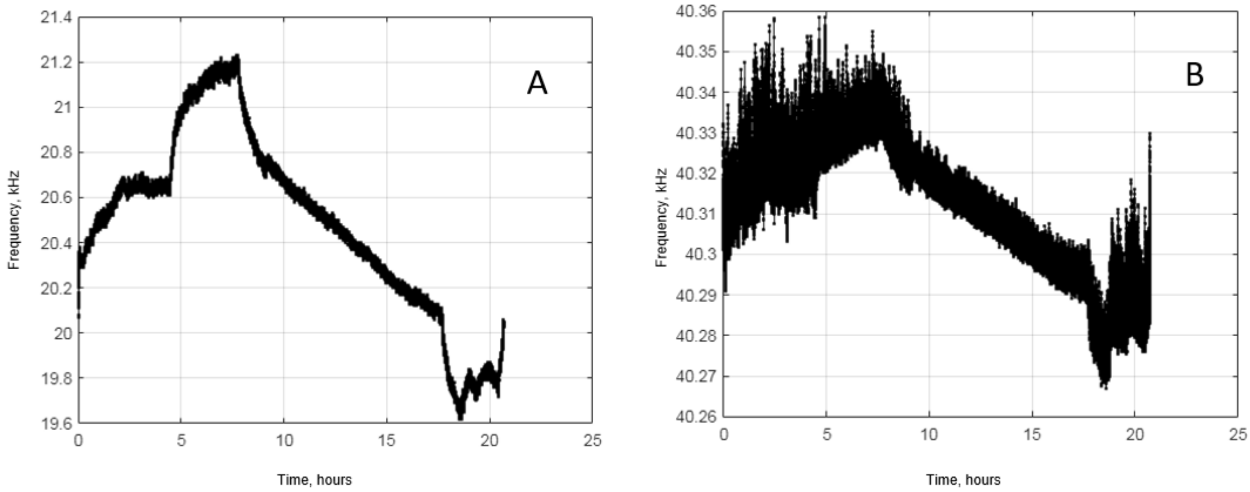

Figure 5.8: Monitored air temperature in an open space recorded by (A) conventional sensor (B) UOTSs at 300 mm over 21 hours (Run 2).

These results are consistent with those obtained during the first run. Figure 5.9 demonstrates a linear relationship with intermittent variations between the two data sets recorded at 300 mm by the conventional sensor and UOTS in open space. The gradient of this relationship is approximately 35 Hz/°C.

This gradient is calculated as follows:

Calculated using equation (4.1)

This gradient is calculated as follows: Temperature Variation: 21.98. (°C) - 20.98 (°C) = 1°C

UOTS Frequency Variation: 40.335 (H)z - 40.300(Hz) = 0.035*1000=35 Hz

Gradient=ΔF/ΔT=35(H)z/1(°C) = 35Hz/°C

This indicates that for each 1°C increase in temperature, the frequency changes by approximately 35 Hz

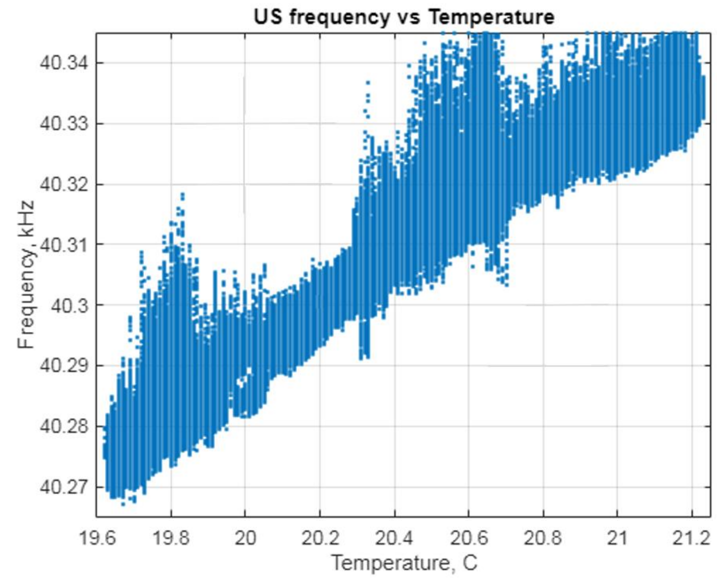

Figure 5.9: Linear relationship between the two data sets recorded at 300 mm by the conventional sensor and UOTSs in the open space over 21 hrs (Run 2).

5.4 Monitoring temperature inside the enclosure at a 500 mm distance

Figure 5.10 shows the collected data of the monitored temperature recorded by both sensors inside the enclosure in December time over roughly 24 hours.

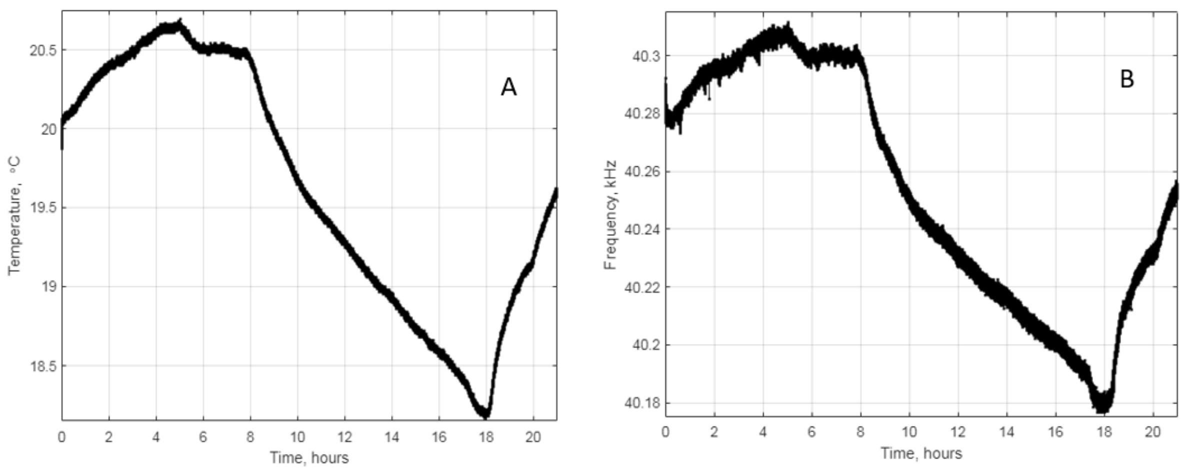

Figure 5.10: The monitored air temperature inside the enclosure was recorded by (A) conventional sensor (B) UOTSs at 500 mm for 21 hours (Run1).

As can be seen in Figure 5.10, the conventional sensor data showed a change in the temperature ranges from 18.15 to 20.75 °C, whereas the UOTSs showed a window from 40.175 to 40.31 kHz. The data recorded and displayed by the A and B curves demonstrate a significant resemblance over a one-day monitoring period.

Figure 5.11 shows the relationship between temperature measurements and UOTS frequency data recorded inside the enclosure over 24 hours.

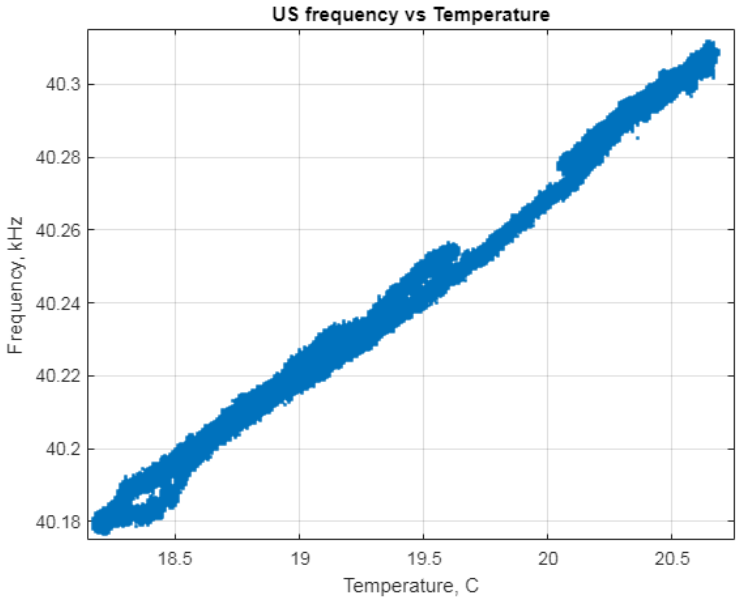

Figure 5.11: The relationship between the monitored air temperature recorded at 500 mm by the conventional sensor and UOTS frequency inside the enclosure over 24-hour intervals (Run 1).

Similar to the experiments conducted at a distance of 300 mm, Figure 5.11 demonstrates a clear linear relationship, with a gradient of approximately 45 Hz per degree Celsius. The temperature variation was Calculated using equation (4.1) as 20 (°C) – 19(°C) = 1°C, and the UOTS frequency variation was determined to be 40.267(Hz) - 40.222(Hz) = 0.045 Hz, which, when multiplied by 1000, equals 45 Hz. Consequently, the gradient is:

Gradient=ΔF/ΔT=45(Hz)/1(°C) = 45Hz/°C

This indicates that for each 1°C increase in temperature, the frequency changes by 45 Hz.

Figure 5.12 shows the experimental results for the second run, when the temperature changed from approximately 18.35 °C to 20.75 °C) during 24 hours, whereas the UOTSs showed a window from 40.1 kHz to 40.275 kHz for. The UOTS frequency output in Figure 5.12 (B) shows more scatter than in Figure 5.10, Run1.

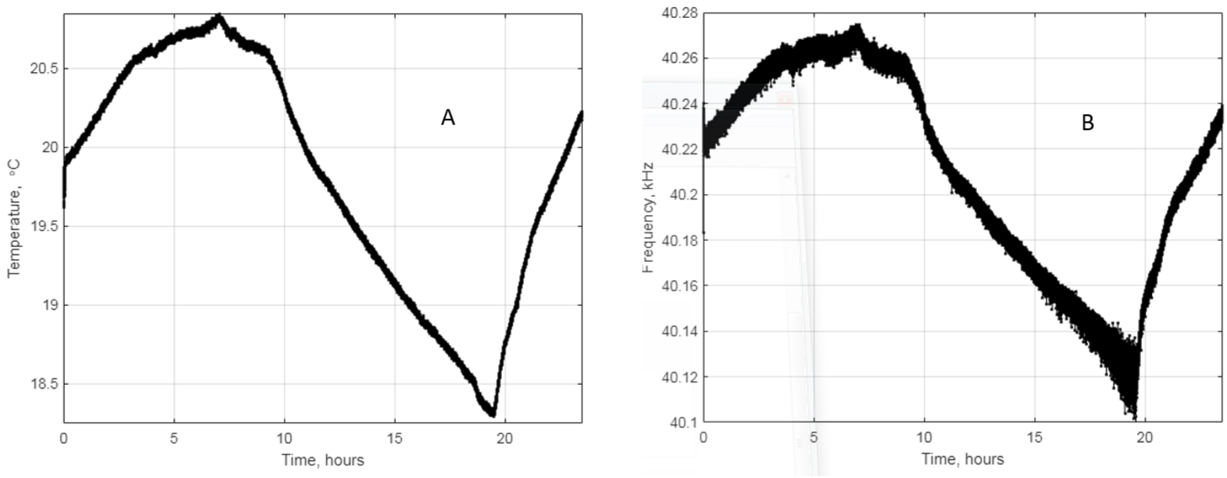

Figure 5.12: The monitored air temperature inside the enclosure was recorded by (A) conventional sensor (B) UOTSs at 500 mm for 24 hours (Run 2).

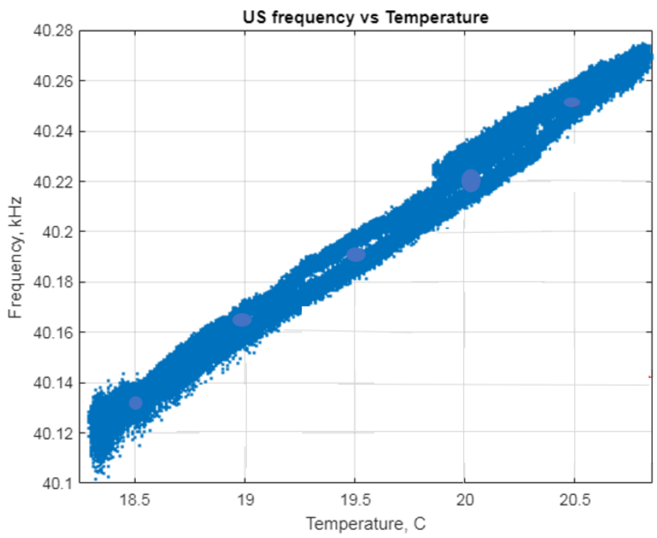

Figure 5.13: The relationship between the monitored air temperature recorded at 500 mm by the conventional sensor and UOTS frequency inside the enclosure over 24-hour intervals (Run 2).

This The scatter plot in Figure 5.13 illustrates a gradient of approximately 55 Hz/°C. This gradient is determined based on the following calculations:

Calculated using equation (4.1)

Temperature difference ΔT=20(°C)-19(°C) =1°C

Frequency difference ΔF=40.220(H)z-40.165(Hz)=0.055*1000=55Hz

Gradient=ΔF/ΔT=55(Hz)/1(°C) = 55Hz/°C

This result indicates that the frequency changes by approximately 55 Hz for each 1°C increase in temperature.

Another experiment was conducted during Christmas time. The setup left monitoring the temperature inside the enclosure, and data was recorded over 450 hours from the conventional and UOTSs collected. The graphs are shown in Figure 5.14.

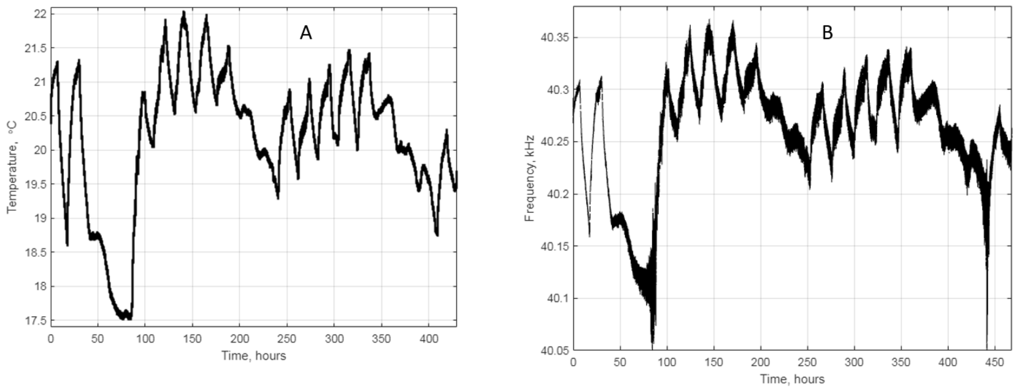

Figure 5.14: Monitored air temperature inside the enclosure recorded by (A) conventional sensor (B) UOTSs at 500 mm over Christmas break (450 hours) (Run 3).

Similar shapes are obtained by both sensors with two unusual, scattered set points recorded at low temperatures at approximately 75 and 440 hours since the start of the experiment. The following Figure 5.15 shows these scattered data zoomed. We are unaware of the cause for these two outliers.

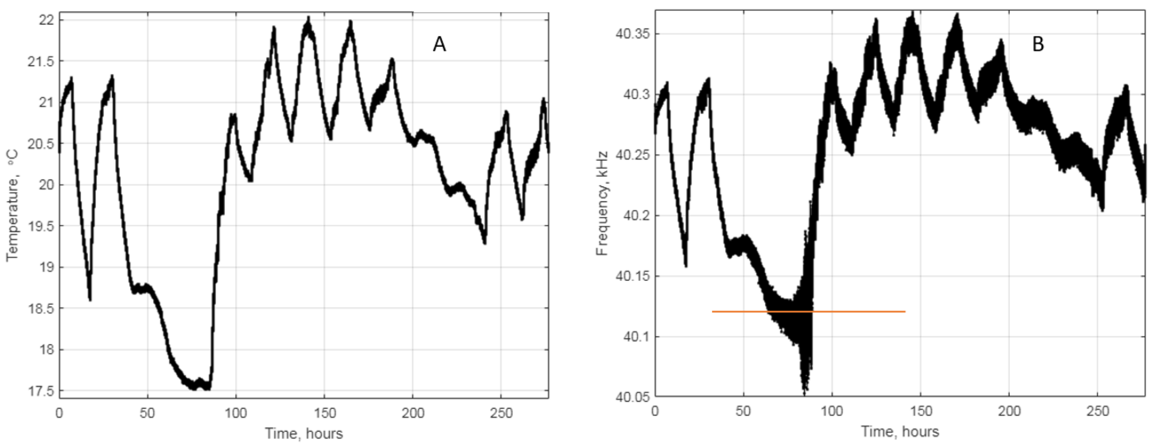

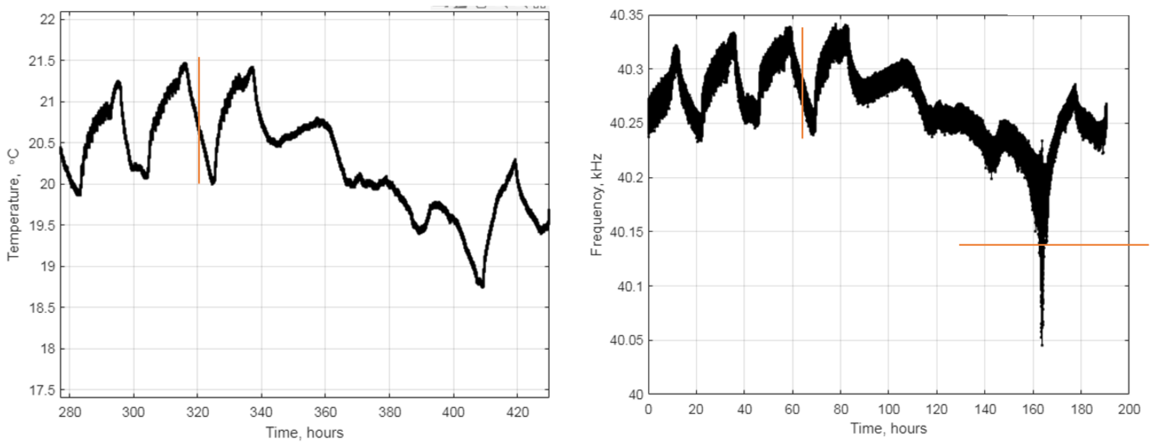

Figure 5.15 Monitored air temperature inside the enclosure recorded over Christmas break zoomed to show the scattered set points corresponding to approximately 75 and 440 hours since the start of the experiment.

5.5 Monitoring the temperature of the open space at a 500 mm distance

The setup was placed on a table inside an open office environment in December and left to record data for over 45 hours. The surrounding environment included operating computers and students moving around during the day. The recorded data for conventional sensors and UOTSs for a weekend are shown in Figure 5.16. The graphs of recorded data showed similar shapes: the open space recordings showed more variability compared to those recorded in the enclosure (for example, Figure 5.10).

Figure 5.17 shows the relationship between temperature measurements and UOTS frequency data recorded in the office over a weekend time. A correlation line was plotted to evaluate the similarity between the two graphs.

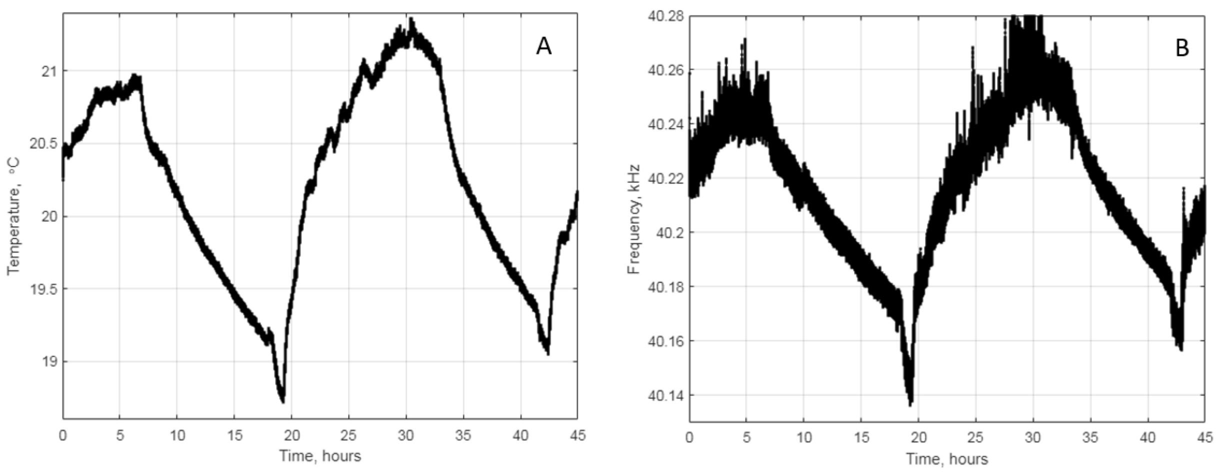

Figure 5.16: The monitored air temperature in an open space recorded by (A) conventional sensor (B) UOTSs at 500 mm over 45 hours.

The relationship between the air temperature recorded at a longer distance (500 mm) by the conventional sensor and the UOTS frequency output is linear and exhibits less divergence than that recorded at 300 mm, as shown in Figure 5.7. A linear relationship was derived from the two data sets, yielding a gradient of approximately 45 Hz/°C.

gradient is calculated as follows.

Calculated using equation (4.1)

Temperature difference ΔT=20.5(°C)-19.5(°C) =1°C

Frequency difference ΔF=40.230(Hz)-40.185(Hz)=0.045*1000=45Hz

Gradient=ΔF/ΔT=45(Hz)/1(°C) = 45Hz/°C

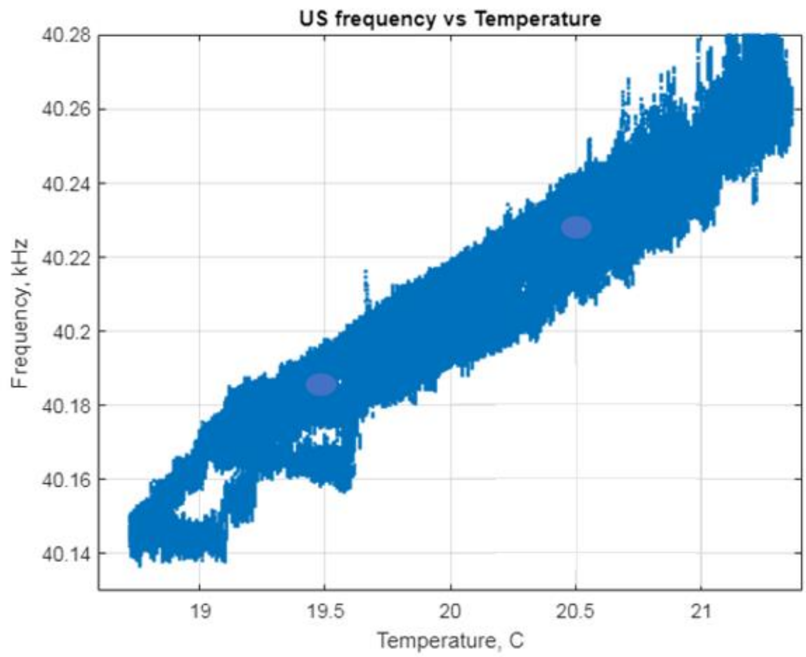

Figure 5.17: The relationship between the monitored air temperature recorded at 500 mm by the conventional sensor and UOTS frequency output in an open space over 45 hrs intervals.

5.6 Discussion

Starting with the observation of the temperature at a 300 mm distance within the cardboard box, the data collected from conventional sensors and UOTSs, as illustrated in (Figure 5.2, Figure 5.3), and (Figure 5.4, Figure 5.5) demonstrated remarkable similarity throughout a weekend-long monitoring period. Both sets of data displayed a strong linear correlation, as shown in Figure 5.3 and Figure 5.5, where the relationship between frequency and temperature exhibited a gradient of approximately 45 and 35 Hz per degree Celsius, respectively.

In Figure 5.2, it was observed that during periods of stability in the readings, a change of roughly 0.04°C corresponded to an approximate 10 Hz shift in the output frequency of the UOTS. The overall temperature range recorded by the conventional sensor during the 70-hour period ranged between (19.7 -21.9) °C. The UOTS frequency output range is (40.28- 40.38) kHz.

The recordings were obtained in open space over a day at a distance of 300 mm, as shown in Figure 5.6 and Figure 5.8; the data collected from conventional and UOTS sensors had similar shapes, indicating consistency in the data. Despite the similar shapes, the open space recordings showed more variability compared to those recorded in the enclosure (Figure 5.2 and Figure 5.4). This variation in the data suggests less controlled conditions led to these variations, which may be attributed to air movement by people walking around or working PCs nearby. These variations appeared especially during working hours and at higher temperatures. In Figure 5.5, the relationship between frequency and temperature seemed to be linear. However, this linear relationship was occasionally diverged, suggesting the presence of some other influences. To understand the level of variation in the data, at 40.3 kHz, for example, the UOTS frequency showed a scatter of 8 Hz corresponding to a variation of 0.2 °C.

At 500 mm distance, the experimental results clearly show that the data collected from the conventional temperature sensors and the Ultrasonic Oscillating Temperature Sensor (UOTS) inside the closure and outside exhibit a remarkable level of agreement. These datasets recorded in open space showed notable UOTS frequency variability; for example, at a high temperature of approximately 20.9°C, the temperature measurements exhibited a scatter of 0.02°C, while the frequency of UOTS exhibited a fluctuation of 40 Hz.

5.7 Conclusion:

Inside the enclosure, the relationship between the readings obtained from the conventional temperature sensor and the frequency output of UOTS collected at 300 mm and 500 mm distances demonstrates strong linearity. This outcome underscores the UOTS's reliability and consistency in temperature measurement, aligning closely with the established performance of conventional sensors.

When monitoring the temperature of the open space, the recordings, collected at 300- and 500-mm distances, exhibited similar shapes to one another but displayed more significant variability in comparison to the ones captured in the enclosure. Despite the seemingly linear relationship between frequency and temperature, it noticeably deviated at higher temperature levels.

This might be due to its sensitivity to both local temperature and air movements between the ultrasonic transducers. These changes occurred in a temperature range roughly between 18.5 – 21.5 °C.

Chapter 6 : Experimentation at the distance of 920 mm between the transducers

This chapter examines the capability of the UOTS to monitor air temperature at a 920 mm distance between the transducers in different scenarios with a comparative analysis of the UOTS's performance with that of conventional temperature sensors. Also, this chapter examines the UOTS's and conventional response to rapid and consistent heating tests using hair dryer and electric soldering iron, respectively.

6.1 Instrumentation and experimental procedures:

Various scenarios were implemented in this chapter to measure temperature within both controlled and open environments at 920 mm distance between the transducers. Figure 6.1 provides a schematic diagram for the experiments conducted in this study. A controlled environment was simulated using a cardboard thermal testing enclosure. to restrict air movement within the enclosure. The experiment conducted outside the cardboard thermal testing enclosure. in an open office aimed to replicate an uncontrolled environment. These conditions were systematically applied across extended time intervals.

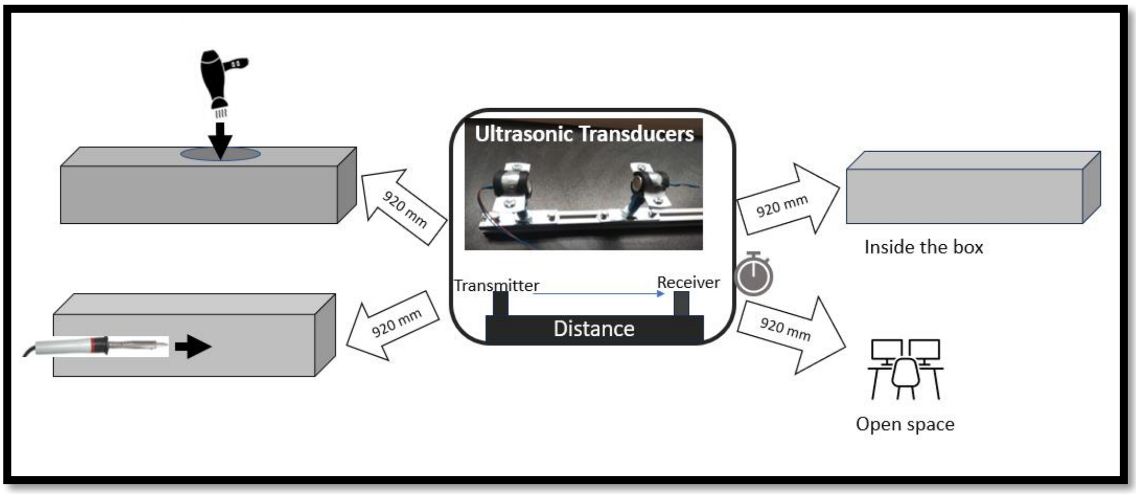

Figure 6.1: Schematic diagram for the Chapter 6 study.

The other scenarios implemented in this study were the rapid heating test and the slow heating test. For the rapid heating test, the temperature monitoring was started for about fifteen minutes before a hair dryer was used to elevate the air temperature inside the cardboard thermal testing enclosure. Via a centrally positioned aperture at the top of the cardboard thermal testing enclosure. The hair dryer operated on a low setting above the opening in the centre by 10 cm for a duration of six seconds before being deactivated, and the temperature was monitored for the first hour. After the initial hour of observation, the hair dryer was reactivated for a duration of ten seconds, and temperature monitoring continued for an additional hour.

To perform the slow heating test in a controlled environment, an electric soldering iron was placed inside the cardboard thermal testing enclosure. The electric soldering iron was operated for a duration of one hour. Then, the experiment was replicated for an extended period of time, where the soldering iron operated for a duration of two hours.

6.1.1 Monitoring temperature inside the enclosure at a 920 mm distance

The experimental arrangement was placed within a cardboard thermal testing enclosure., and temperature monitoring took place throughout the weekend. The records of monitored air temperature from both sensors inside the enclosure over a period of approximately 70 hours in January are shown in Figure 6.2. The figure shows the conventional sensor data indicates a temperature variation ranging from about 19.2 °C to 22.45°. At the same time the Ultrasonic Oscillating Temperature Sensor (UOTS) exhibited a frequency window spanning roughly 40.252 to 40.05 kHz.

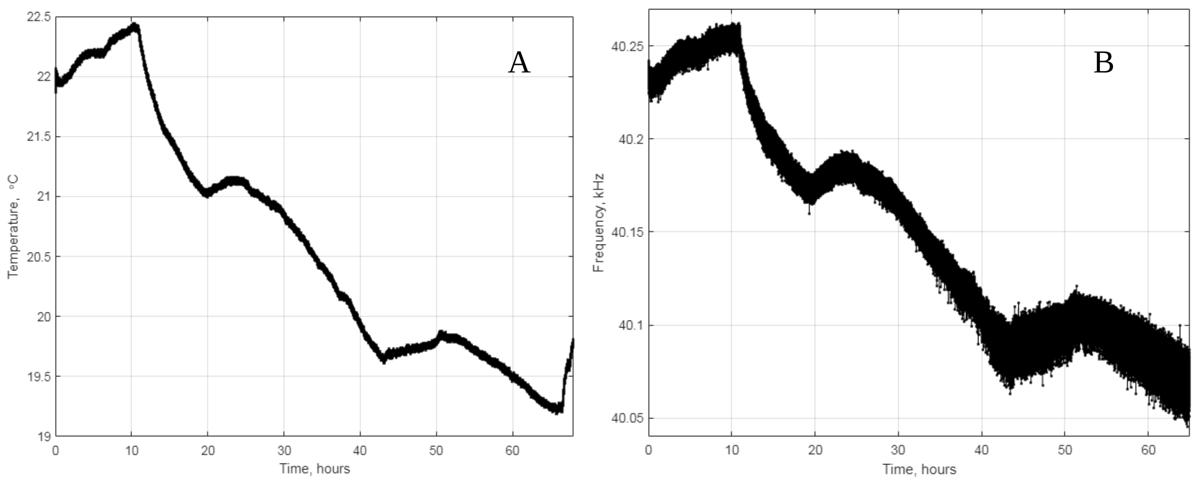

Figure 6.2: The monitored air temperature inside the enclosure was recorded by (A) a conventional sensor (B) UOTSs at 920 mm over 70 hrs intervals (Run 1).

The recorded data shown by the A and B curves in Figure 6.2 exhibit a close similarity over the weekend monitoring interval. Figure 6.3 shows the scatter plot between the frequency of

UOTSs and the conventional sensor-measured temperature Linearity can be seen between the two data sets with a gradient of around 55 Hz/°C.

gradient is calculated as follows.

Calculated using equation (4.1)

Temperature difference ΔT=22(℃)-21(℃) =1℃

Frequency difference ΔF=40.245(Hz)-40.190(H)z=55Hz

Gradient=ΔF/ΔT=55(Hz)/1(℃) = 55Hz/℃

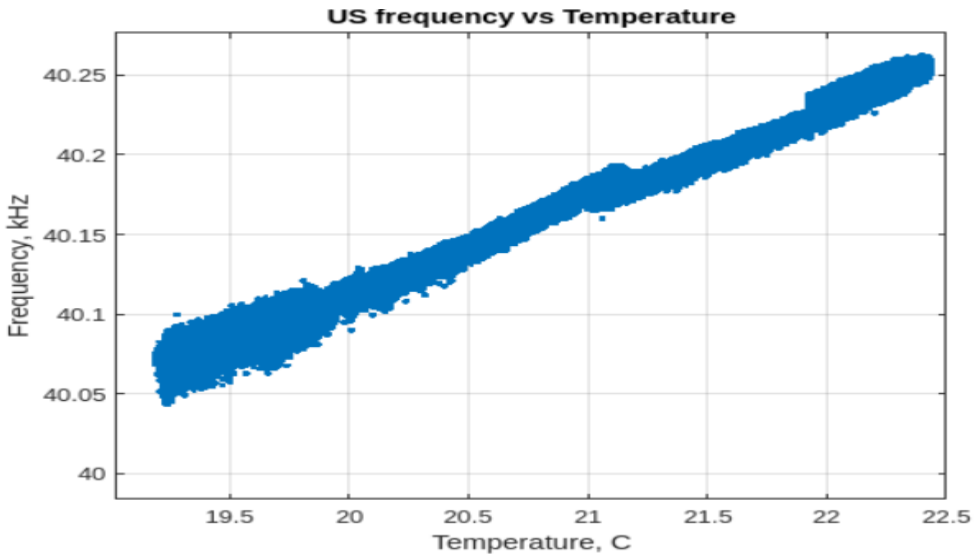

Figure 6.3: (A) The relationship between the monitored air temperature recorded by the conventional sensor and UOTSs inside the enclosure over 60 hrs intervals. (B)Temperature – UOTS frequency relationship (Run 1).

This experiment was repeated for over 20 hours at a distance of 920 mm (Run 2, Figure 6.4).

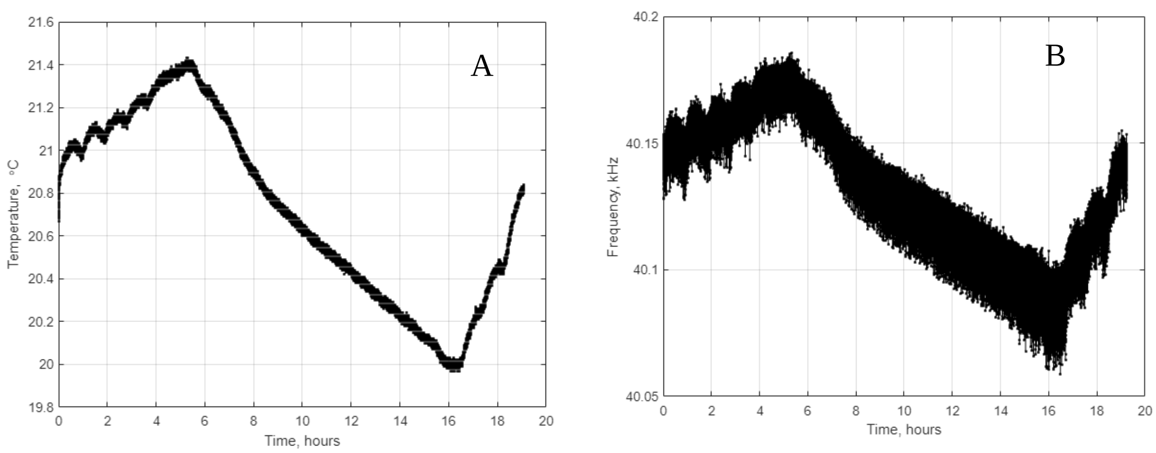

Figure 6.4: The second run of the monitored air temperature inside the enclosure was recorded by (A) a conventional sensor and (B) at 920 mm over 20 hrs interval (Run 2).

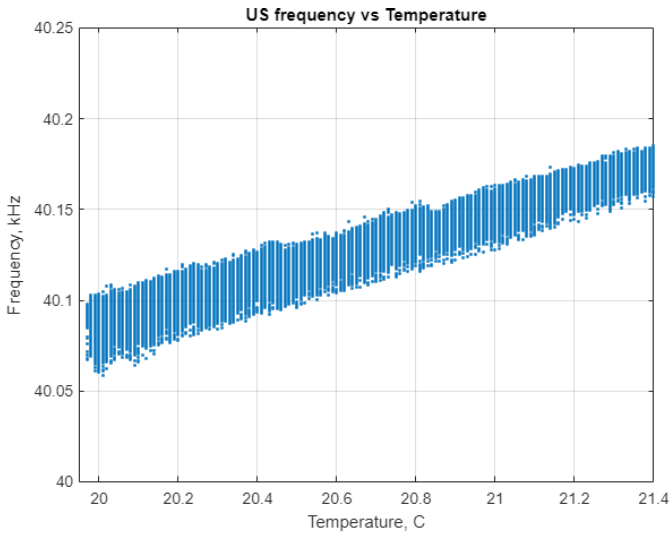

Figure 6.5 The relationship between the monitored air temperature recorded by the conventional sensor and UOTSs inside the enclosure over 20-hour intervals.

Figure 6.5 demonstrates a linear relationship between temperature and UOTS frequency. However, the recorded data exhibit a correlation line with a gradient of 68 Hz per degree Celsius, which is larger than that observed in the first run. The gradient is calculated as follows:

Calculated using equation (4.1)

Temperature difference ΔT=21.2(°C)-20.2(°C) =1°C

Frequency difference ΔF=40.168(Hz)-40.100(H)z= 0.068*1000= 68Hz

Gradient=ΔF/ΔT=68(Hz)/1(°C) = 68Hz/°C

6.1.2 Monitoring the temperature of the open space at a 920 mm distance

The setup was placed on a table inside an open office environment in January and left to record data for over 20 hours. The surrounding environment included operating computers and students moving around for around one day. The recorded data for conventional sensors and UOTSs are shown in Figure 6.6.

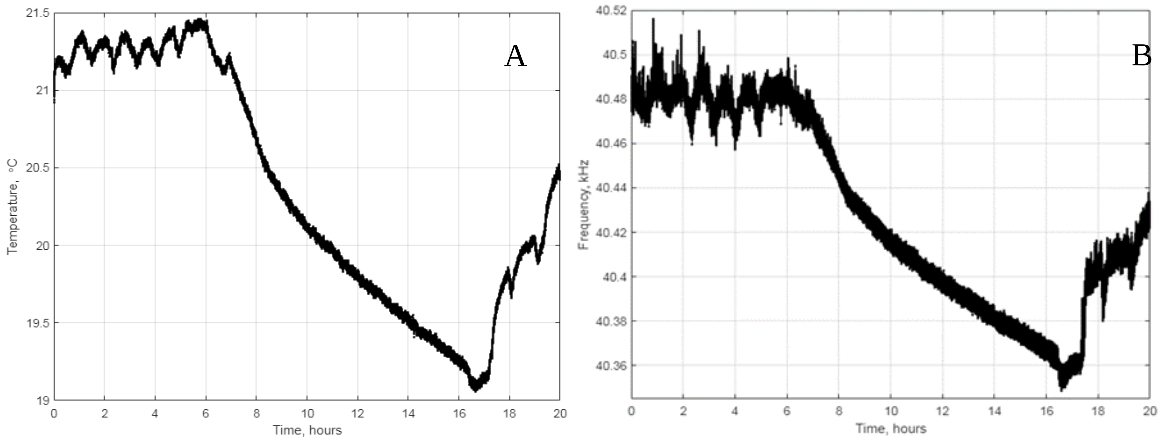

Figure 6.6: The monitored air temperature in an open space recorded by (A) conventional sensor (B) UOTSs at 920 mm over 201 hours (Run 1).

The related scatter plot is shown in Figure 6.7 with the gradient of approximately 55 Hz/°C. There was some hysteresis in the output frequency of the UOTS, as evidenced by different frequency values at the same temperature.

The gradient is calculated as follows:

Calculated using equation (4.1)

Temperature difference ΔT=20.5(°C)-19.5(°C) =1°C

Frequency difference ΔF=40.435(Hz)-40.380(H)z=.055*1000=55Hz

Gradient=ΔF/ΔT=55(Hz)/1(°C) = 55Hz/°C

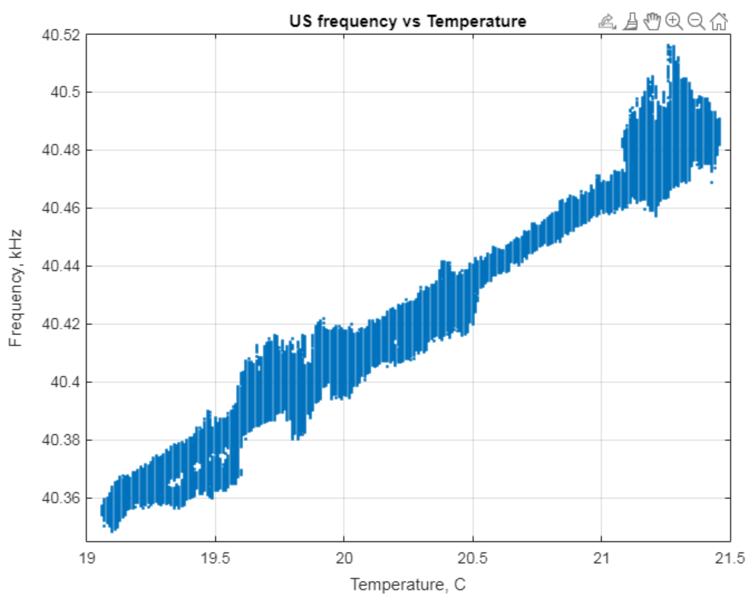

Figure 6.7: The correlation coefficient between the two data sets recorded at 920 mm by the conventional sensor and UOTSs in the open space over 20 hrs (Run 1).

This experiment was repeated on the next day, and Figure 6.8 shows the monitoring temperature outside the enclosure over 20 hours at a distance of 920 mm.

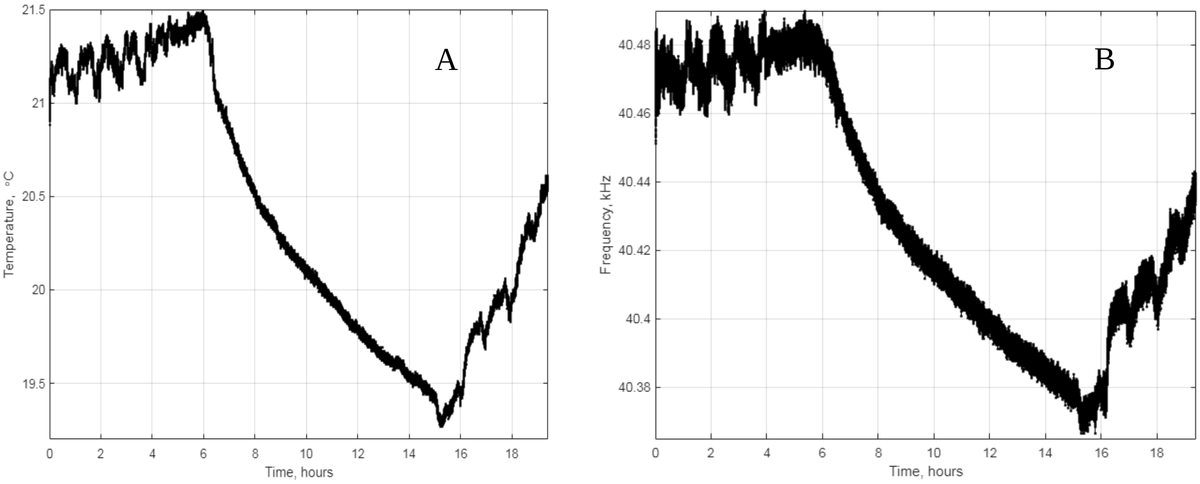

Figure 6.8: The monitored air temperature in an open space recorded by (A) conventional sensor (B) UOTSs at 920 mm over 20 hours (Run 2).

The relationship between frequency and temperature in Figure 6.9 exhibited hysteresis and had an estimated slope of 53 Hz per degree Celsius.

The gradient is calculated as follows:

Calculated using equation (4.1)

Temperature difference ΔT=20.5(°C)-19.5(°C) =1°C

Frequency difference ΔF=40.433(Hz)-40.380(Hz)=.053*1000=53Hz

Gradient=$\Delta F/\Delta T$=53(Hz)/1(°C) = 53Hz/°C

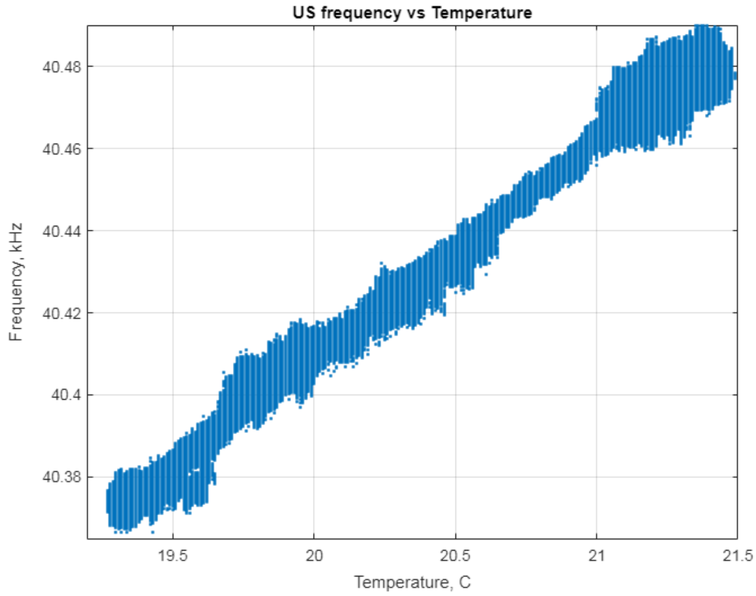

Figure 6.9: Linear relationship between the two data sets recorded at 920 mm by the conventional sensor and UOTSs in the open space over 201 hrs (Run 2).

The UOTS sensor demonstrated reduced output frequency fluctuations during distinct temperature trends. However, the scatter plot shows a few irregular clusters with noticeable hysteresis.

6.2 The rapid heating tests

For this experiment an opening was made at the top centre of the cardboard box; the hairdryer operated at 10 cm above the opening, and the sensors were placed in the centre. The distance between the hair dryer and the sensors was about 30 cm, and it operated at different time intervals with pauses between these operations. Figure 6.10 A & B shows the recorded data for conventional sensors and UOTS when the hair dryer operated on a low setting for a duration of six seconds before being deactivated. The relationship between the monitored air temperature recorded by the conventional sensor and UOTSs is shown in Figure 6.10 C.

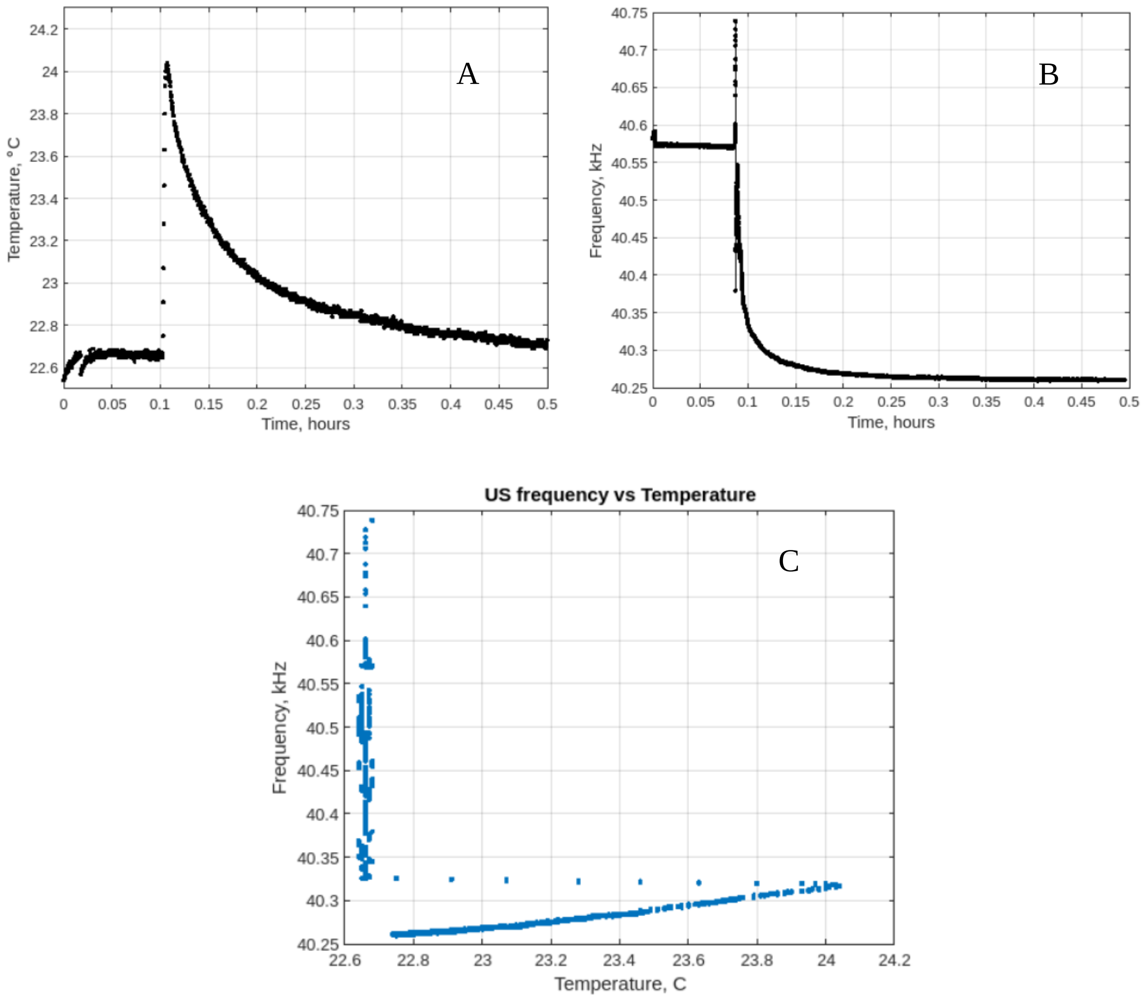

Figure 6.10: Experimental records for the rapid heating test monitoring air temperature before and after hot air was injected by a hair dryer for 6 seconds. (A) conventional sensor, (B) UOTS output at (920 mm distance between transducers) and (C) a linear relationship between the US frequency and temperature.

The results shown in Figure 6.10 are similar to those obtained before and show a simultaneous response of both sensors to the rapid heating test, where the UOTS returned instantaneously to the base line unlike the conventional sensor. The frequency-temperature relationship showed a gradient of 50Hz per degree Celsius (Figure 6.10 C). The gradient is calculated as follows:

Calculated using equation (4.1)

Temperature difference ΔT=23.8(℃)-22.8(℃) =1℃

Frequency difference ΔF=40.320(Hz)-40.270(H)z=.050*1000=50Hz

Gradient=$\Delta F/\Delta T$=50(Hz)/1(℃) = 50Hz/℃

However, this was not the case in Figure 6.11. After the temperature was continued to be monitored for the first hour, the hair dryer was reactivated for a duration of ten seconds, and the temperature monitoring continued for an additional hour (Figure 6.11).

The instantaneous response of the UOTS output that was followed by an immediate return to just above the baseline was subjected to high step jumps. This difference is probably caused by the blowing of hot air into the box where the sensors were placed, and the moving air over-blowing the sensor. The UOTS's data seemed different from the data obtained when the sensors were placed deep inside. The temperature has risen from 20.5 to 37.5 ℃ after the first 6-second hot air shot and from around 21.5 up to 46.5 ℃ after the second 10-second hot air shot. i.e., the total increase is temperature difference ΔT=46.5(℃)-20.5(℃)=26℃ around 26 ℃.

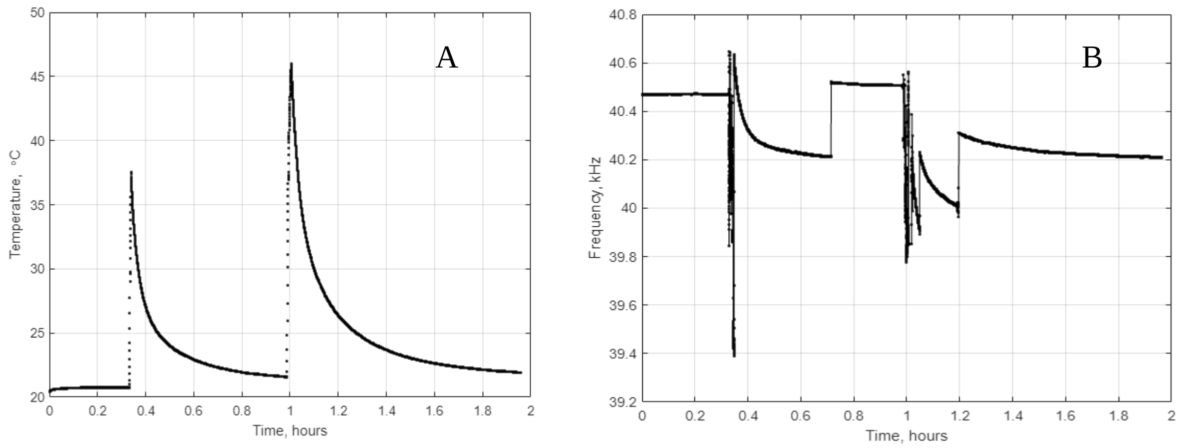

Figure 6.11: Monitoring air temperature before and after hot air was injected by a hair dryer for 6 and 10 seconds and air temperature for an hour after each injection (A) conventional sensor data, (B) UOTSs output at (920 mm distance between transducers).

The box with the transducers had the length of 110 cm (Chapter 4, Section 4.6.1). The rapid heating test experiment was conducted in Chapter 4 by using the hairdryer on a low setting at one end of the cardboard thermal testing enclosure of 110cm L x 25cmW x 25cm H, and the sensors were placed at the other end, i.e., at a distance of 110 cm.

The relationship between the US frequency and temperature after the hairdryer was operated for different time intervals with pauses between these operations shows several parallel peaks with similar slops and an overall increase of the air temperature inside the enclosure.

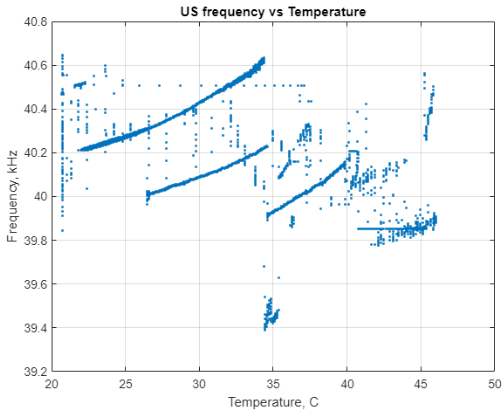

Figure 6.12:UOTS frequency output plotted against temperature recorded by conventional sensors for multiple heating shots injected by a hairdryer inside an enclosure.

6.3 The slow heating tests

In this experiment, an electric soldering iron was positioned at the centre of a closed cardboard thermal testing enclosure. the sensors were positioned at the centre, too, so the iron solder was parallel to the aluminium rail. The soldering iron was switched on for one hour in the initial trial, and the experiment was subsequently repeated for an extended period of two hours. Figure 6.13 shows

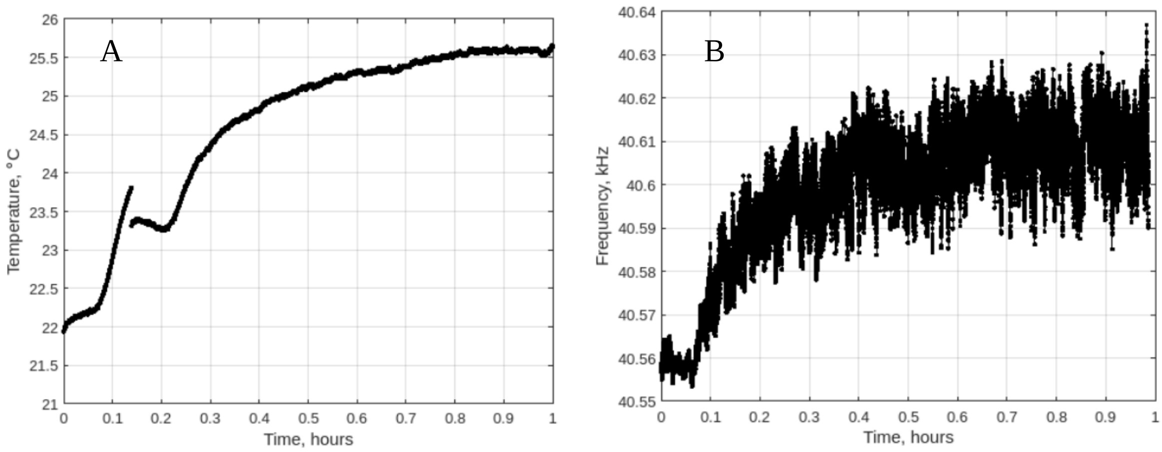

Figure 6.13: The monitored air temperature inside the enclosure recorded by (A) conventional sensor (B) UOTSs at 920 mm over 1 hour in response to an activated nearby soldering iron for one hour (Run 1)

the sensors recorded response to the gradual heating process. Both air temperature monitoring profiles inside the enclosure show similar patterns that exhibit rising air temperature with time.

However, the UOTS exhibited increased data scatter as the temperature rose. The total increase in temperature was calculated as follows:

Temperature difference ΔT=25.5(°C)-21.9(°C) =3.6°C

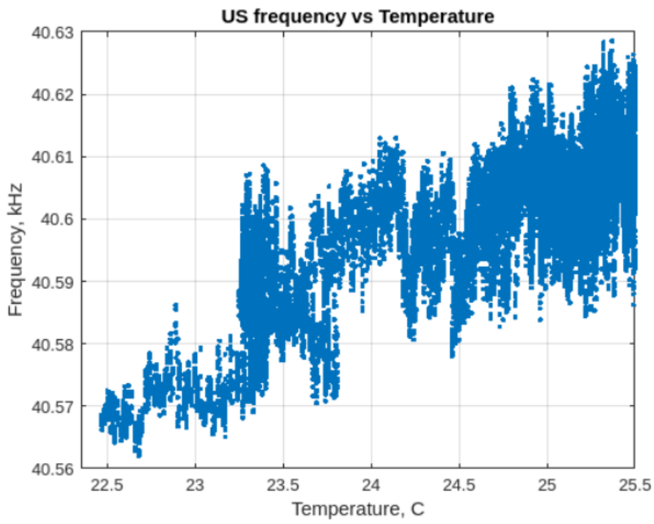

Figure 6.14: UTOS frequency output plotted against temperature recorded by conventional sensor in response to raised temperature by iron solder inside an enclosure.

The relationship plotted in Figure 6.14 between the UTOS frequency output, and the temperature recorded by the conventional sensor shows a direct relational trend despite being nonlinear, probably due to the scattered data pulses.

The repeated experiment, as shown in Figure 6.15, demonstrates a sustained increase in temperature within the first hour, rising from 21.8°C to 26.8°C. This was followed by a slower increase, reaching 27.4°C after two hours, resulting in a total rise of 5.6°C. The temperature difference is calculated as follows: Temperature difference ΔT=27.4(°C)-21.8(°C) =5.6°C

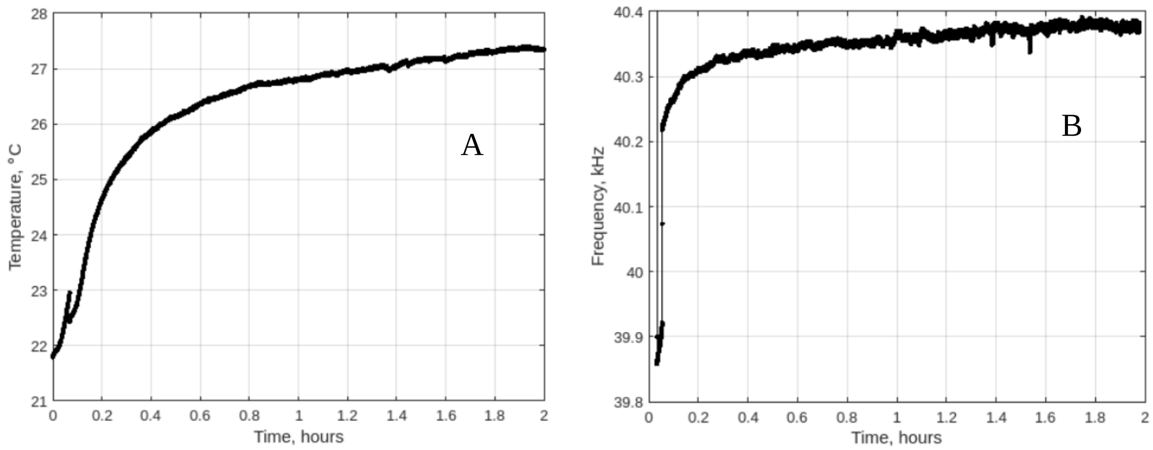

Figure 6.15: The monitored air temperature inside the enclosure recorded by (A) conventional sensor (B) UOTSs at 920 mm over 2 hours in response to an activated nearby soldering iron (Run 2)

The relationship plotted in Figure 6.16 between the UTOS frequency output and the temperature recorded by the conventional sensor shows a direct relationship with less scattered data than the first repeat, which can be seen clearer at low temperatures.

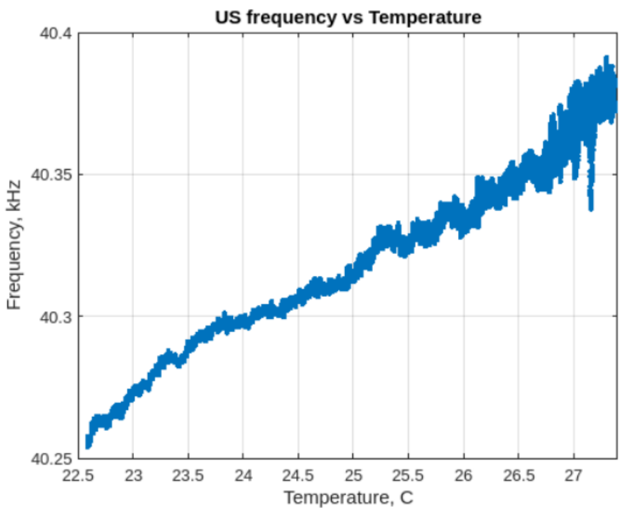

Figure 6.16: UTOS frequency output plotted against temperature recorded by conventional sensor in response to raised temperature by iron solder inside an enclosure.

6.4 Discussion

Starting with the observation of the temperature at a 920 mm distance within the cardboard box, the data collected from the conventional sensor and UOTS, as illustrated in Figure 6.2 and Figure 6.3, demonstrated remarkable similarity throughout a weekend-long monitoring period. Both sets of data displayed a strong linear correlation, as shown in Figure 6.3, where the relationship between frequency and temperature exhibited a gradient of approximately 55 Hz per degree Celsius (Figure 6.2). The figure shows the conventional sensor data indicates a temperature variation ranging from about 19.2 °C to 22.45°C. In contrast, the UOTSs exhibited a frequency window spanning roughly 40.05 to 40.252 kHz during the same time frame.

In the repeat of monitoring temperature for 19 hours shown in Figure 6.4 and Figure 6.5, similar patterns of UTOS scattered data are shown. The correlation line showed a gradient of 68 Hz per degree Celsius, which was notably higher compared to the rest of the collected datasets.

The recordings were obtained in open space over a day at 920 mm, as shown in Figure 6.6 and repeated the next day (Figure 6.8); the data collected from conventional and UOTS sensors had similar shapes, indicating consistency in the data. Despite the similar shapes, the open space recordings showed more variability and hysteresis compared to those recorded in the enclosure (Figure 6.7 and Figure 6.9); the correlation between frequency and temperature revealed a few irregular clusters with noticeable hysteresis.

In the rapid heating test and slow heating test experiments, two heat transfer mechanisms were involved. In the rapid heating test, the hair dryer introduces hot air into the cardboard thermal testing enclosure. With dynamic airflow. As the hot air was blown into the cardboard thermal testing enclosure., it displaced the cooler air, creating a flow pattern. This forced convection helps distribute heat more rapidly, causing a rapid increase in temperature within the enclosure. In contrast, during the soldering iron experiment, heat conduction is the primary mechanism through which the air inside the closed space is heated. The combination of forced and natural convection contributes to the overall heat transfer in the system as heated air becomes less dense and tends to rise, creating a natural convection current where the heated air rises, and cooler air moves in to replace it. The rise in temperature was about 26 °C, and the response of UTOS to sudden increase accompanied by blowing hot air was characterised by high step jumps.

In the slow heating test experiment, the soldering iron directly heats the air in its immediate vicinity, and then the heat is conducted through the air molecules, gradually raising the temperature of the entire volume of air in the box. This resembles the presence of a heater inside the dwelling; the UTOS showed two patterns: scattered data in the first run and more stable data with less variation in the second run of the experiment, which lasted for two hours. The total increase in the temperature was 5.6 °C.

6.5 Conclusion

Inside the enclosure, the experimental data set shows a strong correlation. The relationship between the readings obtained from the conventional temperature sensor and the frequency output of UOTS collected at 920 mm demonstrated remarkable similarity throughout a week-end-long monitoring period. The relationship between frequency and temperature exhibited a gradient of approximately 55 Hz per degree Celsius. This outcome underscores the UOTS's reliability and consistency in temperature measurement, aligning closely with the established performance of conventional sensors. The rapid heating test employs a hair dryer for forced convection, creating dynamic airflow that rapidly increases the temperature within the enclosure. In the slow heating test with a soldering iron, heat conduction is the primary mechanism, complemented by forced and natural convection. The interplay of these mechanisms influences the overall heat transfer, providing insights for tailored thermal processes.

Chapter 7 : SUMMARY AND CONCLUSION

7.1 Chapter 1

Temperature sensors are widely used in science, medicine, industry, and daily life. However, conventional temperature sensors have limitations. They measure temperature at a single localized point and require thermal equilibrium, causing time lags. This increases costs when multiple sensors are needed for accurate monitoring. Their response times are usually several seconds, making them slow to react to sudden temperature changes. Despite these drawbacks, conventional temperature sensors remain essential due to their reliability and effectiveness, with ongoing advancements addressing their limitations.

Ultrasonic temperature sensors offer responsive measurements by utilizing ultrasound velocity's dependence on temperature through pulse-echo and through-transmission principles. These sensors are highly sensitive and can detect fast temperature changes. Unlike conventional sensors, they can measure temperature at multiple points simultaneously, providing aggregate measurement. This makes them a compelling option for various industrial, medical, and scientific applications, offering enhanced performance and reliability over conventional methods.

Extensive past research in acoustic thermometry seeks to overcome traditional sensors' limitations like single-point measurements and thermal equilibrium requirements. UOTS, leveraging ultrasonic sound velocity changes, offers promise for cost-effective, accurate temperature sensing in gases, liquids, and solids. Continued research suggests UOTS could revolutionize temperature sensing with improved performance and affordability.

The present research aims to develop cost-effective UOTS devices with reliability akin to conventional sensors, focusing on measuring aggregate temperature in the air. This involves creating a test rig, integrating calibrated conventional temperature sensors, designing an electronic driver, and conducting validation tests against conventional sensors. Overall, this research’s goal is to develop, fully prototype, and verify an ultrasonic sensor for measuring aggregate temperature in dwellings in order to maintain a comfortable indoor temperature for building occupants.

7.2 Chapter 2

Conventional sensors can be connected to data acquisition systems, control units, recording devices or directly to displays. Their output can be voltage, resistance, or mechanical displacement, which is then converted into temperature values using calibration curves or equations specific to the sensor type and application.

The experiments explore temperature measurement with conventional sensors, revealing challenges in achieving absolute accuracy but highlighting the feasibility of consistent relative measurements, particularly within limited air volume enclosures. The Pt100 RTD and DS18B20 IC sensors were employed alongside I2C combinational sensors (BMP280 and AHT20). While sensor readings generally tracked each other, notable scatter, especially with the DS18B20 sensor, was observed. In a controlled setup with restricted airflow, sensors exhibited minimal deviation, underscoring the importance of environmental conditions and natural variability of temperature field.

7.3 Chapter 3

This chapter provides an in-depth examination of devices and methodologies for recording frequencies in various experimental settings. Ultrasonic transducers are essential instruments, excelling in harsh environments and enabling electrical energy conversion to ultrasound and vice versa.

Auxiliary equipment like the PLJ-8LED-C module and the ISDS205 digital oscilloscope were used for inspecting and quantifying operation of the UOTS. Practical considerations, such as using a cardboard enclosure and a domestic hair dryer for temperature regulation, are also addressed. This chapter integrates theoretical concepts with practical applications to UOTS frequency recording.

An experiment compared the response times of two conventional air temperature sensors, AHT20 and BMP280, with a new ultrasonic air temperature sensor (UOTS). The UOTS showed a significantly faster response to changes in temperature, although precise quantification was unfeasible at that stage.

For accurate quantification, a high-resolution frequency meter is needed to measure the UOTS input frequency multiple times per second. This requires a temperature-controlled crystal oscillator for reference frequency and a microcontroller with capture timers.

This study compared frequency measurement methods using timer peripherals of modern microcontrollers (MCUs) for UOTSes. Accurate measurements were achieved by counting reference pulses over multiple periods of the input signal of interest.

Challenges with the conventional MCU timer's capture mode were mitigated by using direct memory access (DMA) mode, allowing captured values to be stored directly in the MCU's memory without CPU intervention. The STM32G474 MCU captured values at every pulse edge, enabling half-period measurements, and the CPU averaged the data as required.

7.4 Chapter 4

The experimental results revealed several key findings regarding the performance of a conventional temperature sensor and a UOTS in various scenarios at the distance of 150 mm between the transducers. Both sensors were subjected to rapid air heating inside an enclosure and long-term temperature monitoring, both inside the enclosure and in the open space.

The comparison between the conventional sensor and UOTS output frequencies indicated that UOTS captured temperature changes more frequently and responsively compared to the conventional sensors, which provide more coarse and intermittent data. The UOTS output frequency was measured over two distinct time intervals: 0.1 seconds and 6.25 milliseconds. The results were similar, but the latter interval was preferred for more responsive measurements.

During rapid air heating inside an enclosure, UOTS demonstrated faster response times and quicker return to baseline values compared to conventional sensors. It also showed satisfactory agreement with conventional sensor data during extended-term temperature monitoring within the enclosure.

Specifically, UOTS exhibited a variation of 0.05°C at a 2 Hz frequency during a constant reading period, with a hysteresis displayed in the frequency-temperature relationship. Over a 60-hour period, UOTS closely resembled conventional sensors, and within a stable reading period, it showed a deviation of 0.04°C at a 10 Hz output frequency, with a linear relationship between temperature and frequency.

In long-term temperature monitoring in open space, UOTS was found to be more sensitive to air movement, resulting in increased variability. However, it showed few irregular clusters with some hysteresis, highlighting its sensitivity to air movement.

Overall, both sensors exhibited similar temperature patterns, albeit with variations due to the open environment.

7.5 Chapter 5

After examining operation of the UOTS at the shortest distance, further experiments were conducted at the distances of 300 and 500 mm between the transducers.

In the enclosure, the experimental dataset revealed a strong correlation between the readings from the conventional temperature sensor and the frequency output of the UOTS. This highlights the reliability and consistency of the UOTS in temperature measurement, closely aligning with conventional sensors' established performance.

However, when monitoring the temperature of the open space, recordings collected at these distances showed similar shapes, but greater variability compared to those captured in the enclosure. Despite the apparent linear relationship between frequency and temperature, deviations were noticeable at higher temperature levels, possibly due to sensitivity to local temperature and air movements between ultrasonic transducers. Nevertheless, these changes occurred within a controlled temperature environment a manned laboratory with a relatively small temperature variation range from 18.5 to 21.5 °C.

7.6 Chapter 6

At the longest distance between the transducers of 920 mm, experiments within the enclosure and in open space were complimented by rapid and slow heating tests.

Inside the enclosure, the experimental dataset exhibits a strong correlation between readings from the conventional temperature sensor and the frequency output of UOTS over a weekend-long monitoring period. The relationship between frequency and temperature demonstrates a gradient of approximately 55 Hz per degree Celsius, highlighting the reliability and consistency of the UOTS in temperature measurement, closely aligning with conventional sensors' established performance.

In the rapid heating test utilizing a hair dryer for forced convection, dynamic airflow rapidly increases the enclosure's temperature. Conversely, the slow heating test with a soldering iron primarily employs heat conduction, supplemented by forced and natural convection. The interaction of these mechanisms influences overall heat transfer, offering insights for tailored thermal processes.

7.7 Recommendations for future research

During this research and through several experiments conducted, certain limitations require addressing in future work concerning the measurement of air temperature using an ultrasonic oscillating temperature sensor for operation in the air.

1-Verify performance of an UOTS in a temperature-controlled chamber that will also enable more comprehensive study of hysteresis in the output frequency.

2- Verify performance of an UOTS against an array of conventional temperature sensors, independently measuring air temperature along the complete ultrasonic pathway.

3-Extend the distance between the transducers in order to achieve operation at the distance of several meters that is typical for residential buildings.

4-Establish convenient and unobtrusive ways of commissioning an UOTS into a residential environment.

7.8 Overall summary

A low-cost UOTS system has been successfully developed for measuring air temperature. The experimental results quantitatively confirm the significantly faster response time of the UOTS. These advancements and experimental findings pave the way for creating cost-effective ultrasonic temperature sensors that deliver reliable, extended measurements. Data collected over hundreds of hours of experimentation were analysed to optimize the operation and select suitable operating parameters. The developed modular system (transducers' fixture, electronic driver, frequency meter, conventional temperature's datalogger) was proven to be a robust tool for exploring the functionality of ultrasonic oscillating temperature sensors (UOTSs) in air temperature measurement across different setups. Consequently, the aim of the research was successfully achieved.

REFERENCES

[1] Precedence Research: Artificial Intelligence (AI) Sensor Market Report by 2034, Available online: https://www.precedenceresearch.com/sensor-market. accessed Sept 2024

[2] A. Hashmi, A.N.Kalashnikov, Sensor data fusion for responsive high resolution ultrasonic temperature measurement using piezoelectric transducers, Ultrasonics, Volume 99, 2019, 105969, ISSN 0041-624X, https://doi.org/10.1016/j.ultras.2019.105969.

[3] L. Michalski et al, "Temperature Measurement, 2nd," Measurement Science and Technology, vol. 13, (10), pp. 1651-1652, 2002.

[4] Richard Rusby, Introduction to Temperature Measurement. (2nd ed.) United Kingdom: National Physical Laboratory, 2016.

[5] K. E. Jack et al., "A simple thermistor design for industrial temperature measurement," IOSR Journal of Electrical and Electronics Engineering (IOSR-JEEE)e-ISSN: 2278-1676,p-Volume 11, Issue 5 Ver. III (Sep - Oct 2016), pp. 57-66. http://repository.fut-minna.edu.ng:8080/jspui/handl

[6] H. G. Brixy, "Temperature measurement in nuclear reactors by noise thermometry," Nucl. Instrum. Methods, vol. 97, (1), pp. 75–80, 1971.

[7] M. J. McGrath and C. N. Scanaill, Sensor Technologies: Healthcare, Wellness, and Environmental Applications. 2013.

[8] D. Tayurskii and A. Le Méhauté, "The concept of temperature in the modern physics," Thermodynamics-Systems in Equilibrium and Non-Equilibrium, 2011. doi = 10.5772/22082.

[9] J. P. Bentley, "Temperature sensor characteristics and measurement system design," Journal of Physics E: Scientific Instruments, vol. 17, (6), pp. 430, 1984.

[10] M. Duff and J. Towey, "Two ways to measure temperature using thermocouples feature simplicity, accuracy, and flexibility," *Analog Dialogue*, vol. 44, (10), pp. 1-6, 2010.

[11] W. Y. Du, *Resistive, Capacitive, Inductive, and Magnetic Sensor Technologies.* 2014.

[12] I. Sinclair, Sensors and transducers. 3rd edition, Newnes, 2001.

[13] M. Zhu, "A thermometer based on diverse types of thermocouples and resistance temperature detectors," Journal of Shanghai Jiaotong University (Science), vol. 20, pp. 93–100, 2015
.

[14] M. Tirupathamma and V. Niranjan, "PRINCIPLES AND APPLICATIONS OF INFRARED THERMAL IMAGING," *Telecommunications and Radio Engineering,* vol. 79, *(13),* 2020.

[15] I. Ihara et al, "Ultrasonic thermometry for temperature profiling of heated materials," Advancement in Sensing Technology: New Developments and Practical Applications, pp. 211-236, 2013.

[16] J. D. N. Cheeke, Fundamentals and Applications of Ultrasonic Waves. 2010.

[17] T. B. A. Senior & J. H. Richmond. (1975). *Ultrasonic Thermometry and its Application in Industry*. *Journal of Acoustical Science*. Retrieved from Acoustical Society Publications

[18] C. Abram, B. Fond and F. Beyrau, "Temperature measurement techniques for gas and liquid flows using thermographic phosphor tracer particles," *Progress in Energy and Combustion Science*, vol. 64, pp. 93–156, 2018.

[19] D. Hurle, "*Fundamentals: Thermodynamics and Kinetics*". 2013.

[20] M. Z. Aslam et al, "Advances in the surface acoustic wave sensors for industrial applications: Potentials, challenges, and future directions: A review," Measurement, vol. 222, pp. 113657, 2023. .

[21] D. Morgan, Surface Acoustic Wave Filters: With Applications to Electronic Communications and Signal Processing. 2010.

[22] C. K. Campbell, "Applications of surface acoustic and shallow bulk acoustic wave devices," Proc IEEE, vol. 77, (10), pp. 1453–1484, 1989.

[23] J. Monchalin, "Laser-ultrasonics: Principles and industrial applications," in Ultrasonic and Advanced Methods for Nondestructive Testing and Material Characterization Anonymous 2007.

[24] D. S. Ballantine Jr et al, Acoustic Wave Sensors: Theory, Design and Physico-Chemical Applications. 1996.

[25] S. Sherrit et al, "BAW and SAW sensors for in situ analysis," in Smart Structures and Materials 2003: Smart Sensor Technology and Measurement Systems, 2003. Available:

https://www.researchgate.net/publication/253799355_BAW_and_SAW_sensors_for_in-situ_analysis accessed Sept 2024.

[26] L. C. Lynnworth et al, "Nuclear reactor applications of new ultrasonic transducers," IEEE Trans. Nucl. Sci., vol. 18, (1), pp. 351–362, 1971.

[27] T. Liao, W. Tsai and C. Huang, "A new ultrasonic temperature measurement system for air conditioners in automobiles," Measurement Science and Technology, vol. 15, (2), pp. 413, 2003.

[28] L. C. Lynnworth, D. R. Patch and E. H. Carnevale, "No title," Ultrasonic Profile Measuring Apparatus, 1972.

[29] Malyarenko, D. I., Joines, W. T., & Grissom, W. A. *Ultrasonic System Thermometry for Monitoring Temperature Changes in Cancer Radiation Therapy*. IEEE Transactions on Biomedical Engineering, 55(9), 2175-2183. https://doi.org/10.1109/TBME.2008.919346.2008.

[30] Lévesque, D., Desbiens, A., & Moreau, A. *Ultrasonic Measurement of Bore Temperature in Small Firearms: Applications in Heat Transfer and Structural Analysis*. *Journal of Dynamic Systems, Measurement, and Control*, 138(11), 110904. https://doi.org/10.1115/1.4034279 2016.

[31] A. Afaneh et al., "Ultrasonic measurements of temperature in aqueous solutions: why and how," Physics Research International, , 2011. https://doi.org/10.1155/2011/156396

[32] Smith, J., & Brown, High-Resolution Time-Delay Measurement in Advanced Radar Systems. IEEE Transactions on Instrumentation and Measurement, accessed Sept 2024

[33] Yuan, J., & Liu, Y. *Time-of-Flight Measurements in Ultrasonic Systems: A Review of Techniques and Applications*. *Ultrasonics*, 44(1), 25-38. 2006. https://doi.org/10.1016/j.ultras.2005.06.00

[34] P. Popejoy et al, "*Comparison of implementations of driving electronics for ultrasonic oscillating sensors*," in 2012 IEEE International Ultrasonics Symposium, 2012,

[35] L. C. Lynnworth, Ultrasonic Measurements for Process Control: Theory, Techniques, Applications. 2013.

[36] S. Alzebda and A. N. Kalashnikov, "Ultrasonic sensing of temperature of liquids using inexpensive narrowband piezoelectric transducers," IEEE Trans. Ultrason. Ferroelectric. Freq. Control, vol. 57, (12), pp. 2704–2711, 2010. .

[37] A. Afaneh et al, "Ultrasonic measurements of temperature in aqueous solutions: why and how," Physics Research International, vol. 2011, (1), pp. 156396, 2011. .

[38] A. Hashmi, A. N. Kalashnikov and R. A. Light, "Experimental evaluation of ultrasonic oscillating temperature sensors (UOTS) under cyclically changing temperatures," in 2015 IEEE International Ultrasonics Symposium (IUS), 2015,

[39] Dyer, S. A. *High-Precision Ultrasound Measurements: Addressing Hysteresis and Feedback Control Issues*. *IEEE Transactions on Ultrasonics, Ferroelectrics, and Frequency Control*, 52(8), 1383-1392. https://doi.org/10.1109/58.942547 *.2005.*

[40] Market Research Future (MRFR). Temperature Sensors Market Research Report *2023–2032*. Available at: https://www.marketresearchfuture.com/reports/temperature-sensors-market-11037. accessed Sept 2023

[41] L. Cole, "No title," How to Cut Carbon Out of Your Heating, BBC Future, 17 Nov 2020

[42] Lynnworth, L. C., & Liu, Y. *Ultrasonic Measurements for Process Control and Monitoring*. *IEEE Transactions on Ultrasonics, Ferroelectrics, and Frequency Control*, 53(12), 2332-2345. https://doi.org/10.1109/TUFFC.2006.1629. 2006

[43] W. Manthey, N. Kroemer and V. Magori, "Ultrasonic transducers and transducer arrays for applications in air," Measurement Science and Technology, vol. 3, (3), pp. 249, 1992. .

[44] C. R. Hill, J. C. Bamber, Gail R. Ter Haar, Physical Principles of Medical Ultrasonics, January2004 ISBN:9780471970026 |OnlineISBN:9780470093979 |DOI:10.1002/0470093978

[45] Lynnworth, L. C. *Ultrasonic Measurements for Process Control: Theory and Applications*. Academic Press. https://doi.org/10.1016/B978-012460465-4/50012-0. (1999)

[46] Seeeduino XIAO Arduino Controller, SAMD21 Cortex M0+ - 102010328. Available: https://cpc.farnell.com/seeed-studio/102010328/microcontroller-arduino-seeeduino/dp/SC15646.

[47] A. Elyounsi and A. N. Kalashnikov, "Using ultrasonic oscillating temperature sensors (UOTSes) to measure aggregate temperatures in liquid and gaseous media," *in 2021 IEEE UFFC Latin America Ultrasonics Symposium (*LAUS), 2021.

[48] Sinha, D. N. *Ultrasonic Sensing and Measurements in Liquid Environments*. *Ultrasonics*, 52(2), 140-146. https://doi.org/10.1016/j.ultras.2011.07.007 .(2012).

[49] N. V. Kirianaki, S. Y. Yurish and N. O. Shpak, "Methods of dependent count for frequency measurements," Measurement, vol. 29, (1), pp. 31-50, 2001

[50] Brodie, R. & Lindsay, M. *Microcontroller Development: Implementing DMA with ARM Cortex-M Processors*. *Embedded Systems Programming Journal*, 45(3), 123-134. (2017).

[51] Yiu, J. (2015). The Definitive Guide to ARM Cortex-M3 and Cortex-M4 Processors (3rd ed.)